R. Wahyu Widanarto

Gas Detection with Floating Gate Field Effect Transistor

Cuvillier Verlag Göttingen

Universität der Bundeswehr München
Fakultät für Elektrotechnik und Informationstechnik

Gas Detection with Floating Gate Field Effect Transistor

R. Wahyu Widanarto

Vorsitzender der Promotionsausschusses : Prof. Dr. H. Baumgärtner
1. Berichterstatter : Prof. Dr. I. Eisele
2. Berichterstatter : Prof. Dr. H. Meixner

Tag der Prüfung 12.03.2007

Mit der Promotion erlangter akademischer Grad:
Doktor-Ingenieur
(Dr.-Ing.)

Neubiberg, den 14.03.2007

Der Druck dieser Arbeit wurde durch Haushaltsmittel der Universität der Bundeswehr München gefördert.

Bibliografische Information Der Deutschen Bibliothek
Die Deutsche Bibliothek verzeichnet diese Publikation in der Deutschen Nationalbibliografie; detaillierte bibliografische Daten sind im Internet über http://dnb.ddb.de abrufbar.
1. Aufl. - Göttingen : Cuvillier, 2007
Zugl.: München, Univ., Diss., 2007

978-3-86727-193-6

„Gedruckt mit Unterstützung des Deutschen Akademischen Austauschdienstes“

Nonnenstieg 8, 37075 Göttingen
Telefon: 0551-54724-0
Telefax: 0551-54724-21
www.cuvillier.de

1. Auflage, 2007
Gedruckt auf säurefreiem Papier

978-3-86727-193-6

Abstract

Gas detection with the FG-FET sensor system has been demonstrated within this thesis. According to the goal of the thesis, metal and metal oxides were employed as gas sensitive films. Work function changes of metal and metal oxides with respect to gas concentrations have been measured as a function of temperature and humidity.

Ag_2O films were deposited by thermal evaporation a pressure of $2x10^{-2}$ mbar under oxygen atmosphere. The H_2S sensitivity of the film was characterized in the FG-FET sensor system. The sensing characteristics, which are derived from the work function change of the film, depend strongly on H_2S concentration and temperature. Ag_2O sensors exhibit best performance in H_2S detection at operating temperature of 95°C. Its signals increase with increasing H_2S concentration. From 5 ppm up to 50 ppm the t_{50} response time is about 10 s, whereas at 2 ppm the response time is very slow (t_{50}~7 min). No significant humidity effect can be observed during H_2S measurement for elevated relative humidity. An experiment corresponding to the cross sensitivity of the sensor shows that the sensor responds strongly to H_2S with positive signals and NO_2 with negative signals. Furthermore, the sensor shows good the long-term stability.

In a second experiment, ZnO films were investigated in the FG-FET sensor system as NO_2 sensitive films. 200 nm of ZnO film was deposited by thermal evaporation a pressure of $2x10^{-2}$ mbar under oxygen atmosphere. Interaction between the resulting ZnO film and NO_2 was directly analyzed by using XPS. It has been found that the interaction occurs due to ion exchange at the surface and the bulk conduction electron near the surface. The ZnO sensor signal depends strongly on NO_2 concentration and temperature. It shows best performance in 2-20 ppm NO_2 detection at operating temperature of 165°C, at which negligible base line changes and a fast response time t_{50}~10 s as well as reversible signals to NO_2 can be observed. At low operating temperature, the sensor signals need more than 15 min to return to the base line. Humidity affects the output of the signals. The height of the

signals decreases with increasing humidity due to the formation of OH-groups at the ZnO surface. The high selectivity of the sensor can be observed at this operating temperature under dry condition. The sensor responds strongly only to NO_2 exposure. An experiment related to the long-term stability shows that the signal pattern of the sensor remains stable after 1.5 months. Unfortunately the sensor needs high temperature of 190°C to detect NO_2 at low concentrations below 2 ppm.

In order to detect low NO_2 concentrations below 2 ppm, a SnO_2 film modified with Cu clusters was used as gas sensitive film in the FG-FET sensor system. The clusters, which are distributed at the SnO_2 surface, were employed to dissociate NO_2 molecules. The XPS characterization shows that the SnO_2/Cu surface adsorbs nitrogen after exposing it to 2 ppm NO_2 for 15 min at room temperature under dry conditions. Obviously this causes the work function change of SnO_2. The sensing properties of SnO_2/Cu were tested by exposing the SnO_2/Cu sensor to NO_2 concentrations from 200 ppb up to 2000 ppb at elevated temperatures under dry conditions. The sensor signal depends strongly on NO_2 concentration and temperature. Its sensitivity increases with increasing temperature. The sensor exhibits best performance at operating temperature of 165°C under dry conditions.

With the goal improving Pt sensors for H_2 detection, Pt films modified with SnO_2 and $TiSi_2$ were investigated by using the FG-FET sensor system. As has been known signals of the Pt sensor are unstable with temperatures and humidities due to oxygen chemisorption and formation of OH-groups at the Pt surface. In the new system, the Pt film was used as a catalyst, which will dissociate H_2 or O_2 molecules into hydrogen or oxygen atoms species. Due to the spill-over effect, SnO_2 and $TiSi_2$ were employed as material, which adsorbs the resulting dissociated molecules, so that reduction and oxidation reactions at the Pt surface can be avoided.

The Pt/SnO_2 sensor proves to be very stable with temperatures up to 135°C and shows long-term stability as well as high selectivity. Unfortunately, the response of the sensor to H_2 exposure is slow, particularly at temperatures below 95°C. Obviously the H_2 molecules must diffuse through SnO_2 film to reach the Pt surface because the interaction between H and O^- atoms occur at the SnO_2 surface after Pt catalyst dissociated H_2 molecules.

Therefore, the molecules need more time and higher temperature. Moreover, the sensor is quite sensitive to relative humidity. Signals of the sensor decrease rapidly with increasing humidity at temperatures below 100°C.

Accordingly, new materials and strategies were used to improve the Pt sensor. For this propose $TiSi_2$/Pt films were employed as gas sensitive films. The gates, which have been coated with 110.6 nm of Ti and 249.4 nm of Pt films, were annealed by using horizontal furnace in oxygen at 800°C for 30 min. It was found that nano-grains of $TiSi_2$ grow inside the films whereas large Pt islands remains. The Pt islands dissociate directly H_2 and O_2 molecules into H and O^- atoms, and then the atoms spill over onto nano-grains of $TiSi_2$.

The $TiSi_2$/Pt sensor is very stable with temperature. Its response to H_2 exposure is nearly independent of temperature up to 135°C. No significant change of the response time (t_{90}~10 s) can be observed due to elevated temperatures and concentrations. Signals of the sensor increase linearly with increasing H_2 in concentration range between 3000 ppm and 20000 ppm at room temperature under dry conditions. No significant relative humidity effect up to 70% is observed during measurements of 9000 ppm H_2 at room temperature. Furthermore, the cross sensitivity and long-term stability of the sensor are very well.

Zusammenfassung

In dieser Dissertation ist die Gasdetektion mit Hilfe eines FG-FET Sensor-Systems demonstriert worden. Entsprechend dem Ziel dieser Arbeit, wurden Metall und Metalloxide als sensitive Filme für die Detektion von Gasen eingesetzt. Hierbei wurden Austrittsarbeitsänderungen des Metalls bzw. der Metalloxide in Abhängigkeit von der Gaskonzentration, Temperatur und Feuchtigkeit gemessen und ausgewertet.

Die Präparation der ersten untersuchten sensitiven Schicht, Ag_2O (50nm), erfolgte durch thermisches Aufdampfen bei einem Sauerstoffpartialdruck von $2x10^{-2}$ mbar. Zur Charakterisierung des Ag_2O-Films im Hinblick auf H_2S-Sensivität wurde dieser in ein FG-FET Sensor-System eingebaut. Die Sensoreigenschaften, die sich aus den Austrittsarbeitsänderungen des Filmes ableiten, hängen stark von der H_2S-Konzentration und der Temperatur ab. Der Ag_2O-Sensor zeigt die besten Resultate bezüglich der H_2S-Detektion bei einer Betriebstemperatur von 95°C. Dabei wird bei zunehmenden H_2S-Konzentrationen ein Anstieg des Signals beobachtet. Während die Antwortzeit t_{50} bei einer Konzentration zwischen 5 ppm und 50 ppm H_2S bei etwa 10 Sekunden liegt, verlängert sie sich bei der Konzentration von 2 ppm auf ca. 7 Minuten. Es konnten keine nennenswerten „Feuchtigkeits-Effekte“ während der H_2S-Messung bei höheren relativen Feuchtigkeiten beobachtet werden. Ein Experiment zur Untersuchung der Querempfindlichkeit des Sensors zeigte ein starkes positives Signal bei H_2S-Beaufschlagung und ein starkes negatives Signal bei NO_2. Darüber hinaus zeigt der Sensor sehr gute Resultate im Hinblick auf Langzeitstabilität.

In weiteren Experimenten wurden ZnO Filme mit Hilfe von FG-FET Sensor-Systemen für die Detektion von NO_2 untersucht. Die Präparation der 200 nm dicken ZnO Schichten erfolge durch thermisches Aufdampfen bei einem Sauerstoffpartialdruck von $2x10^{-2}$ mbar. Anhand von XPS-Messungen konnte die Reaktion zwischen dem abgeschiedenen ZnO Film und dem NO_2 analysiert werden. Hierbei wurde ein Ionenaustausch nachgewiesen. Der ZnO Sensor-Signal zeigt ebenfalls eine starke Abhängigkeit von der NO_2

Konzentration sowie der Temperatur. Die besten Resultate zeigt dieser bei einer Konzentration von 2-20 ppm NO_2 und einer Betriebstemperatur von 165°C. Dabei wurden vernachlässigbare Verschiebungen der Grundlinie, eine schnelle Antwortzeit t_{50} von ca. 10 Sekunden sowie die Reversibilität NO_2-Signale beobachtet. Bei einer niedrigen Betriebstemperatur benötigen die Sensor-Signale mehr als 15 Minuten, um zur Grundlinie zurückzufinden. Mit zunehmender Feuchtigkeit verringert sich die Signalhöhe, da sich OH-Gruppen an der ZnO-Oberfläche anlagern. Die hohe Selektivität des Sensors bei dieser Betriebstemperatur kann daher nur in trockener Umgebung beobachtet werden. Zudem reagiert der Sensor stark auf NO_2-Beaufschlagung. Ein Experiment zur Untersuchung der Langzeitstabilität des Sensors zeigte noch nach 1,5 Monaten ein stabiles Signalmuster. Leider benötigt der Sensor die hohe Temperatur von 190°C um NO_2 bei niedrigen Konzentrationen unterhalb 2 ppm zu nachzuweisen.

Um eine niedrige NO_2 Konzentration unterhalb 2 ppm detektieren zu können, wurde eine mit Cu-Clustern modifizierte SnO_2-Schicht als sensitiver Film integriert in einem FG-FET Sensor-System untersucht. Die Cluster, die an der SnO_2 Oberfläche verteilt werden, dienen zur Aufspaltung des NO_2-Moleküls. Aus den XPS-Messungen geht hervor, dass die Beaufschlagung der Schicht mit 2 ppm NO_2 für 15 Minuten bei Raumtemperatur in trockener Umgebung zur Absorption von Stickstoff auf der SnO_2/Cu Oberfläche führt. Offensichtlich wird die Absorption durch die Austrittsarbeitsänderungen des SnO_2 verursacht. Zur Untersuchung der Eigenschaften der SnO_2/Cu-Schicht wurde der Sensor bei NO_2 Konzentration zwischen 200 ppb und 2000 ppb, bei erhöhten Temperaturen und in trockener Umgebung betrieben. Dabei zeigte das Signal eine starke Abhängigkeit von der NO_2-Konzentration und der Temperatur. Die Sensitivität nimmt bei steigender Temperatur zu. Die besten Resultate konnten bei einer Betriebstemperatur von 165°C und in trockener Umgebung nachgewiesen werden.

Eine weitere Aufgabe bestand in der Optimierung des Pt Sensors für den Nachweis von Wasserstoff. Hierzu wurden in einer weiteren Versuchsreihe mit SnO_2 und $TiSi_2$ modifizierte Pt Schichten untersucht. Wie bereits bekannt, werden die Signale der Pt Sensoren stark durch Temperatur und Feuchtigkeit beeinflusst. Der Grund hierfür ist einerseits die

Chemisorption des Sauerstoffs und andererseits die Bildung von OH-Gruppe an der Pt Oberfläche. Bei dem neu entwickeltem System dient die Pt-Schicht als Katalysator für die Dissotiation der H_2- oder O_2-Moleküle. Getreu dem „spill over“ Effekt adsorbieren SnO_2 und $TiSi_2$ die dissozierten Moleküle und verhindern damit jegliche Reduktions- bzw. Oxidationsreaktionen an der Pt-Oberfläche.

Der Pt/SnO_2-Sensor zeigt ein stabiles Verhalten bis zu einer Temperatur von 135°C. Daneben konnte die Langzeitstabilität sowie eine hohe Selektivität nachgewiesen werden. Leider zeigt der Sensor ein langsames Antwortverhalten bei Beaufschlagung mit H_2. Dies wird bei Temperaturen unter 95°C besonders deutlich. Offensichtlich müssen die H_2-Moleküle durch die SnO_2-Schicht diffundieren, da die Reaktion zwischen H und O Atomen an der SnO_2-Oberfläche erst nach der Dissotiation des H_2-Moleküls durch den Pt Katalysator, erfolgt. Folglich benötigen die Moleküle mehr Zeit und eine höhere Temperatur. Zudem zeigt der Sensor eine starke Reaktion auf Änderung der relativen Feuchtigkeit. Es wird ein rasches Absinken des Sensorsignals bei zunehmender Feuchtigkeit und gleichzeitig einer Temperatur unter 100°C beobachtet.

Aus diesem Grund wurden zur Verbesserung des Pt-Sensors neue Materialen und Strategien untersucht. Als sensitive Schichten kamen $TiSi_2$/Pt Filme zum Einsatz. Ein Schichtsystem aus 110,6 nm Ti und 249,4 nm Pt wurde in einem Rohrofen in Sauerstoff-Atmosphäre bei 800°C für 30 Minuten getempert. Die Schichten zeigten ein Wachstum von $TiSi_2$-Nano-Körnern unterhalb größerer Pt-Inseln auf. Die Pt Inseln dienen zur Zerlegung der H_2 und O_2 Moleküle in H und O^- Atome. Die Atome wandern zu den zu $TiSi_2$-Nano-Körnern und werden dort adsorbiert.

Der $TiSi_2$/Pt Sensor verfügt über eine sehr gute Temperaturstabilität. Seine Sensitivität gegenüber H_2 ist nahezu unabhängig von der Temperatur bis zu 135°C. Die Antwortzeit (t_{90} ~ 10 Sekunden) ist aufgrund der höheren Temperatur und Konzentration annährend konstant. Bei Raumtemperatur und H_2-Konzentrationen bis 9000 ppm ist der „Feuchtigkeit Effekt“ ist bis zu einer relativen Feuchtigkeit von 70 % vernachlässigbar. Darüber hinaus weist der Sensor sehr gute Resultate im Hinblick auf Querempfindlichkeit und Langzeitstabilität auf.

Contents

Introduction

A gas sensor is a device, which allows for the determination of information about the ambient gas atmosphere. It consists of a gas sensitive film and a signal transfer component, which is called transducer. The transducer converts physical and chemical change of the sensitive film into an electrical signal. The sensor's ability to detect certain gas can be optimized by an appropriate choice of gas sensing material and by suitable technology.

Over the past 20 years, a great deal of research effort has been directed towards the development of small dimensional gas sensing devices for practical applications in detection of polluting and inflammable gases as well as manufacturing process monitoring. Detection of polluting and inflammable gases is becoming increasingly important for environmental and human protection.

- Nitrogen dioxide (NO_2) is one of the indicators of poor air quality and can cause photochemical smog and corrosion.
- Hydrogen sulfide (H_2S) is a toxic gas and very dangerous for people, who live in surroundings of volcanoes. H_2S appears in blast furnaces, petroleum-refineries, in gasworks, and also in the viscose-industry, cell-wool-, cell-glass-, and rayon-manufacturing. Already small concentrations of approximately 200 ppm H_2S can cause irritation of the mucous membranes (eyes, breath-ways), nausea, sickness, headaches, diarrhea, breathing difficulty, unconsciousness and cramps.
- Hydrogen (H_2) is predicted to be an alternative energy carrier in the future. It will be used in automotive industry and in local fuel cells. This

energy can decrease the problem related to the green house warming by CO_2. On the other hand, hydrogen is dangerous due to its explosive character. Already a concentration of 4% can cause an explosion. Hydrogen is also a produced gas in the very early stage of fire. It has been shown that hydrogen sensors can detect a fire earlier than the smoke detectors used up to now [1].

Metal oxides like SnO_2, ZnO and TiO_2, which are used as gas sensitive films in sensor systems, are playing an important role in the gas detection. The systems are mostly based on conductivity change measurement of the metal oxides due to reaction between surface of the metal oxides and the ambient gas atmosphere [2-6]. One disadvantage of the systems is that they need high temperature above 200°C to obtain interaction between the material and gas molecule. Since it is necessary to actively heat the sensor for proper operation, it is difficult to use it in mobile systems due to the limited energy supply. Therefore the high operating temperature of the systems is a serious problem to be considered. Intense efforts are being made to reduce it. A well known strategy is to modify the gas sensitive films by doping with metallic catalyst e.g. platinum (Pt), palladium (Pd) and various nano-dimensional architectures [7-10]. However, the temperature can not be decreased yet. Moreover, application of noble metals as gas sensitive films or doping in the systems creates a new problem with selectivity.

Accordingly, it has become very important to develop new gas sensors and sensing materials, which offer high sensitivity, selectivity, stability and reproducibility to certain gas as well as low cost of ownership and power consumption. The sensors should also allow for continuous monitoring of the gas concentration in their environment of application.

For this propose new transducer principles are necessary. One possible approach is to measure surface effects instead of bulk effects. A well known surface effect is work function change due to interactions between the surface and ambient gases. Work function measurements can be carried out with Kelvin Probe (BESOCKE DELTA PHI[1]), which however needs a mechanically vibrating electrode or Field Effect Transistor (FET).

[1] BESOCKE DELTA PHI GmbH, Tuchbleiche 8, D-52428 Jülich

The first Gas-FET has been introduced by I. Lundström in 1978 for hydrogen detection in ppm range [11]. A heated Pd gate was used as sensing element. Hydrogen modifies the work function of Pd and modulates in this way the channel conductance. Afterwards the Gas-FET was developed towards more versatile hybrid structures with an air gap from the FET channel. In 1996 the Hybrid Suspended Gate FET (HSGFET) and the Capacitive Controlled Gas FET (CC-FET) have been developed by J.S. Chung [12] and Z. Gergintschew et al [13] respectively in order to improve ability of the Gas-FET principle.

In this thesis, metal and metal oxides are used as gas sensitive films in the Floating Gate Field Effect Transistor (FG-FET) sensor system. The system has been developed from the HSGFET and CC-FET principle. It uses a Field Effect Transistor (FET) as transducer to measure work function change $\Delta\Phi$ of the gas sensitive films and convert it into an electrical signal. The advantages of the system are its sensitivities to work function changes due to physisorption, chemisorption and chemical reaction as well as ionosorption, which are occurring at gas sensitive films [14-18]. The gas sensitive films and the transducer can be separately developed. Additionally this system solves the problem of high power consumption [19].

The goal of the thesis is to develop and characterize new gas sensing materials and optimize sensing materials. This work concentrates on new sensing materials for hydrogen sulfide (H_2S), nitrogen dioxide (NO_2) and hydrogen (H_2) detection. For this propose, silver oxide (Ag_2O), zinc oxide (ZnO), tin oxide/copper (SnO_2/Cu), platinum/tin oxide (Pt/SnO_2) and titanium silicide/platinum ($TiSi_2$/Pt) were employed in the FG-FET to detect target gases. Different gas sensitive films were used in order to obtain gas sensors with high sensitivity, selectivity and reproducibility as well as well long-term stability.

Chapter 1

Fundamental theory

In this chapter, the fundamental theory and process of gas sensing based on work function change measurement will be discussed. The effects, which lead to gas sensing mechanism is emphasized on gas and metal oxides interface.

1.1 Work function

The work function is the minimum energy (usually measured in electron volts) which is needed to remove an electron from the Fermi energy level in a metal or semiconductor to a point at infinite distance away outside the surface. The work function is also generally defined as the difference between energy of an electron at Fermi energy level E_F and the local vacuum energy level E_l^{Vac} [20].

The local vacuum energy level E_l^{Vac} is defined as the energy of a resting electron at a certain place, so as if it would not be exposed to the solid potential. It is very important to understand the difference between the local (E_l^{Vac}) and the absolute vacuum potential E^{Vac}. E^{Vac} is defined as the reference energy of a resting electron, which is at infinite distance away outside the surface. In Fig. 1.1 the illustration of energetic conditions for an electron in a semiconductor can be seen.

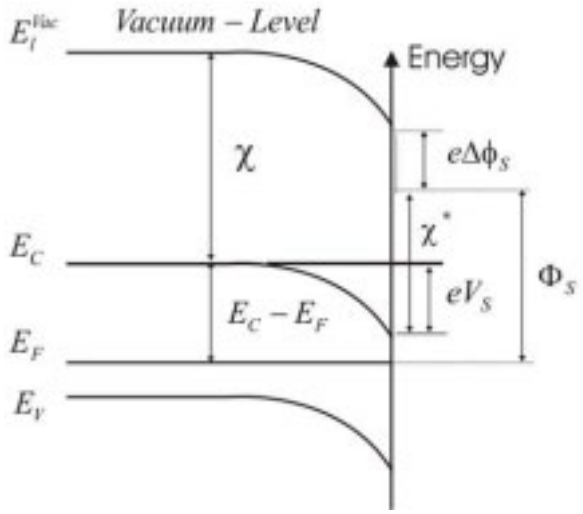

Figure 1.1. Energy band structure of a semiconductor surface.

The electron affinity is defined as energy difference between local vacuum level and conduction band level:

$$\chi = E_l^{Vac} - E_C \tag{1.1}$$

The surface dipoles can be present in this case, so that the effective electron affinity χ^* can be differentiate from the bulk affinity. These surface dipoles have atomic size and to become manifest as stage in the local vacuum energy level. Therefore the work function Φ_S can be wrote as follow

$$\Phi_S = \left(E_C - E_F\right)_{bulk} - eV_S + \left(\chi - e\Delta\phi_S\right) \tag{1.2}$$

$$= \left(E_C - E_F\right)_{bulk} - eV_S + \chi^*$$

with V_s is surface potential or barrier potential.

In metals, the charge carrier density is high enough, so that no space-charge zones can be formed. Therefore, the electron affinity χ and the surface dipole potential $\Delta\phi_S$ determine the work function Φ_S The Fermi energy level coincides with the conduction energy level $E_{C.}$

$$\Phi_S = \chi - e\Delta\phi_S = \chi^* \tag{1.3}$$

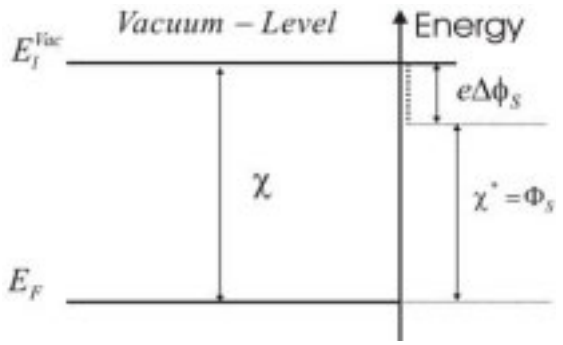

Figure 1.2. Energy band structure of a metal surface.

1.1.1 Adsorption on the surface

There are several ways that the gaseous ambient can change the work function. Some of these are unacceptable for the application of the gas sensors. Physical and chemical adsorption of gas molecules on the surface are famous processes, which can yield the work function change.

Adsorption is the attraction of molecules, atoms or ions of a substance to a solid surface. It is traditionally referred to as either physical or chemical. In discussions of adsorption a distinction has been made between physical adsorption and chemisorption. A set of criteria are often used which hopefully allows a separation to be made. Physical adsorption is considered to be reversible and non-activated while chemisorption is irreversible at one temperature and may also be non-activated and reversible at a high temperature. Furthermore the other difference is energy of bonding at the surface.

The interaction between gases and solid surfaces is a basic process, providing an understanding of the working principle of gas sensors. The adsorption of different gases depends on the surface structure composition and gas molecules. The adsorption can take place in different ways. In the following different types of adsorption are roughly described.

Physical adsorption

Physical adsorption is a weak adsorption in which the forces involved are intermolecular forces (van der Waals forces) of the same kind as those responsible for the imperfection of real gases and the condensation vapors, and which do not involve a significant change in the electronic orbital patterns of the species involved.

The Lennard-Jones potential-energy diagram, which is shown in Fig. 1.3, has already been used to discuss the adsorption at solid surfaces [21]. Here the energy of the system is plotted against a coordinate related closely to the distance of the adsorbate from the surface. Curve A shows the energy of the adsorbate molecule as a function of the distance. It can be seen that the lowest energy occurs if the molecule has reached a distance d_P from the surface. In this condition the physical adsorption occurred with ΔE_P, whereas curve B confirms the system energy if two atoms are close to the surface. The strong chemisorption occurred at a distance d_C from the surface with ΔE_C whereas ΔE_∞ is the potential energy which is needed to separate the molecule (dissociation of molecule).

ΔE_A is the threshold energy or the activation energy that must be overcome in order to a chemical reaction to occur. Activation energy may otherwise be denoted as the minimum energy necessary for a specific chemical reaction to occur. In generally the activation energy nearly always appears at the adsorption process. Exception is only in van der Waals adsorption.

Chemisorption

Chemisorption (or chemical adsorption) is adsorption in which the forces involved are valence forces of the same kind as those occurring in the formation of chemical compounds. The chemical nature of the adsorptive(s) may be altered by surface dissociation or reaction in such a way that on desorption the original species cannot be recovered. In this sense chemisorption may not be reversible and leads to radical changing in the electronic structure of the solid state surface and particles.

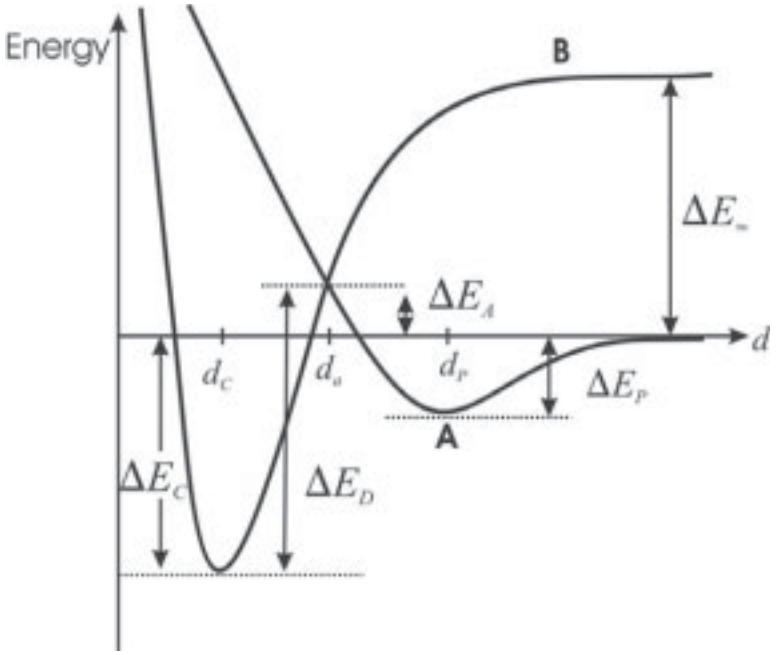

Figure 1.3. Lennard-Jones potential energy of physical adsorption and chemisorption. A). Physical adsorption of molecule. B). Chemisorption of molecule.

The chemisorption may be reversible if the molecule receives again a minimal energy ΔE_C+ΔE_A, which is called with desorption energy (ΔE_D), as depicted in Fig. 1.3. ΔE_C and ΔE_A are not constant. The both values depend strongly on surface coverage θ (interactions). Mostly ΔE_C decreases and ΔE_A increases with increasing θ [22].

Ionosorption

Ionosorption is a special type of chemisorption. By ionosorption atoms or molecules are ionized through capturing of an electron from the bulk (conduction band) during the adsorption process. Therefore ionosorption can be seen as delocalized chemisorption. As a consequence of the charge transfers between molecules and surface, the chemical reactivity of the molecules, as well as their electronic and geometrical structures, are strongly influenced.

1.1.2 Desorption from the surface

An adsorbed species present on a surface at low temperatures may remain almost indefinitely in that state. However as the temperature of the substrate is increased, there will be reached a point at which the thermal energy of the adsorbed species is high enough that one of several things may occur:

1. A molecular species may decompose to yield either gas phase products or other surface species.
2. An atomic adsorbate may react with the substrate to yield a specific surface compound, or diffuse into the bulk of the underlying solid.
3. The species may desorb from the surface and return into the gas phase.

The last of these options is the desorption process. In the absence of decomposition the desorbing species will generally be the same as that originally adsorbed but this is not necessarily always the case.
The rate constant for the desorption process may be expressed in an Arrhenius form [23]

$$k = k_0 \cdot \exp\left(\frac{-E_D}{R \cdot T}\right) \tag{1.4}$$

where k_0 is the frequency factor and E_D is the activation energy for desorption measured in KJ mol^{-1}. The frequency factors are usually calculated on the basis of the theory of absolute reaction rate.

Surface residence times

One property of an adsorbed molecule that is intimately related to the desorption kinetics is the *surface residence time*. This is the average time that a molecule will spend on the surface under given conditions (in particular, for a specified surface temperature) before it desorbs into the gas phase. The surface residence time is expressed by Frenkel equation [24]

$$\tau = \tau_0 \cdot exp\left(\frac{E_D}{k \cdot T}\right) \tag{1.5}$$

where τ_0^{-1} is the order of the vibration frequency of the adsorbate-surface bond and is frequently taken to be about 10^{-13} s.

1.2 Metal oxide

To understand the gas sensing with metal oxide as gas sensitive film, it is necessary to study oxygen adsorption on surface of the metal oxide because detection of reducing gases is depended on the existing oxygen ions at the surface. Furthermore, an additive metallic catalyst on the surface is important to be known because sensitivity of the metal oxide to gaseous ambient can be improved by it.

1.2.1 Energy band structure of metal oxide

Metal oxide is naturally a semiconductor. Electronic effect of the adsorption of different gases on the metal oxide surfaces can be described by the band model. There are two cases. First case is an accumulation layer that arises if a strong reducing agent injects electrons into an n-type semiconductor or a strong oxidizing agent injects holes (extracts valence electrons) into a p-type semiconductor. The second case is an inversion layer that occurs if a very strong oxidizing agent (acceptor surface state) appears on an n-type semiconductor or a very strong reducing agent (donor surface state) is provided on a p-type semiconductor [25].

In the following, the energy band structure of the semiconductor and its changes due to adsorption processes will be described. For simplification, influence of the adsorption processes on the energy band structure of n-type semiconductor will be shown on the basis of oxygen molecule adsorption.

Oxygen adsorption at surface of the n-type semiconductor generates an acceptor surface state because the adsorbed oxygen captures electron from the bulk conduction band. This causes a broadening of the depletion layer in the semiconductor near the surface. Thus, the energy band near the

surface and the work function increase. The broadness of this band bending can be calculated using the Schottky model. However, it should be note that the oxygen adsorption is limited because of the band bending. The chemical adsorption cannot take place anymore, if the Fermi level of the bulk is equal to the energy of the highest occupied surface states.

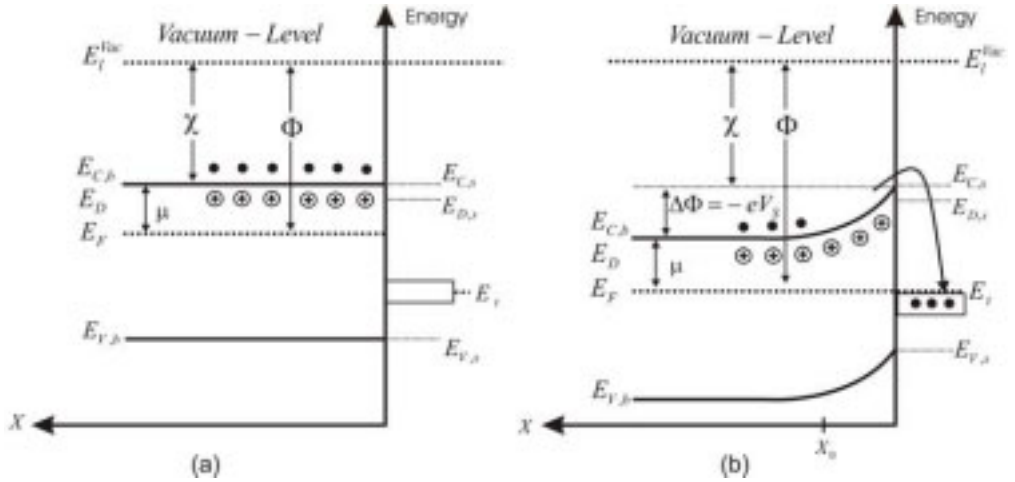

Figure 1.4. Energy band bending structure of the n-type semiconductor before (a) and after (b) the oxygen molecule adsorption.

The potential Φ must of course obey the basic Poison equation in one dimension

$$\frac{d^2\Phi}{dx^2} = -\frac{\rho}{\varepsilon \cdot \varepsilon_0} \tag{1.6}$$

where

ρ : The charge density C/m^3
ε : The dielectric constant
ε_0 : The permittivity of free space

In general the charge in the space charge region by this model is $\rho = e \cdot (N_D - N_A)$ for $x < x_0$ and $\rho = 0$ for $x > x_0$. Substituting into the eq. (1.6) and double integrating yields

$$\Phi_b - \Phi_x = \frac{e \cdot (N_D - N_A)(x - x_0)^2}{2 \cdot \varepsilon \cdot \varepsilon_0} \tag{1.7}$$

$$V_S = \Phi_b - \Phi_x \tag{1.8}$$

or

$$V_S = \frac{e \cdot (N_D - N_A)(x - x_0)^2}{2 \cdot \varepsilon \cdot \varepsilon_0} \tag{1.9}$$

where

e : Elementary charge
N_A : Acceptor density
N_D : Donor density
Φ_b : Potential in bulk
Φ_x : Potential in the edge layer

From the equation can be obtained the Schottky barrier at $x = 0$

$$V_S = \frac{e \cdot (N_D - N_A) \cdot x_0^{\,2}}{2 \cdot \varepsilon \cdot \varepsilon_0} \tag{1.10}$$

Another form of this important relation is obtained by recognizing that the number of charges per unit area on the surface (N_s) arising from electron exhausted at a distance $x = x_0$ from the surface is given by

$$N_s = -(N_D - N_A) \cdot x_0 \tag{1.11}$$

so that the Schottky barrier relation at eq. (1.10) can be expressed in terms of N_s

$$V_S = \frac{e \cdot N_s^2}{2 \cdot \varepsilon \cdot \varepsilon_0 \cdot (N_D - N_A)} \tag{1.12}$$

The Schottky barrier V_S describes a potential between the surface and the inside of the semiconductors which electrons must overcome during the free charge exchange. The charge density in the conduction band (in the case of an n-type semiconductor) depends on the Fermi function that is approximated by a Boltzmann distribution. In this approximation the height of the potential barrier is considered into it. So for the n-type semiconductor is applied in the case of fully ionized donors: [25, 26]

$$n_s = N_c \cdot \exp\left(\frac{-(e \cdot V_S + E_C - E_F)}{k \cdot T}\right) = n_b \cdot \exp\left(\frac{-e \cdot V_S}{k \cdot T}\right) \tag{1.13}$$

n_s : The electrons density in the conduction band at the surface (per unit volume)

n_b : Bulk electrons density in the conduction band
N_c : Effective density of states in the conduction band
T : Temperature
k : Boltzmann constant

The electrons density in the conduction band at the surface can be expressed if V_S in eq. (1.13) is substituted with V_S from eq. (1.12)

$$n_s = n_b \cdot exp\left(\frac{-e^2 \cdot N_s^2}{2 \cdot \varepsilon \cdot \varepsilon_0 \cdot k \cdot T \cdot \left(N_D - N_A\right)} \right) \tag{1.14}$$

1.2.2 Oxygen adsorption and desorption on metal oxide

A well understood chemisorption is oxygen chemisorption on tin dioxide [27, 28]. Therefore tin dioxide is used as model for adsorption process at many other semi-conducting metal oxides. The species found on the metal oxide semiconductor surfaces of adsorbed O_2 are manifold and depend on temperature [29]. Oxygen species can be adsorbed in several forms: in molecular O_2^- and atomic O^-, O^{-2}. Adsorbed oxygen species transform at the surface according to the general scheme:

$$O_{2\,gas} \leftrightarrow O_{2\,ads} \tag{1.15}$$

$$O_{2\,ads} + e^- \leftrightarrow O_2^- \tag{1.16}$$

$$O_2^- + e^- \leftrightarrow 2\,O^- \tag{1.17}$$

$$O^- + e^- \leftrightarrow O^{-2} \tag{1.18}$$

At room temperature O_2 form is physically adsorbed, being the coverage of the species at the surface restricted by space charge effects (Weisz limit) [30]. In this process the coverage with negatively charged species is limited to 10^{12}-10^{13} molecules cm^{-2}. With increasing temperature $O_{2\,ads}$ and O_2^- forms convert to O_2^- and O^- forms with taking one electron from the bulk, respectively as shown in eq. (1.16) and (1.17). The study of Electron Paramagnetic Resonance Spectroscopy (EPR) indicated that the O^- form is more reactive than other [31]. This specie is a dominant contributor to the

negatively charged surface state referred to eq. (1.12), providing the surface charge $e.N_s$.

Fig. 1.5 shows adsorbed oxygen species at polycrystalline of n-type semiconductor. The potential barrier appears at contact between the grains and affect on the depletion region near the surface leading to conductivity and work function change of the semiconductor. The conductivity G can be written as [32]

$$G = G_0 \cdot \exp\left(\frac{-e \cdot V_S}{k \cdot T}\right) \tag{1.19}$$

where G_0 contains of all other portions contributing to the conductivity.

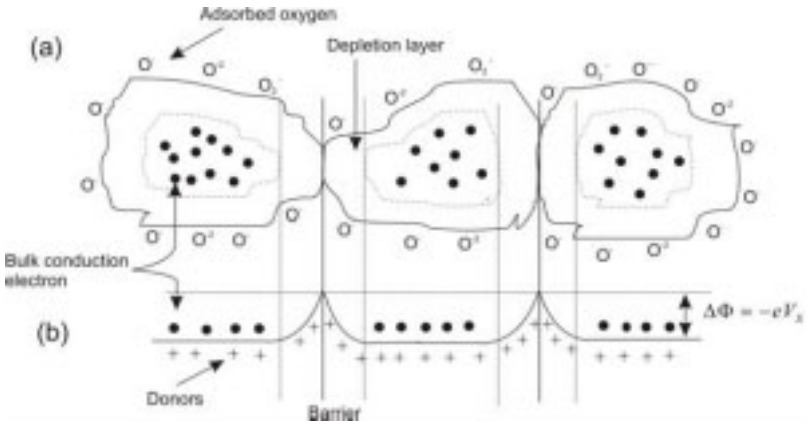

Figure 1.5. Model of the polycrystalline n-type semiconductor with the adsorbed oxygen species at the surface [33]. (a). Physical model. (b). Energy band structure model.

According to Yamazoe et al. [34], oxygen desorbs with a maximum temperature of desorption as physisorbed O_2 at 80°C, as O_2^- at 150°C, O^- or O^{-2} at 520°C.

1.2.3 Reaction on surface of metal oxide

Adsorbed oxygen species influence on the surface state. The surface becomes acceptor surface state. If the surface is introduced to reducing gases R such as H_2, CH_4, C_2H_6 and CO, the adsorbed oxygen will interact with them. The general reaction between adsorbed oxygen and reducing gas is as follow [35]

$$R + O^- \rightarrow RO + e^- \quad (1.20)$$

The dynamic equilibrium will be established between the reaction of eq. (1.17) and eq. (1.20) if a reducing gas is exposed in the atmosphere. Oxygen is adsorbed at the semiconductor surface and is removed by reaction with a reducing gas.

1.2.4 Catalysis

Catalysis is defined as the initiation of chemical reaction or a change in its rate by the action of substances called catalysts. The catalysts take part in the reaction but do not appear in the final product. The catalyst bears no stoichiometric relation to the reaction yield. In positive catalysis the reaction rate is accelerated, whereas in negative catalysis it is slowed. The term catalysis usually denotes the former. Negative catalysts are called anticatalysts or inhibitors, though an inhibitor is sometimes defined as a substance which stops chain reaction. An increase in the rate of reaction under the influence of a final or intermediate product is called autocatalysis.

In order to improve the sensing properties catalysts are often added. These additives can affect the sensing behavior of a gas sensor significantly. They can result in faster response and recovery times, in an enhancement of sensitivity or selectivity as well as in a better reproducibility.

The effect of catalyst on semiconductor surface is explained by two alternative models. Both models assume that the catalyst particles are located at the surface of much bigger grains of metal oxide and are homogenously distributed on the surface.

First model is spill-over or catalytic effect. In this case catalyst particles on the surface are able to activate certain gas molecules, e.g. dissociation of oxygen or hydrogen. The spill-over is a mechanism where the oxidation of the reducing agents on the semiconductor can be accelerated by the presence of dispersed metallic catalyst. Well known examples for the spill-over are the spill-over of hydrogen and oxygen from metal catalysts onto the semiconductor support [36]. The spill-over occurs due to the presence of Pt.

This phenomenon can be explained as follow: The bonding energy of Pt atoms to hydrogen atoms is not so different from bonding energy of one hydrogen atom to another. Therefore little energy is needed to dissociate hydrogen molecules. This argument is similar for dissociation of oxygen molecule. As a result the catalyst reduces the energy normally needed for dissociation. Thus the spill-over onto the semiconductor support is possible after breaking the weak bonds between hydrogen or oxygen and Pt, respectively. Fig. 1.6 illustrates the phenomenon that the catalyst dissociates O_2 into O atoms and allows them to spill-over onto the semiconductor, so active oxidation reaction on its surface occurs. As a result electrical properties of the semiconductor change.

Second model is Fermi energy control: By this effect the sensor signal is determined mainly by the electronic contact of the semiconductor with the catalyst. Oxygen species at the surface of the catalyst trap electrons from the semiconductor. Since the density of electrons in the bulk has changed by this process, a depletion layer is created and band bending occurs. The catalyst particles become oxidized in the ambient gas atmosphere.

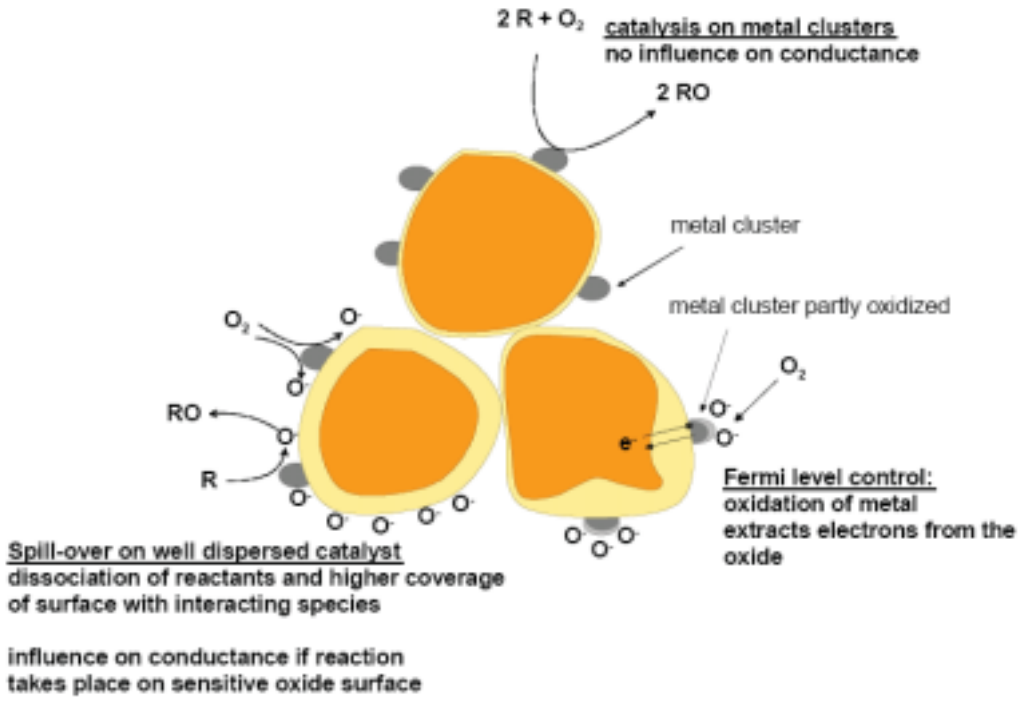

Figure 1.6. Different effects of catalyst. Spill-over effect (left bottom) and its reaction with reducing gases, Fermi level control (right bottom) [26, 29].

1.2.5 Electronic contact of metal oxide with catalyst

The contact of the metal oxide semiconductor with catalyst creates a barrier that is fully characterized by the electron affinity of the semiconductor, the work function of the metal and the density of surface states of the semiconductor that are located inside the energy band gap. All of these three contributions generate a Schottky barrier through the formation of a depletion region in the semiconductor surface in contact with catalyst. Fig. 1.7 illustrates energy band structure of metal (catalyst) and n-type semiconductor contact [20].

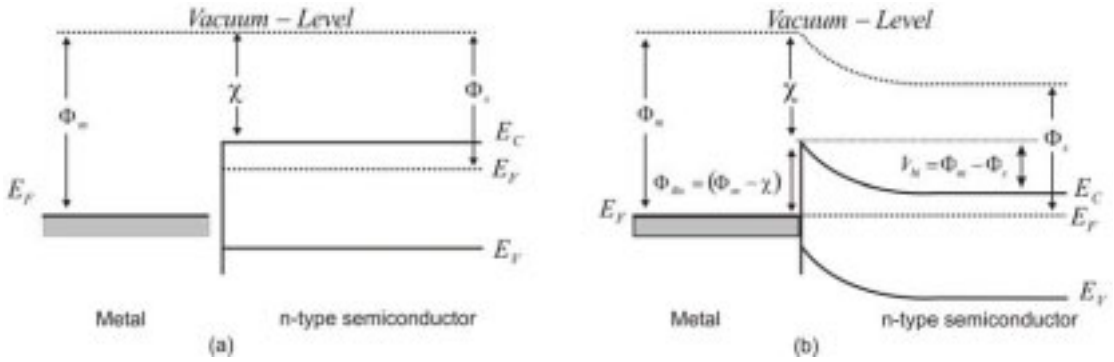

Figure 1.7. (a) Energy band structure of an isolated metal adjacent to an isolated n-type semiconductor under non-equilibrium condition. (b) Energy band structure of metal-semiconductor contact in thermal equilibrium.

When the metal makes intimate contact with semiconductor, the Fermi level in the two materials must be equal at thermal equilibrium and the vacuum level must be continuous. These two requirements determine a unique energy band structure for the ideal metal-semiconductor contact as shown in Fig. 1.7b. For this ideal case the barrier height Φ_{Bn} is simply the difference between the metal work function and the electron affinity χ of the semiconductor.

$$\Phi_{Bn} = \left(\Phi_m - \chi\right) \tag{1.21}$$

and the built-in potential V_{bi} for the n-type semiconductor is give

$$V_{bi} = \Phi_{Bn} - V_n \tag{1.22}$$

where Φ_{Bn} is the barrier height of the real metal-semiconductor contact and V_n is the potential difference between the Fermi level and $E_{C.}$

1.3 Work function change measurement

To determine an absolute value of the work function is very difficult. The photoemission spectroscopy under ultra high vacuum condition, thermal emission and field emission were employed to measure it [37]. In the gas sensor, work function changes $\Delta\Phi$ which occur as a result of adsorption or chemisorption on the surface are of greater interest than the absolute value Φ.

1.3.1 Kelvin Probe

Kelvin Probe measurements are one of the methods to determine work function change of the material surface with high precision due to the adsorption of gases. This method was firstly introduced by William Lord Kelvin of Largs in (1824-1907) [38]. Schematic of the Kelvin Probe can be seen in Fig 1.8.

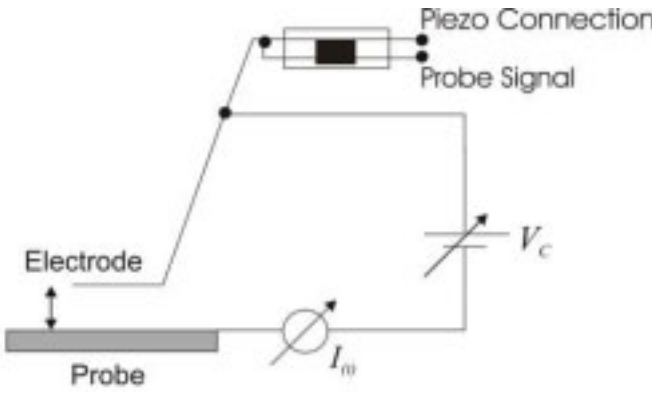

Figure 1.8. Schematic of the Kelvin Probe.

Kelvin Probe measurements are essentially based on the detection of a current induced by the change of the capacitance value of a capacitor. An electrode, which is attached parallel to the surface of the sample, forms a capacitor. This electrode is mechanically moved at a given frequency. The oscillation of the electrode causes a change of the capacity, so that an alternating current signal $I_{(t)}$ is produced, whose amplitude is proportional to

the contact potential difference V_{CPD} or work function change ($\Delta\Phi$) between sample and electrode.

$$I_{(t)} = \dot{Q} = \dot{C} \cdot V \tag{1.23}$$

where V is the potential difference, which is generated between the two electrode plates.
The alternating current can be adjusted to null by the balancing voltage V_C which is arranged to against the contact potential difference.

$$I_{(t)} = \dot{Q} = \dot{C} \cdot \left(V - V_C\right) = 0 \tag{1.24}$$

The gas adsorption at the surface of the sensitive layer can generate the work function change ($\Delta\Phi$) leading to the potential change of the electrode plates V. Therefore the electronics of the Kelvin Probe must readjust V_C in order to regulate $I_{(t)}$=0, in accordance with:

$$I_{(t)} = \dot{Q} = \dot{C} \cdot \left\{\left(V + \Delta\Phi\right) - \left(V_C + \Delta V_C\right)\right\} = 0 \tag{1.25}$$

It can be seen that the change of the balancing voltage ΔV_C is the same as in the value of work function change which is generated by the gas adsorption.

$$\Delta V_C = \Delta\Phi \tag{1.26}$$

Although the Kelvin Probe does not measure the absolute value of the work function, this method has a special advantage, because changes of the work function can be pursued during the adsorption or desorption. Furthermore the integration of new materials in this method is very simple in order to first observation. Unfortunately the measurement has the disadvantage of extreme sensitivity to other mechanical vibration.

Sensitivity of germanium to ethanol in Kelvin Probe is described in Fig. 1.9. It can be observed that work function change of the germanium film decrease with increasing ethanol concentrations. The best result is shown at an operating temperature of 130°C.

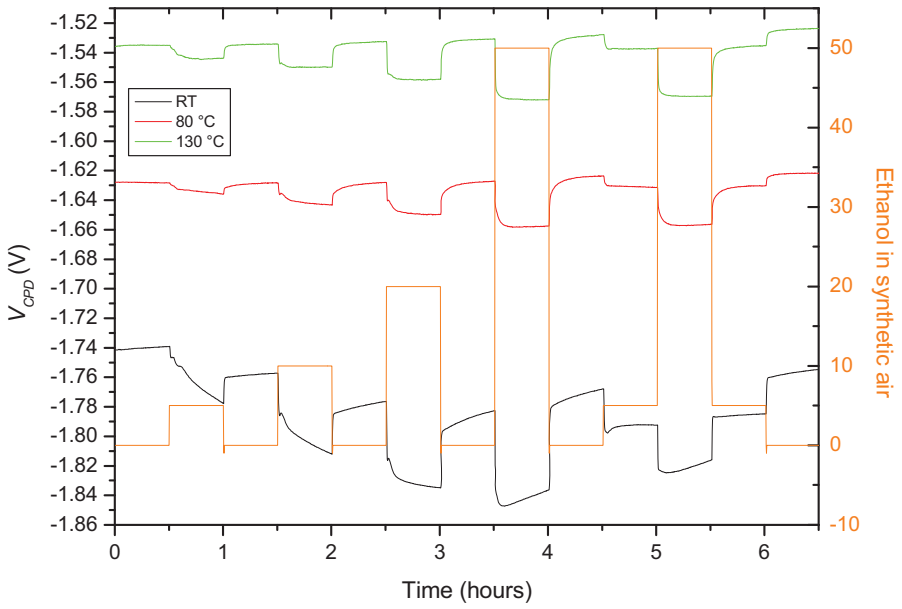

Figure 1.9. Sensitivity of germanium to ethanol in the Kelvin Probe at room temperature, 80°C and 130°C.

1.3.2 Floating Gate Field Effect Transistor (FG-FET)

A versatile design with respect to deposition methods of chemically sensitive films is the FG-FET, which was developed from the HSGFET and CC-FET principle. It combines the hybrid design with the large amplification of conventional MOSFETs (Metal Oxide Semiconductor FET). The FG-FET was firstly introduced by M. Burgmair et al at UniBw Munich (*Universität der Bundeswehr München*). Fig 1.10 shows the new design of the FG-FET with a gas sensitive film mounted silicon gate [39, 40]. The sensor consists of two parts. The lower part consists of a conventional p-channel MOSFET and the upper part is p-doped silicon with a gas sensitive film as top electrode or gate. The top electrode and a capacitance-well (n) together form a capacitor. The floating gate is electrically pinned between them by means of a capacitive potential divider. Furthermore, it acts as a gate electrode of the MOSFET. The dividing sensor is aimed to simplicity develop the gas sensitive film and transducer.

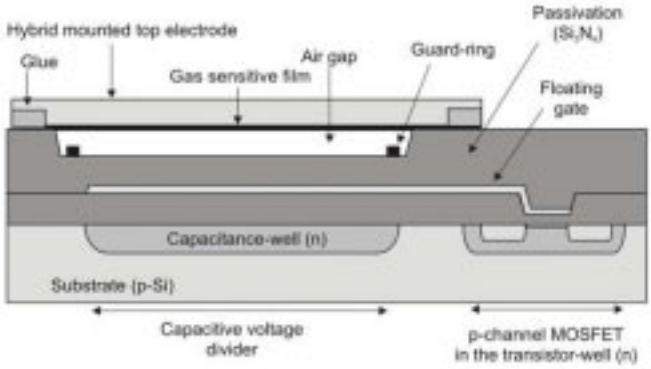

Figure 1.10. Schematic of the FG-FET.

The gas sensitive film is a part of the capacitive voltage divider. Physisorption or chemisorption at the film on the top electrode or gate can generate a reversible potential difference $\Delta\Phi$. The potential difference causes source-drain voltage changes of a conventional p-channel MOSFET via a capacitive voltage divider. The equivalent circuit diagram of the sensor is shown in Fig. 1.11.

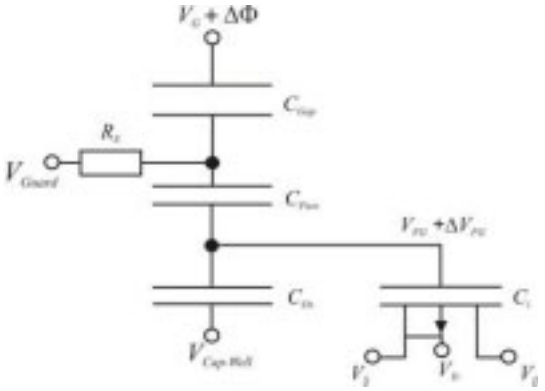

Figure 1.11. Equivalent electrical circuit of the FG-FET.

If the surface resistance (R_s) is neglected, then drain-source current I_{DS} can be written as

$$I_{DS} = \mu \frac{W}{L} C_i \left(\frac{C_1 V_G + C_{Ox} V_{Cap}}{C_1 + C_{Ox}} - V_T \right) V_{DS} \tag{1.27}$$

V_{FG} : Floating Gate Voltage, W : Channel width, L : Channel length, V_{DS} : Source-Drain Voltage, μ : Charge carries-mobility, V_T : Voltage of MOSFETs, C_i : Capacitance between floating gate and channel.

with $$\Delta V_{FG} = \frac{C_1}{C_1 + C_{Ox}} \Delta\Phi \tag{1.28}$$

and $$\frac{1}{C_1} = \frac{1}{C_{Pass}} + \frac{1}{C_{Gap}} \tag{1.29}$$

Chapter 2

Preparation and characterization of metal oxides

The hybrid gates have been made out of p-doped silicon. For the deposition of the metal oxides on the gates intermediate layers are needed to assure good adhesion as well as base line stability. They consist of titanium (Ti) and platinum (Pt) [14, 41], which were serially deposited by DC sputtering for 110.6 nm and 249.4 nm thicknesses, respectively. The deposition of Ti was carried out at P_0 = 6x10^{-5} mbar and P_{argon} = 8x10^{-3} mbar for 5 min whereas Pt deposition was done at P_0 = 6x10^{-5} mbar and P_{argon} = 8x10^{-3} mbar for 10 min. SEM image of the gates cross section is shown in Fig. 2.1.

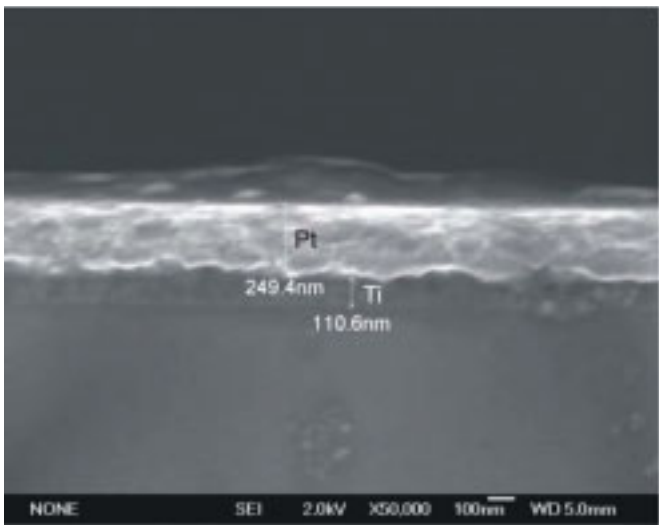

Figure 2.1. SEM image of a gate cross section.

Afterwards, metal oxides are grown on them by thermal evaporation in a vacuum chamber. In order to obtain interaction between metals and oxygen, oxygen is injected into the vacuum chamber through a micro leak. The Leybold evaporation apparatus is shown in Fig. 2.2.

Figure 2.2. The Leybold evaporation apparatus with oxygen source.

2.1 Silver oxide (Ag_2O)

Pure silver (Ag) was thermally evaporated on the gate at a pressure of $2x10^{-2}$ mbar under oxygen atmosphere. The evaporation rate was kept between 0.5-0.6 nm/s for a total film thickness of 50 nm. Thickness of Ag_2O film was measured by using a quartz micro balance frequency of 6 MHz.

The XPS characterization method was employed to study the surface of the resulting films. The method is from the group of the electron-spectroscopic procedures. The special strength of the method is appropriate for the possibility to determine the elementary composition also the chemical bond, in which an atom within the analyzed sample range is presented. Therefore it is used frequently for the proof of chemical compounds and/or the bond kind of a certain element (e.g. catalyst surfaces, clarifying of detention problems, contamination of surfaces, etc.).

The XPS method is based on the photoelectric effect: the surface is irradiated with photons (in this case X-rays), which are then absorbed by the atoms of the sample. Thereby the energy $h\nu$ of the photon is transferred to an electron and there is the emission of a photoelectron (see Figure 2.3).

The kinetic energy (E_k) of the emitted electron is measured in most cases by means of a hemispherical analyzer. The obtained value allows calculating the binding energy, E_b, of the electron [42]:

$$E_b = h\nu - \Phi - E_k \tag{2.1}$$

where $h\nu$ is the energy of the primary X-ray source and Φ the work function of the spectrometer (obtained by calibration). The binding energy is conventionally referred to the Fermi level.

A typical XPS spectrum normally shows the number of detected electrons plotted against their binding energy. The latter has a characteristic value for each different orbital of each atom and therefore it is possible to assign each peak to a certain orbital of a certain element, obtaining in this way the elemental composition of the surface. With an information depth of 5-10 nm (depending on the investigated material) this technique is especially suitable for the analysis of thin layers on sample surfaces.

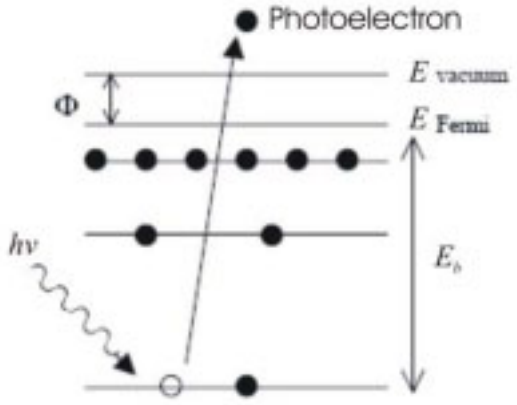

Figure 2.3. Emission of a photoelectron.

Chemical compositions of the films are confirmed in Fig. 2.4. Core level peaks of silver and oxygen dominate the XPS spectrum with concentrations 65% and 30%, respectively. Accordingly, stoichiometry of Ag_2O films can be almost achieved with this simple preparation technique.

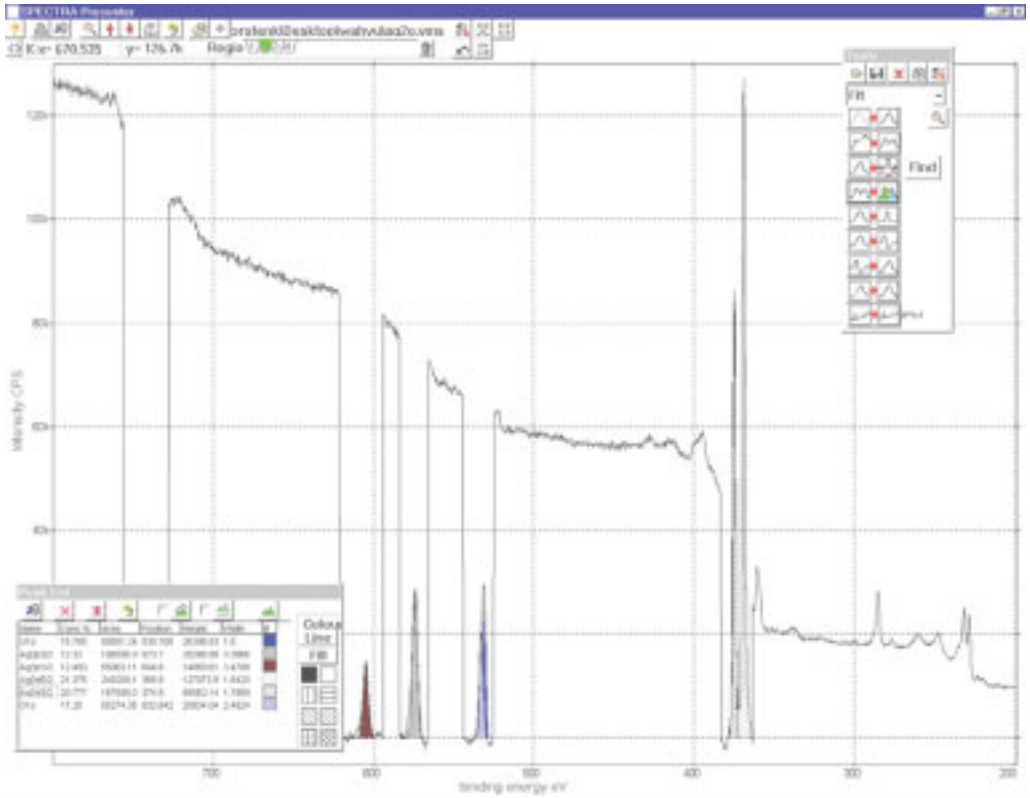

Figure 2.4. Typical XPS survey spectrum of Ag_2O surface.

Gas sensitivity of silver was characterized in a Kelvin Probe with the gold as a reference electrode. Twelve gas species were serially exposed to the silver film at room temperature, 80°C and 130°C. Changes of the contact potential difference (CPD) between the gold and the film in the Kelvin Probe prove that the adsorption or chemisorption is occurring at the surface of the film.

For the measurement in the Kelvin Probe related to the experimental FG-FET structure with gas sensitive film was driven the following attempt profile: After stabilization of the operating temperature of 80°C and 130°C, the measurement chambers are rinsed for half hours with 200 ml/min synthetic air in order to stabilize the Kelvin Probe. Twelve different gases are serially exposed to the film for total time of 16.5 hours. Each gas is exposed for 30 min. Between exposing the chambers are rinsed again with the synthetic air for one hour in order to prevent influences of the previous gases.

The result shows that the film reacts to H_2S, NH_3, NO_2 and Cl_2 concentrations as which can be seen in Fig. 2.5. The reversible V_{CPD} signal

change can be observed only when the film is exposed to H_2S. Accordingly, the film is applied as a H_2S sensitive film in the experimental FG-FET structure. Furthermore interaction between the Ag or Ag_2O and H_2S was characterized by using XPS [43]. The results show that at room temperature until 150°C, silver or silver oxide reacts with hydrogen sulfide to silver sulfide. Silver oxide decomposes to silver and oxygen at temperatures above 200°C.

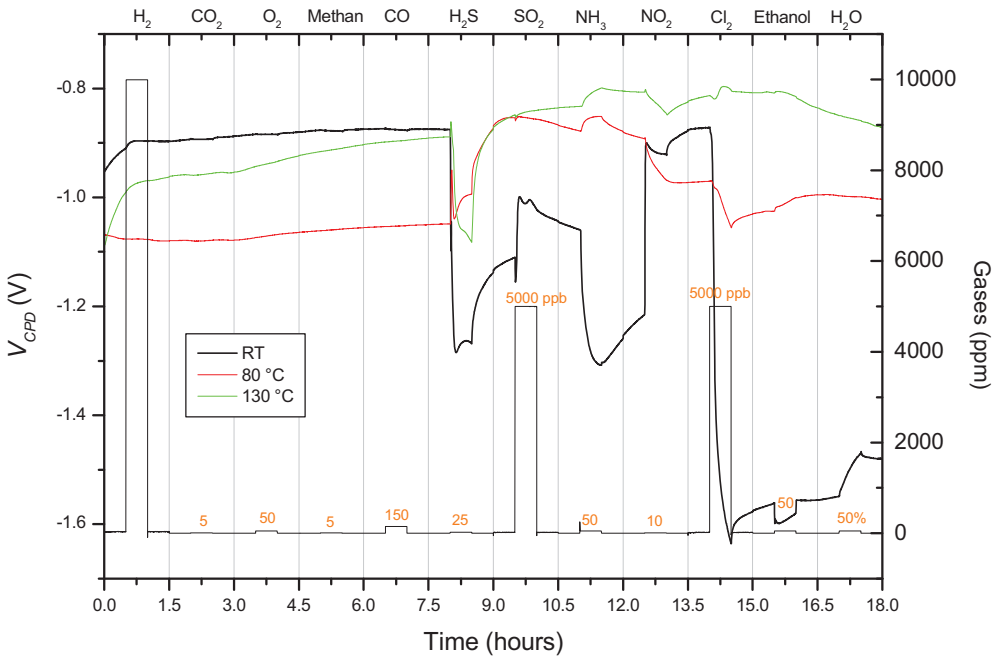

Figure 2.5. Screening test of the Ag film in the Kelvin Probe at different temperature and under dry conditions.

2.2 Zinc Oxide (ZnO)

With the same method, pure zinc (Zn) was thermally evaporated at a pressure of $2x10^{-2}$ mbar under oxygen atmosphere. The evaporation rate was kept between 0.5-1 nm/s for a total film thickness of 200 nm.

SEM was employed to study the surface morphology of the obtained films. SEM image of the film is shown in Fig. 2.6. It can be seen that surface of the obtained films is very rough but the surface roughness is smaller than air gap of ~1.6 μm. The roughness has to below the air gap in order to avoid contact with reference electrode.

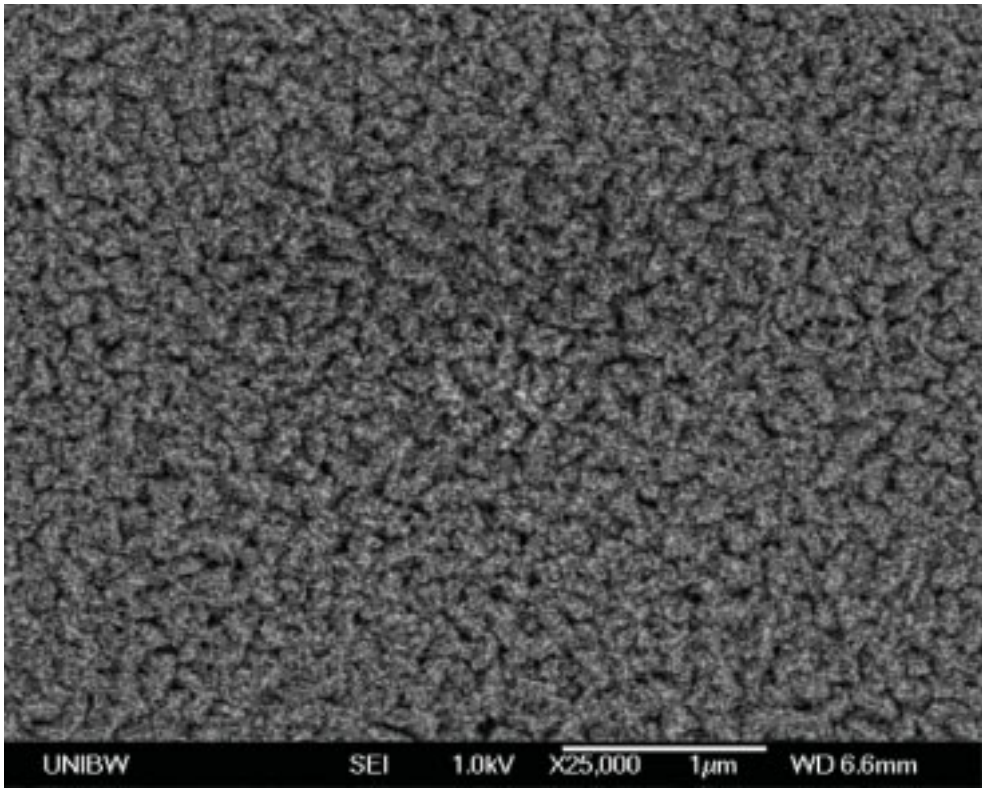

Figure 2.6. SEM image of the ZnO surface.

The surface was also characterized by using EDX to determine its qualitative composition. This technique is used in conjunction with the SEM method. An electron beam strikes the surface of a conducting sample. This causes X-rays to be emitted from the point the material. The energy of the emitted X-rays depends on the material under examination.

The characterization was done at 5 keV primary electron energy, 6 nA beam current and (4 μm x 3 μm) area. These parameters have been used to make sure that the characterization is only at the surface. At these parameters, electron beam strikes the surface of a conducting sample up to a depth of 50 nm.

Fig. 2.7 shows that the EDX spectrum is dominated by three energy peaks: $Zn-L\alpha_{1,2}$ at 1.011 eV, $Zn-L1$ at 884 eV and $O-K\alpha_{1,2}$ at 524 eV. This result makes sure that the interaction is only ZnO surface and NO_2.

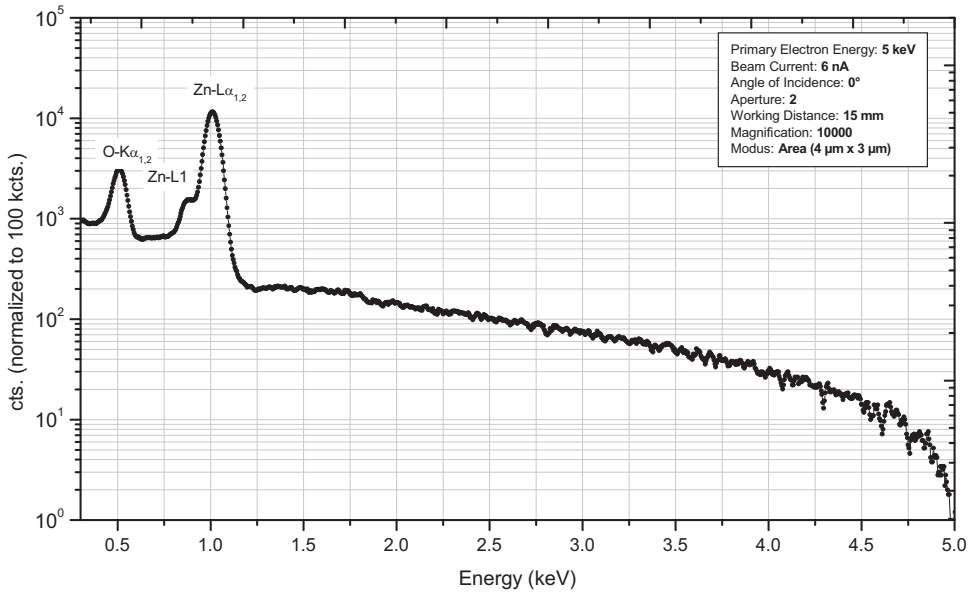

Figure 2.7. EDX characterization of the ZnO surface.

The interaction between ZnO surface and NO_2 was directly analyzed by using the XPS method before and after NO_2 exposure. First, the surface was characterized by using the XPS to observe initial of the surface before NO_2 exposure. Then the surface was induced to 5 ppm NO_2 in the sensor chamber at FET measurement station. The inducing was carried out at room temperature under dry condition for 15 min. This is expected that the surface residence time of NO_2 is long. Afterwards the surface was characterized again by using the XPS to obtain the chemical compound after NO_2 exposure. In order to avoid interaction between the surface and air as well as evaporation of adsorbed gas, the characterization was immediately carried out after NO_2 exposure. The corresponding XPS spectra of the surface are depicted in Fig. 2.8 and 2.9.

Fig. 2.8 shows the surface before NO_2 exposure. Two peaks of oxygen (O1s line) are observed. Peak A appears at a binding energy of 533.7 eV with concentration of 22% and peak B appears at 531.6 eV with concentration of 77%. Peak A corresponds to O^- ions adsorbed at the ZnO surface. Peak B is related to the O-peak of ZnO.

Fig. 2.9 represents the condition of the surface after exposing it to NO_2 at room temperature under dry conditions. Accordingly the concentration of peak A increases significantly up to 47%, whereas the concentration of peak B decrease down to 53%. One possible explanation is that NO_2 adsorption at the surface generates surface acceptor states because NO_2 molecules capture electrons from the bulk conduction band of the ZnO film [25]. With further adsorption the surface becomes more negatively charged, which corresponds to increasing concentration of peak A. This causes a broadening of the depletion layer near the surface and thus the work function changes.

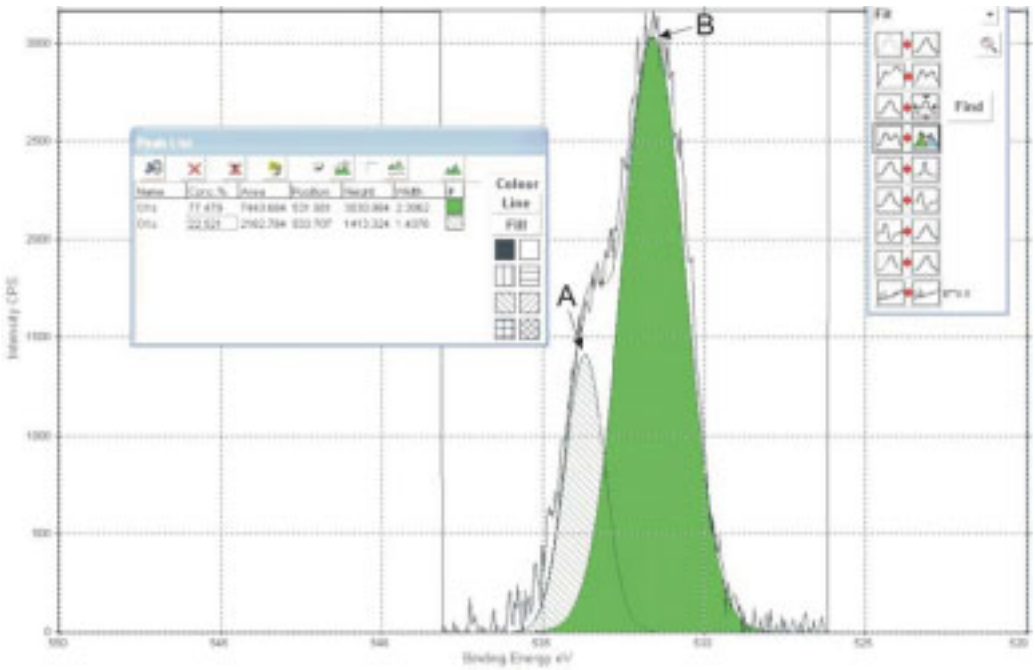

Figure 2.8. XPS spectra for the O1s region of ZnO before NO_2 gas exposure. Peak A: O^- ions-peak adsorbed on the ZnO surface. Peak B: O-peak of ZnO.

The detection of NO_2 can be related to the following reaction [44]

$$NO_2 + e^- \Leftrightarrow NO + O^-_{ads} \qquad (2.2)$$

The consumed electrons in this reaction are captured from the bulk conduction band of the ZnO semiconductor thus the work function of ZnO raises.

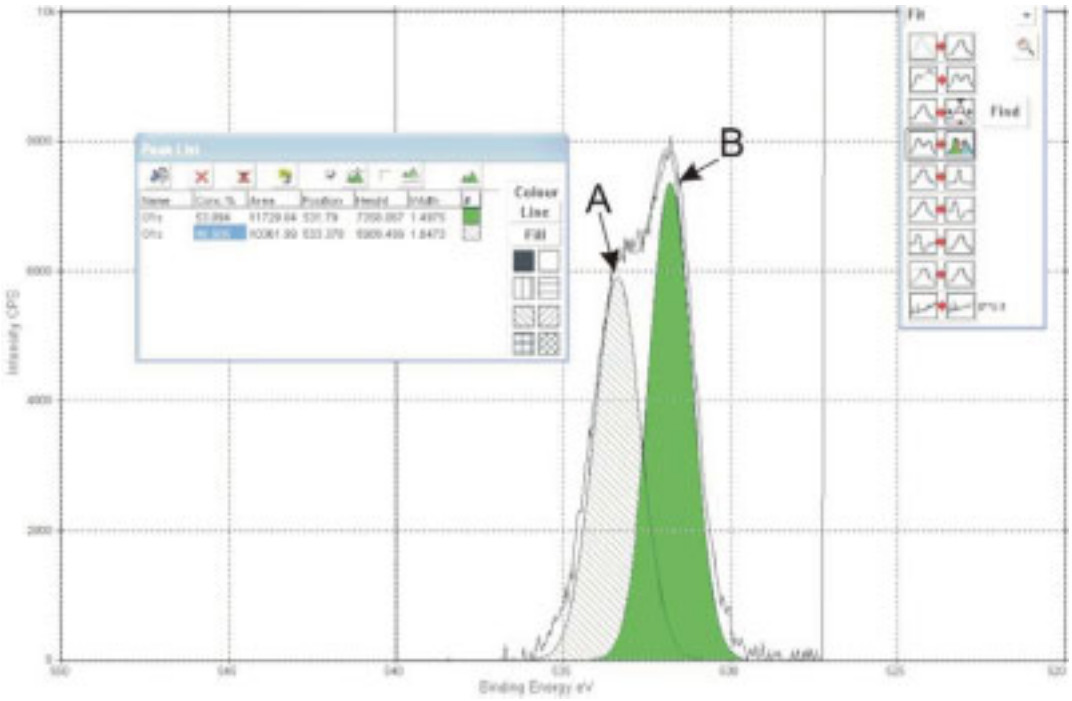

Figure 2.9. XPS spectra for the O1s region of ZnO after exposing it to 5 ppm NO_2 gas at room temperature.

2.3 Tin Oxide/Copper (SnO_2/Cu)

In order to obtain porous SnO_2/Cu films, pure tin was thermally evaporated on the gates and wafers under oxygen atmosphere at total pressure of $2x10^{-2}$ mbar. Thickness of the obtained films is about of 50 nm. Then pure Cu was thermally evaporated on them at $2x10^{-4}$ mbar for 25 s with the evaporation rate of 0.5-0.6 nm/s.

Surface of the obtained films was characterized by using SEM. The surface morphology is shown in Fig 2.10. It can be seen that the Cu clusters distribute at the SnO_2 surface with high contrast. Size of the cluster is smaller than 1 μm. Moreover the surface was characterized by using EDX. The EDX characterization (see Fig. 2.11) shows that the typical EDX spectrum is dominated by Sn, O and Cu energy peaks.

Interaction between the surface and NO_2 was analyzed by using XPS. The typical XPS spectrums of the SnO_2/Cu surface before and after NO_2 gas exposure is shown in Fig. 2.12. The black one is the spectrum before NO_2 gas exposure whereas the red one is the spectrum after NO_2 gas exposure at 100°C for 15 min. The XPS spectrums related to the nitrogen content in the surface are confirmed in binding energy range between 297 - 400 eV. It can

be seen that the spectrum shift appears after NO_2 gas exposure although the shift is very small. The small shift is caused by low NO_2 concentration (2000 ppb) exposure and fast surface residence time of the nitrogen due to temperature. With these results, the SnO_2/Cu films are possible to be used as gas sensitive films in the FG-FET principle for NO_2 detection at low concentration.

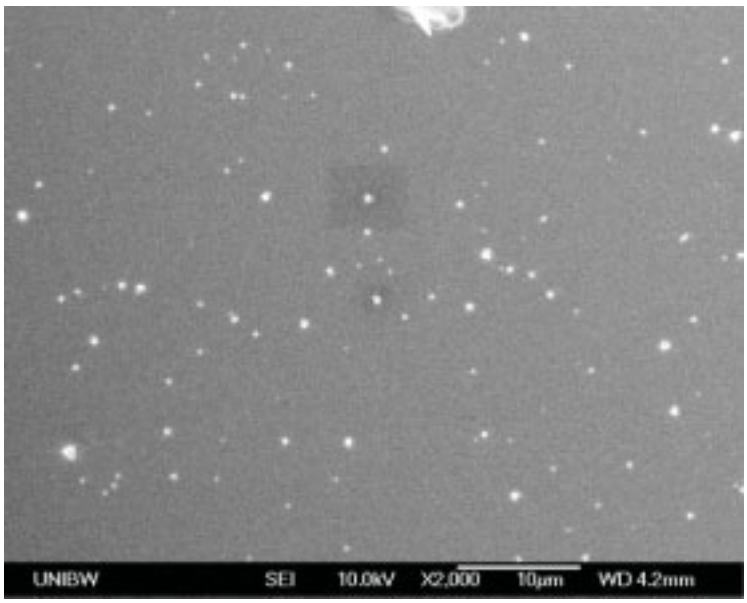

Figure 2.10. SEM image of the SnO_2/Cu surface.

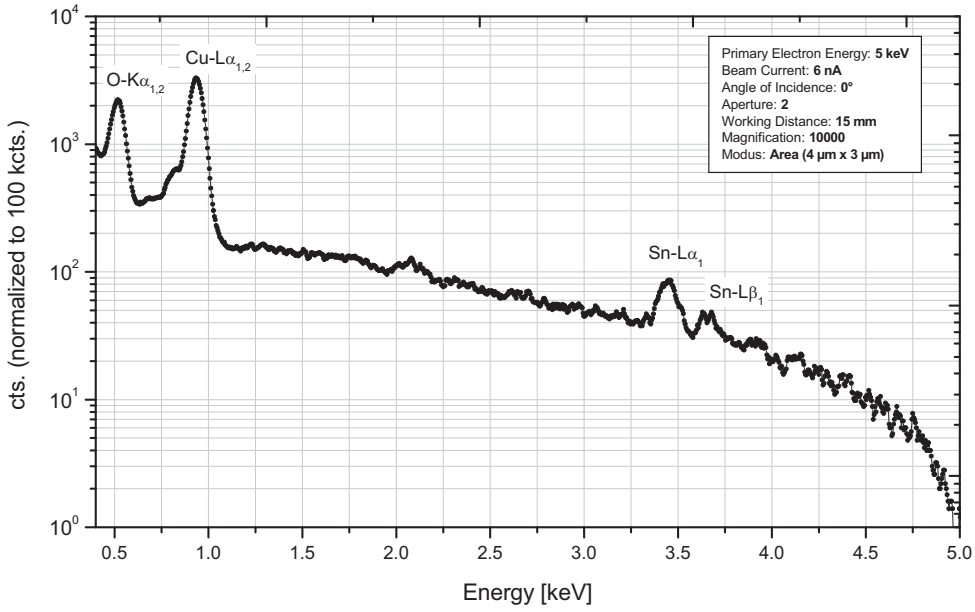

Figure 2.11. EDX characterization of the SnO_2/Cu surface.

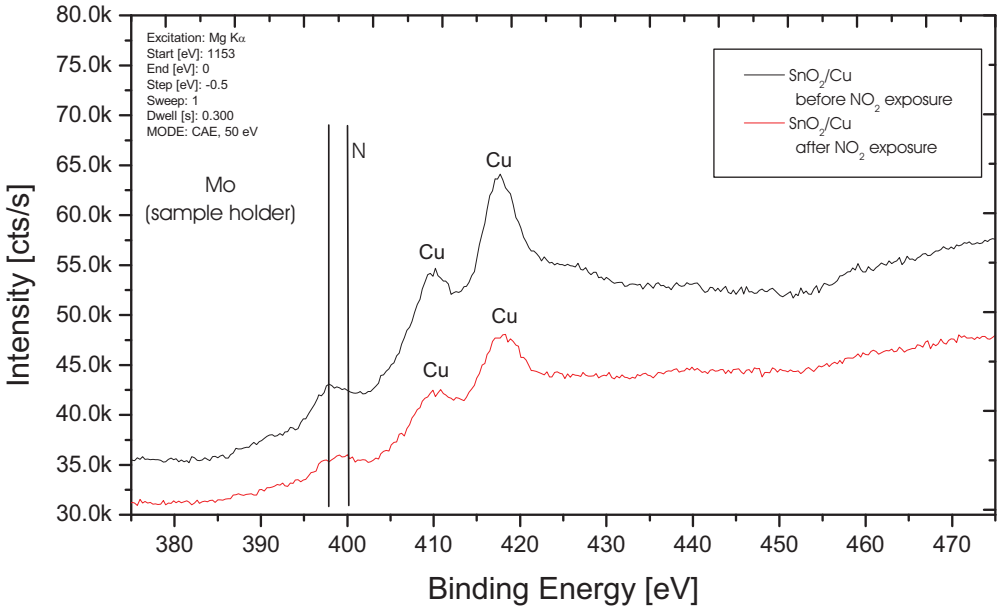

Figure 2.12. The typical XPS spectrums of the SnO_2/Cu surface before and after NO_2 exposure.

Chapter 3

Sensor technology

3.1 The FG-FET

The industrial-realization of the FG-FET sensor system is carried out by Micronas[2]. In scope of the research the sensor 12 is used to detect gas concentration. The sensors consist of five identical transistors as transducer with aluminum gate and PECVD-silicon nitride-passivity (see Fig. 3.1). Electrostatic Discharge Protection (EDP) and integrated heating with temperature control are an advantage of the sensor. The EDP was first presented by Dr. T. Knittel [43]. Furthermore the silicon nitride passivity offers the best performance of the sensor signal concerning humidity and cross sensitivity.

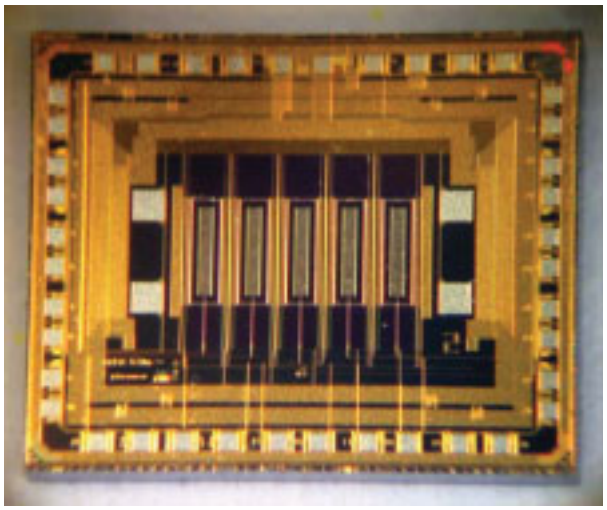

Figure 3.1. Transducer (FG-FET) with five equal channels.

[2] MICRONAS GmbH, Postfach 840 79008 Freiburg

3.1.1 Hybrid gates

Each transducer electrode used as reference has a different size and characteristic. Therefore suitable gates are developed. The p-doped silicones as gates are manufactured with lithography processes. They are 3 mm length and 2 mm width with four pits (the dimension 0.5x2 mm) which are not used at present. In addition they have two pits at the left and right edge, which function as sticking place. The hybrid gate can be seen in Fig. 3.2.

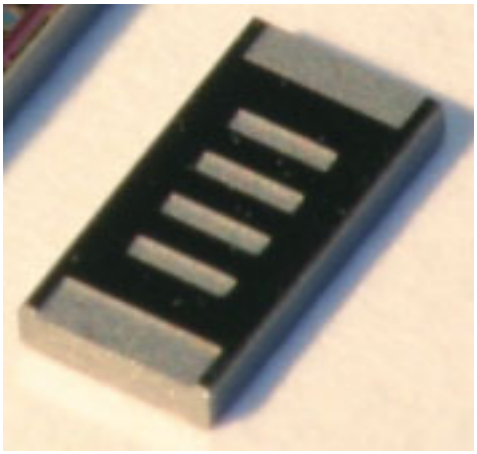

Figure 3.2. The hybrid p-doped silicon gate.

The gates must be firstly cleaned to make them dust free before they are coated with gas sensitive films. The ultrasonic process with alcohol and isopropanol is used to clean them. The ultrasonic bowl is filled 2/3 water. Then, the water is heated about 50-60°C. If the temperature has been reached, the ultrasonic is switched on and glass with 550 ml alcohol is adjusted in the bowl. The gates are immersed into the glass. After the process ran 10 min, the gates are taken from the glass and the glass is also taken from the bowl. After that, glass with 550 ml isopropanol is put in the bowl to make the further cleaning. The gates are immersed again for 10 min into the glass. Finally, the gates are heated in oven at a temperature of 125°C for 10 min.

3.1.2 Integrating gates on the transducers

The integration of gates, which were already coated with gas sensitive layers, on the transducers is done by Flip Chip Bonding in clean room at UniBw Munich. For this, four aluminum pads on the transducer chip are

carefully incised with a small needle. Then small points of the epoxy glue are put on them. The incising aluminum pads are aimed to make good mounting. A special microscope is used in which the gate and the transducer chip one on the other can be viewed in the same time so that both of them can be exactly placed. Finally the gate is mounted on the chip with an air gap (1.6 μm) at a temperature of 150°C and 10 N forces for 5 min. An air gap is kept with distance holder from aluminum in order to provide free access for the test gas species to the film.

3.1.3 Integrated heater and thermal isolator

There are two kinds of integrated heater at the Micronas's sensor 12: the power transistor- and poly resistance-heater. At the moment only the poly resistance heater is used as a heat source to obtain an optimal operating temperature of the sensor. The power transistor heater with heater control can not work properly because each control which is regulated by the filament voltage affects to temperature signal.

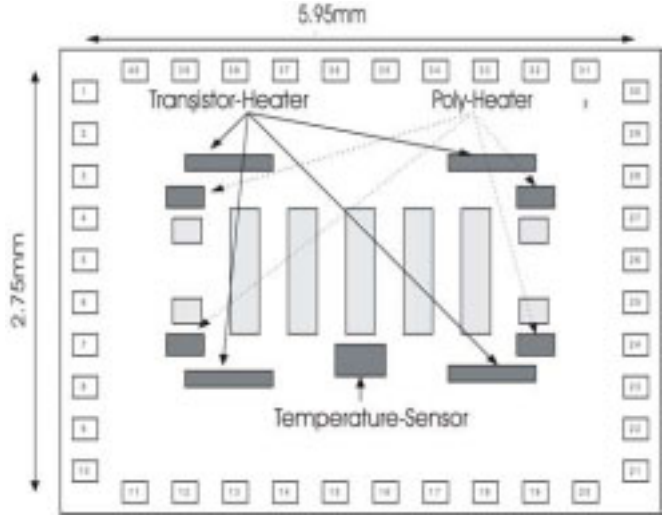

Figure 3.3. Schematic of the integrated heater at the Micronas's sensor 12.

In order to prevent the heat creep at the TO 16-sockets the separation is necessary placed between the transducer and the TO 16-sockets. Some various materials have been tested. The glass and epoxy plat show the best results. But in future the glass is used as a thermal isolator. The mounted transducer on the TO16-sockets with separation glass is shown in Fig. 3.4.

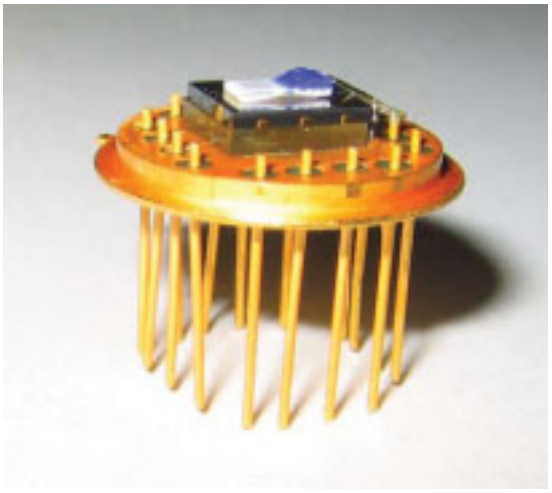

Figure 3.4. The mounted transducer on the TO 16-sockets with separation glass.

Actually the transducer is provided with a temperature sensor, unfortunately the temperature sensor can not be used because its voltage control sensor affects to the signal output, which is generated by the heater. Therefore the heater must be calibrated to obtain certain temperature value. The temperature calibration was done by using Pt_{100}.

For the calibration the Pt_{100} is stuck on the transducer with epoxy glue as shown in Fig 3.4. Then the controlled current is applied to the heater from 0 to 200 mA. Increasing current of the heater generates heat which causes resistance changes of the Pt_{100}. The resistance changes are measured for three minutes at each current value in order to obtain stabile condition. By using available resistance table of the Pt_{100} towards the temperature relation between the poly heater current and temperature can be obtained. The relation can be observed at the red line in Fig. 3.5. The temperature increases exponentially with the increasing current. The black and blue lines are the first and second measurements respectively whereas the green line is the average of the measurements.

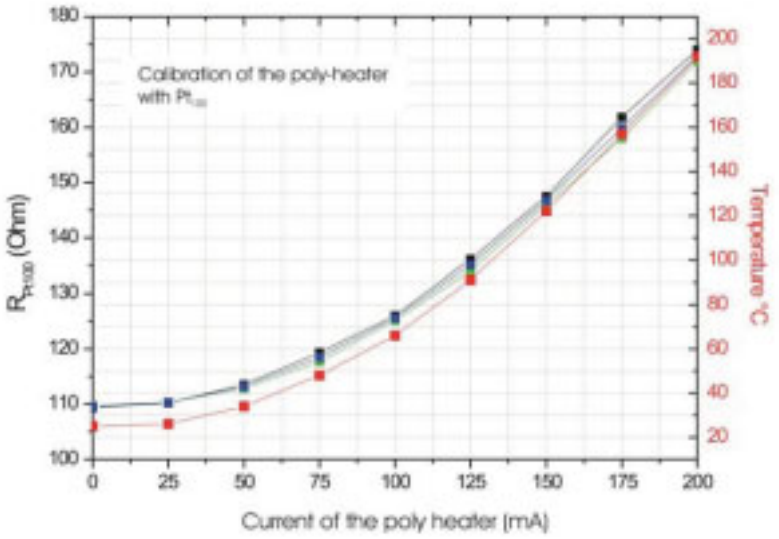

Figure 3.5. Calibration of the poly heater with Pt_{100}.

3.1.4 Electronic contacts

After the transducer was stuck on the TO 16-sockets with separation glass, the electronic contacts between the transducer pads and the sockets are created by using the wedge bonding with 0.25 μm aluminum wire. 14 pads were bonded with the sockets, 10 contacts for source-drain of the five transducers, 2 contacts for the poly heater and 2 contacts for gate and substrate. The gate and substrate are grounded. The sockets are contacted to the electronic circuit via a sub-D connector (25 cables) for measuring electronic. The sensor, which was already bonded on the TO 16-sockets, can be seen in Fig. 3.6.

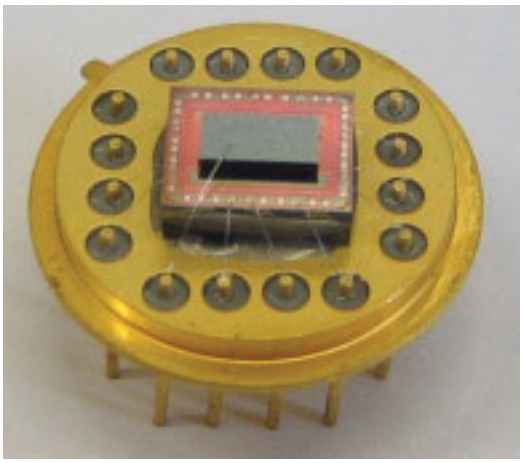

Figure 3.6. Complete assembled FG-FET sensor, stuck on TO 16-sockets.

3.1.5 Protection of the wire bonding

The wire bonding at the transducer and TO 16-sockets is very weak and very sensitive to mechanical disruption. In order to protect it, the sensor is covered with steel plate cap. The hole with 3 mm diameter is made at top side of the cap in order to give access for the test gases to the sensor. A filter for preventing the sensor from dust is not used because pure interaction between the sensitive film and the gas is expected.

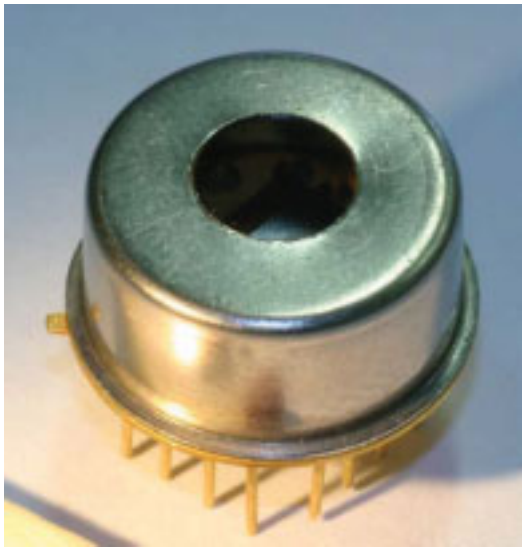

Figure 3.7. The sensor with the steel plate cap.

3.2 Measurement stations

For characterization of the sensor, four measurement stations which were built by Dr. M. Burgmair are available [39]. The measurement stations consist of four components,

1. The supply lines with dry synthetic air and six differently test gases.
2. Magnetic valves with three mass flow controllers (MFC).
3. A computer with GPIB[3] interfaces for the control and signal recorded.
4. Sensor chamber

In new development of the measurement stations to the supply lines of gases six lines are added so that with the new stations 12 synthetic test gases can be simultaneously induced into the sensor chamber. The available gases at the station are as follow

[3] GPIB: General Purpose Interface Bus

Gas	Concentrations
H_2	20000 ppm
CO_2	100000 ppm
CO	300 ppm
O_2	100000 ppm
H_2S	50 ppm
SO_2	10 ppm
NH_3	10 ppm
NO_2	2 – 10 ppm
Cl_2	0.5 – 100 ppm
Methane	500 ppm
Ethanol	1000 – 100000 ppm
H_2O	0 – 100 %
Synthetic Air	0 – 100 %

The test gases can be humidified by flowing dry synthetic air through a water bubbler. The stations are also provided with high quality temperature and humidity sensors which measure permanently the temperature and humidity in a flowing gas.

Kelvin Probe and FET measurements can be accomplished in this station. In case of the Kelvin Probes, the new material can be measured in three Kelvin Probes at different temperatures in the same time. The material is characterized with all test gases at room temperature, 80 and 130°C, whereas with the FET measurement station one can measure two sensors or ten different transistors at the same time. The signals of the transistor are recorded at the personal computer (PC) via a 10-channel multiplexer card of the Keitley-2001 after the signals were gained in the appropriate electronic circuit.

Operating temperature of the sensor can be indirectly regulated here by a fully automated climatic chamber, which is integrated into the appropriate software at the PC. In case of the new type sensor 12, which has been provided with the integrated poly heater, the operating temperature associated to the heater current can be directly controlled with the Keithley-SMU's 2400 in the software at the PC so that the current can be automatically adjusted. Schematic of the new measurement station with 12 test gases is shown in Fig. 3.8.

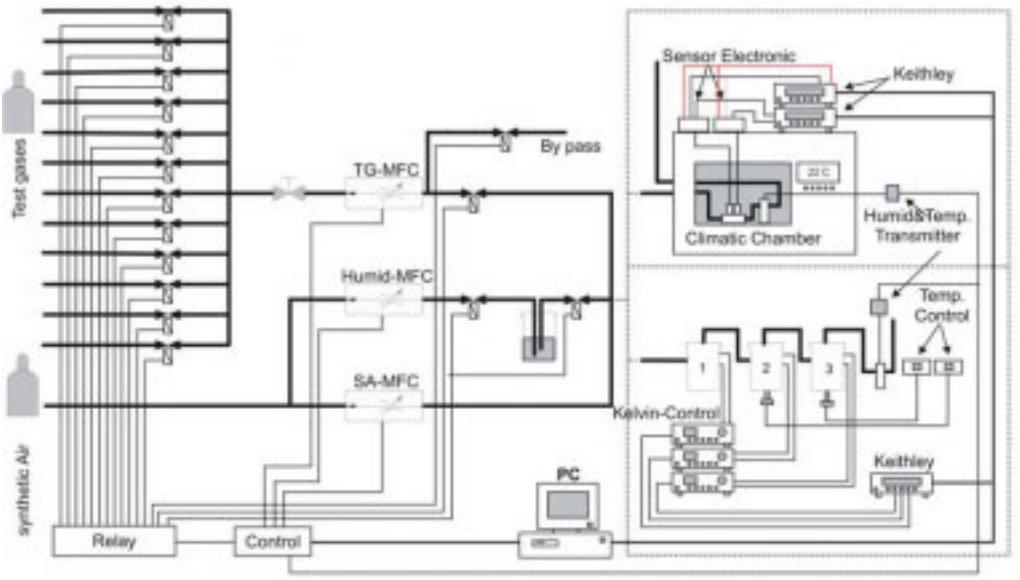

Figure 3.8. Schematic of the new measurement station.

Figure 3.9. The Kelvin Probe-measurement station with three Kelvin Probe chambers and different operating temperature.

Figure 3.10. The FET measurement station. The sensor chamber is put in the climatic chamber. Two same or different sensors with ten transistors can be characterized.

3.3 Sensor signal

The expected information about a gas measurement can be determined with an analysis of the sensor signal associated to the work function change. The signal can be a positive or negative peak depends on what kind of the used film and detected gas. Plotting the signal and the gas concentration as a function of the time can be used to explain response, stability and reversibility of the sensor to the detected gas.

Fig. 3.11 shows the comparison between the ideal signal and the real signal. The ideal signal (orange line) is value of the gas concentrations which are controlled by Mass Flow Controllers (MFC) and the integrated program in the PC whereas the real signal (black line) is signal output of the sensors due to gas adsorption or chemisorption on the film.

The sensor response can be estimated with calculating t_{90}-time. The t_{90}-time is the time which is needed to reach 90% of the final measurement

value or the maximal signal at certain gas concentration. For the measurement result in Fig. 3.11 e.g. the t_{90}-time is about 4 minutes after exposing gas concentrations.

Stability of the sensor can be observed from stability of the signal related to the gas concentration. As is shown in Fig. 3.11 the signal height remains stabile with value of 42 mV at 10000 ppm test gas for 25 min whereas reversibility of the sensor can be proved with reversibility of its signal. The signal returns fast to base line after test gas exposure is turned off. Furthermore, the reversible signal proves also that the poisoning is not occurring at surface of the film due to test gas interaction. It can be seen from Fig. 3.11 that the signal needs less than 30 min to return to base line.

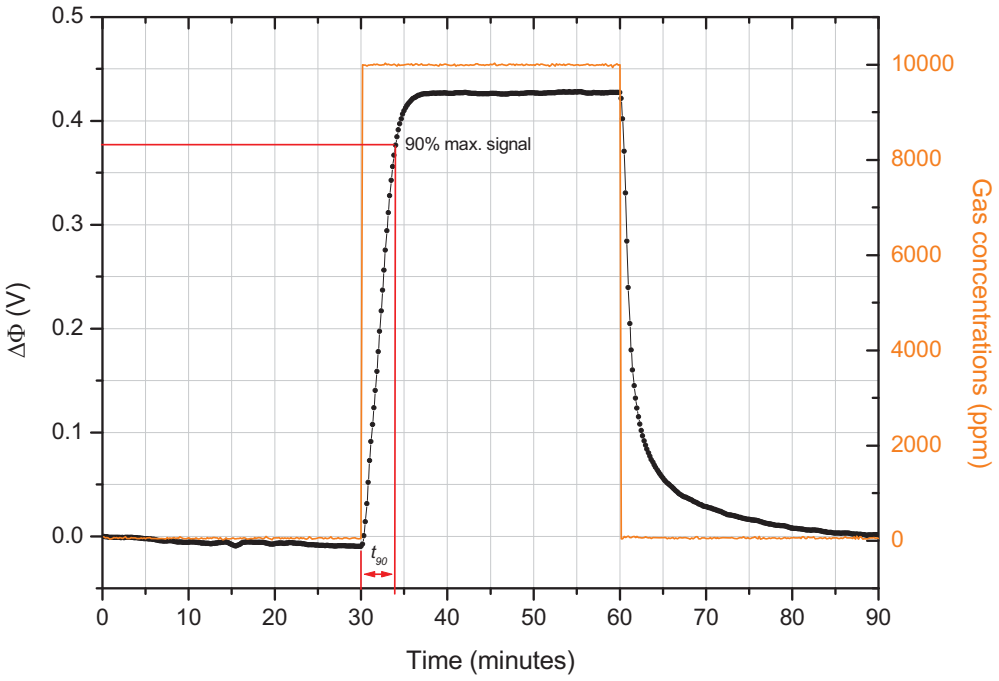

Figure 3.11. Analysis of the sensor signal.

3.4 Surface passivation

The humidity in the ambient air is not constant but dependent on the weather conditions. In the measurement station a relative humidity can be adjusted with flowing dry synthetic air through a water bubbler. The water dipoles remain not only at the gas sensitive film but also at the passivation depending on the used material. This makes a possible increasing surface conductance that generates a short circuit current in the air gap so that the sensor can not work properly.

In order to reduce influence of the humidity the guard ring is made at the transducer surface that forms an equipotential surface around the gate, although it is not enough to prevent the FG-FET from the humidity effect (see Fig. 3.12). The signal drift can be observed at the humidity above 50%. It means that the guard ring can not prevent the sensor from humidity effect anymore.

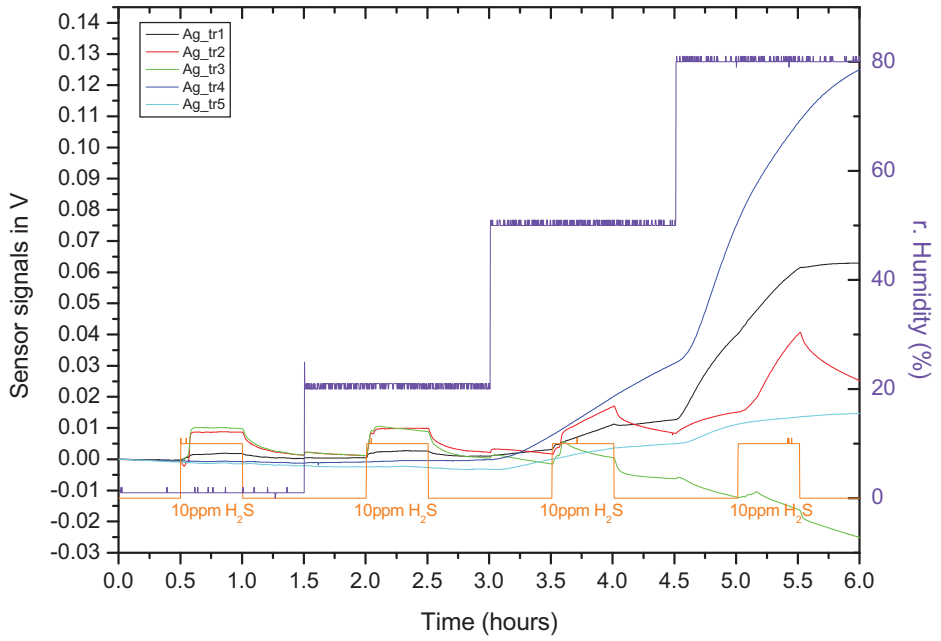

Figure 3.12. Influence of humidity on the FG-FET, which has been provided with the guard ring at room temperature. 10 ppm H_2S in synthetic air measurements at room temperature under different humidity conditions.

A hydrophobic surface passivity with n-octadecyltrichlorsilan (ODTS) is the other possibility to reduce the humidity influence. The ODTS passivation was introduced by Dr. T. Knittel [43]. The main advantage of ODTS is the

formation of a self-assembling monolayer on any silicon containing surface, where it forms binding sites to the silicon atoms. After the passivation the surface remains hydrophobic and is stable with respect to oxidizing gases. Furthermore, the monolayer is insensitive to acid. This acid-proof character of the passivation is especially important for the detection of aggressive gas species like H_2S to avoid transducer damage and to keep long term stability.

For the fabrication of the ODTS passivation, a glass is filled with 50 ml toluol, and then 2 drops of the ODTS are added. The solution is swiveled briefly, so the ODTS in toluol distributes itself. The solution must always be freshly set and directly use. Cleaned and dried wafers are put into the solution. Tweezers are used to keep the surface upward and wafers not one above the other. The glass is covered with aluminum foil to avoid the solution to evaporate.

The solution is carefully swiveled each 2 min. After 20 min the wafers are taken out using tweezers and immersed immediately into 2 glasses with clean toluol in order to wash the remaining ODTS which is bonded at the surface. After that the wafers are washed with DI water. If the passivation was successful, the wafers will float on the water. Finally binding of the silan layer is kept at temperature of 125°C for 15 min. The passivation is stable with increasing temperature until about 200°C.

After the passivation, the sensor signals are stable to different relative humidity up to 80%, only smaller effects still occur at change of the humidity. However it should be noted that the humidity effect can be strongly reduce with the ODTS passivation.

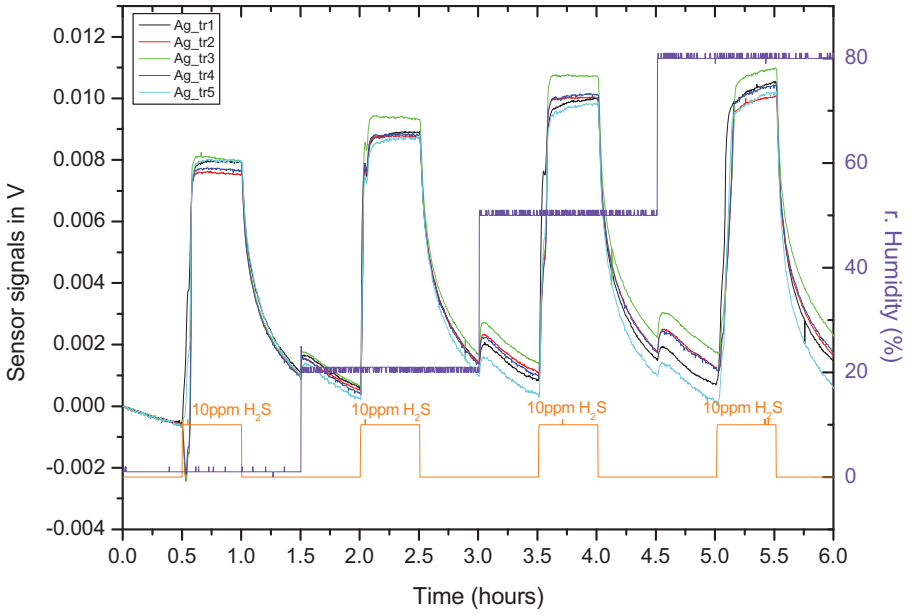

Figure 3.13. Reducing influence of humidity on the FG-FET with the ODTS passivation. 10 ppm H_2S in synthetic air measurements at room temperature under different humidity conditions.

Chapter 4

Metal oxides as gas sensitive films

Gas sensors based on metal oxides can be used for the detection of combustible and noxious gases in air [44-50]. Their gas sensing properties have been widely studied with respect to both the oxidizing and reducing gases. The sensor systems are mostly based on conductivity change measurements of the metal oxide due to gas exposure. Huge efforts have been carried out in order to improve their sensitivity by doping catalytic metals. However, this system still requires high operating temperature above 200°C to obtain interaction between sensitive materials and gas molecules.

In this chapter the Ag_2O, ZnO and SnO_2/Cu films are used as gas sensitive films in the FG-FET sensor system for H_2S and NO_2 detections, respectively. An interesting advantage of this system is its sensitivity to work function changes due to physisorption, chemisorption and chemical reaction as well as ionosorption, which are occurring on the surface of the films. Moreover, it can be operated at low temperature, which is necessary for mobile systems.

4.1 Silver oxide (Ag_2O) for hydrogen sulfide (H_2S) detection

Application of silver (Ag) films in the FG-FET as a hydrogen sulfide sensor was done by Dr. G. Freitag [14]. Operating at 135°C, the sensors show very good stability and sensitivity characteristic as are represented in Fig. 4.1. Two transistors show comparably signal heights at the same concentration. The positive sensor signal depends on the H_2S concentration.

The sensor is sensitive to H_2S concentrations of 2-50 ppm. Unfortunately the difference of the measured values between 5 and 50 ppm H_2S is only 10 mV and the maximum signal is only approx. 65 mV at 50 ppm H2S. Operating at 95°C, the Ag sensor signals saturate at about 5 ppm H_2S but the signals are not stable and show a significant drift.

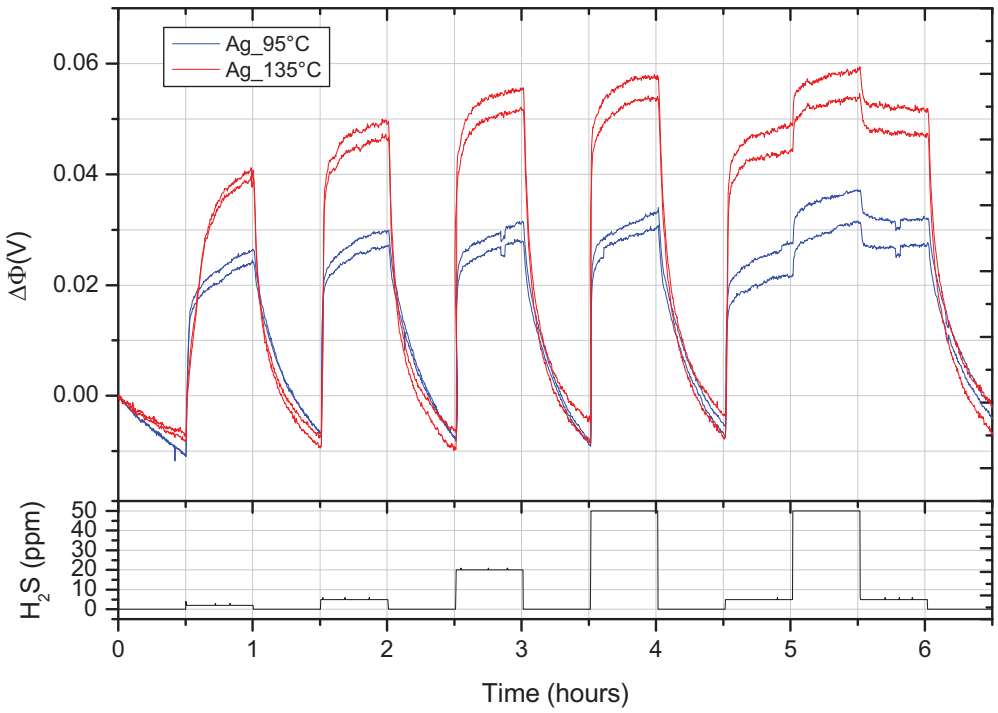

Figure 4.1. Response time of the Ag sensor to H_2S concentrations at operating temperature of 95 and 135°C under 0% relative humidity.

In order to improve the ability of the Ag sensor, silver oxide is used as a gas sensitive film. By adding oxygen it is expected that ion exchange processes with the surface can be improved. An Ag_2O sensor based on the FG-FET was investigated as a H_2S detector in a constant flow of dry synthetic air (100 ml/min) with interrupted 2-50 ppm H_2S. The measurements were carried out at different temperatures to obtain optimum operating temperature of the sensor because adsorption and desorption processes are temperature activated as presented in chapter 1.

Equilibrium on the film surface can be achieved by exposing the sensor to a constant flow of dry synthetic air (100 ml/min) for 15 min. To investigate the H_2S sensitivity of the sensor, it is exposed to H_2S in the concentration

range between 2 and 50 ppm for 15 min. This cycle is repeated for several times in order to investigate its reliability and reproducibility

4.1.1 Thermal behavior of the Ag_2O sensor

The thermal behavior of the Ag_2O sensor to H_2S concentrations at room temperature, 95°C and 135°C under dry condition is described in Fig. 4.2. It can be seen that signals and response time of the sensor increase with increasing temperature. Operation at 95°C confirms that the sensor offers reversible signals with negligible base line drift and fast response time t_{50}~10 s.

A possible explanation is as follow: at a temperature of 95°C the Ag_2O surface adsorbs H_2S to form silver sulfide. The sulfide at the surface injects electrons into the bulk conduction band of the Ag_2O film (n-type semiconductor). Consequently, an electron accumulation layer appears near the surface. Thus, the work function of the films changes. It is proved by increasing the sensor signal.

$$Ag_2O + H_2S \rightarrow Ag_2S + H_2O \quad (4.1)$$

The signal returns faster to the base line when a constant flow of dry synthetic air is added. It proves that this compound is not very stable because it decomposes into Ag_2O again. Oxygen at the surface causes the surface to behave acceptor like so that electrons are transferred from the conduction band to the surface. As presented previously, electrons transferred to the surface generate a depletion layer, and the band returns to the original condition before the adsorption process. Therefore silver oxide can be used as sensitive thin film for H_2S detection. The back reaction can be described as follow:

$$2Ag_2S + 3O_2 \rightarrow 2Ag_2O + 2SO_2 \quad (4.2)$$

At an operating temperature of 135°C the signal needs more time to return to the base line because silver oxide decomposes to silver. It means that the material composition at the surface has been modified by the temperature.

$$2Ag_2O \rightarrow 4Ag + O_2 \quad (4.3)$$

Whereas operating at room temperature, the generated signal is very low because transferring electrons from the band to the surface and injection electrons from the surface to the band are activated processes, which depend on temperature.

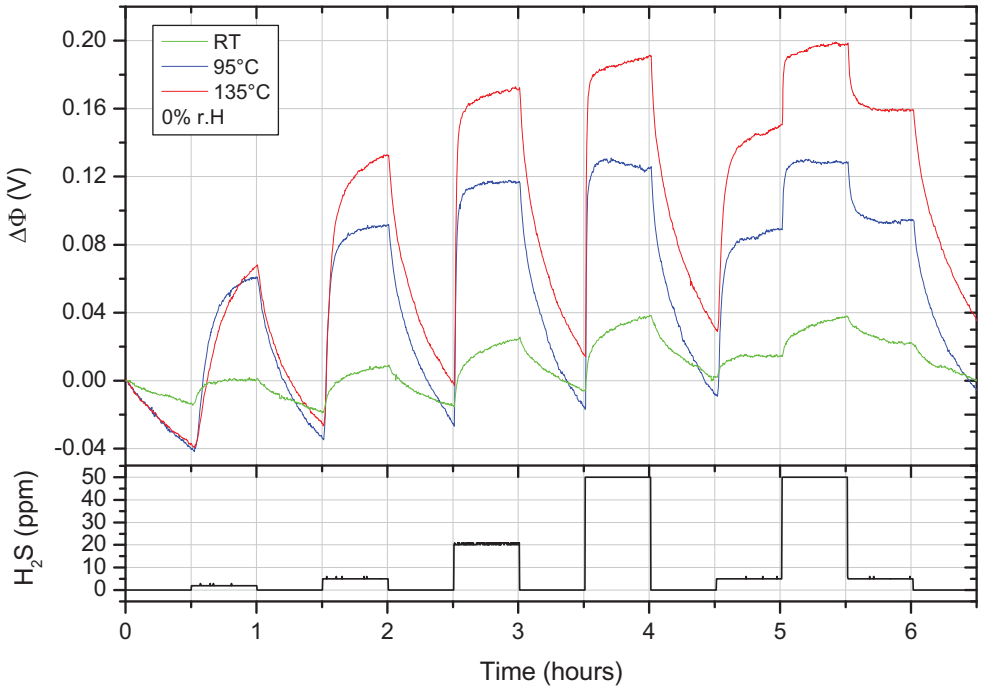

Figure 4.2. Thermal behavior of the Ag_2O sensor to H_2S under dry conditions.

4.1.2 H_2S concentration dependence of the Ag_2O sensor

After the operating temperature was obtained, the Ag_2O sensor is characterized by exposing it to various H_2S concentrations for 3.15 hours in order to investigate the sensor's reliability and reproducibility. The electrical response of the sensor with four different transducers to 2-50 ppm H_2S at 95°C under dry condition is shown in Fig. 4.3. It can be observed that the sensor distinguishes well between H_2S exposures in a concentration range of 2-50 ppm. The sensor signals conducted work function change increases with increasing H_2S concentration. The signals reach 100 and 125 mV at 5 and 50 ppm H_2S concentrations, respectively. Furthermore the signals are not in saturation at each elevated concentration.

At 2 ppm H_2S, the signals do not level after more than 15 min. The signal height is about 80 mV and the response time t_{50} about 7 min. This means that the electron transfer from a donor surface state to the bulk conduction band runs slowly. The signals are in steady state after less than 15 min with t_{50} ~10 s at H_2S exposure in a concentration range of 5-50 ppm.

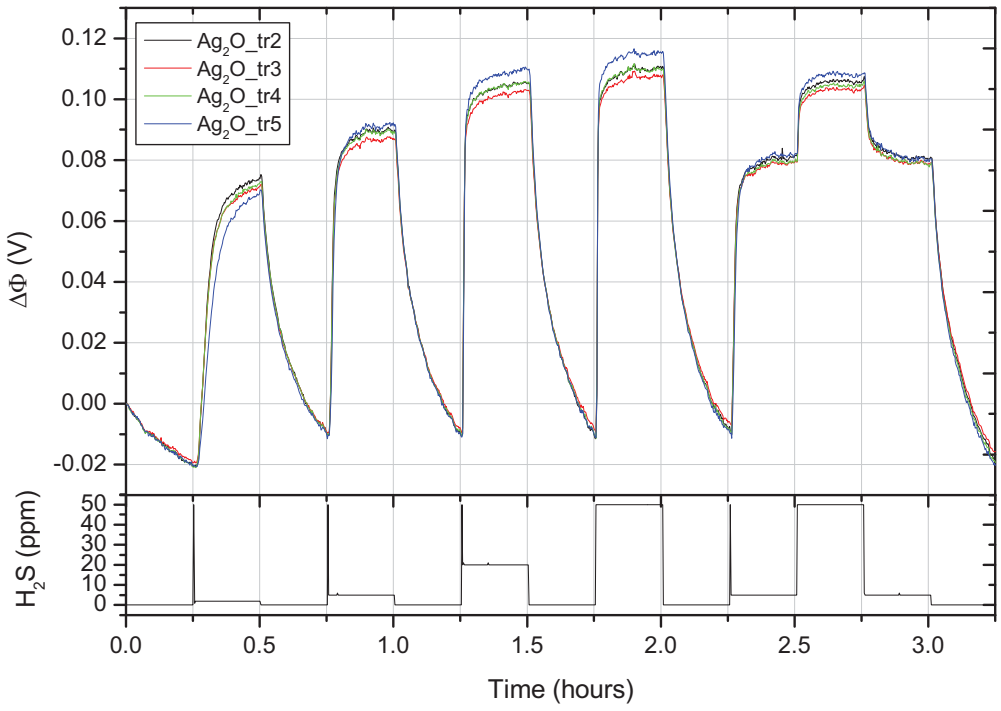

Figure 4.3. Dynamic response of the Ag_2O sensor to various H_2S concentrations at 95°C under dry conditions.

4.1.3 Humidity effect on the Ag_2O sensor

In order to investigate the influence of humidity on the Ag_2O sensor, the relative humidity was varied in a range of 0-80%. Each value of humidity was investigated for 45 min. A cycle of measurement is divided into three steps. In step 1 the humidity is exposed for 15 min in order to obtain a stable signal in humid condition. In step 2 the sensors are exposed to H_2S for 15 min to analyze the gas behavior. In step 3 the humidity is still exposed without H_2S in order to investigate reversibility of the signal.

Investigation of the humidity influence is shown in Fig. 4.4. The humidity has only little effect on the sensor. Above 60% relative humidity, the signal is not in saturation condition when the sensor is exposed to H_2S gas.

However, it should be noted that the signals are reversible, stable and nearly no base line drifts occur in humid condition.

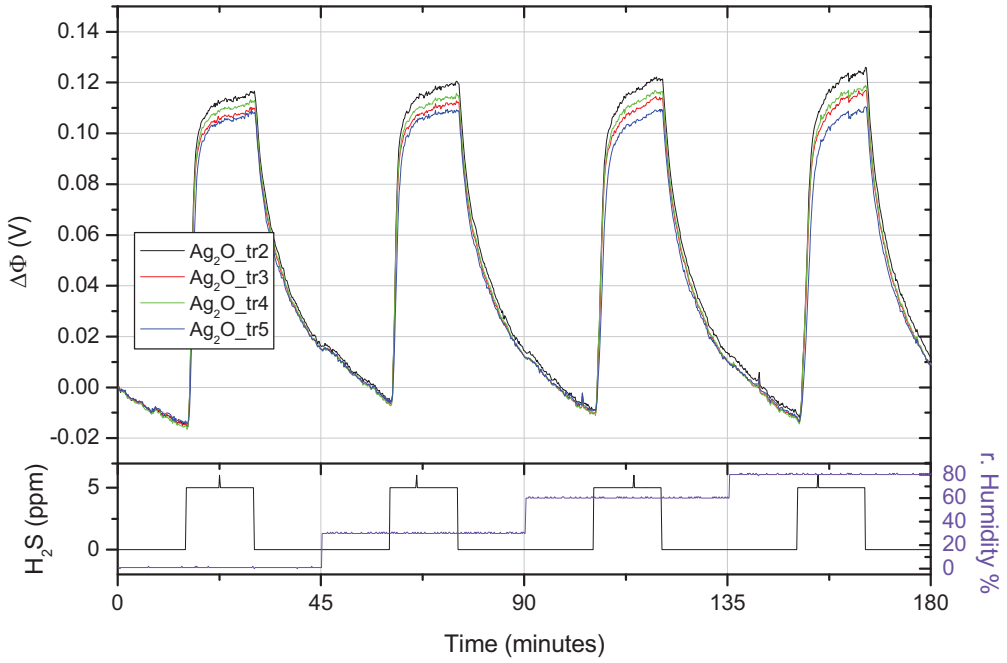

Figure 4.4. Influence of the elevated humidity on the Ag_2O sensor during measurements of 5 ppm H_2S at 95°C.

4.1.4 Cross sensitivity of the Ag_2O sensor

Cross sensitivity of the Ag_2O sensor to other gas species was characterized by exposing it to H_2, O_2, CH_4, CO_2, CO, H_2S, SO_2, NH_3, NO_2 and H_2O at 95°C under dry condition. The result (see Fig. 4.5) shows that the sensor also reacts with NH_3 and NO_2. When NH_3 gas penetrates into the sensor, small positive signals are generated whereas significant negative signals are generated, when the sensor is exposed to NO_2. A possible explanation is as follows: NO_2 adsorption at the Ag_2O surface causes an acceptor surface because NO_2 molecules capture electrons from the bulk conduction band. This causes a broadening of the depletion layer of the free charges near the surface. Thus the work function of the films changes. In this condition, a significant negative signal can be observed. After 10 exposures, the sensor sensitivity to H_2S decreases because contamination occurs at the film during interaction with NO_2 gas. It is verified with the decreasing sensor signals.

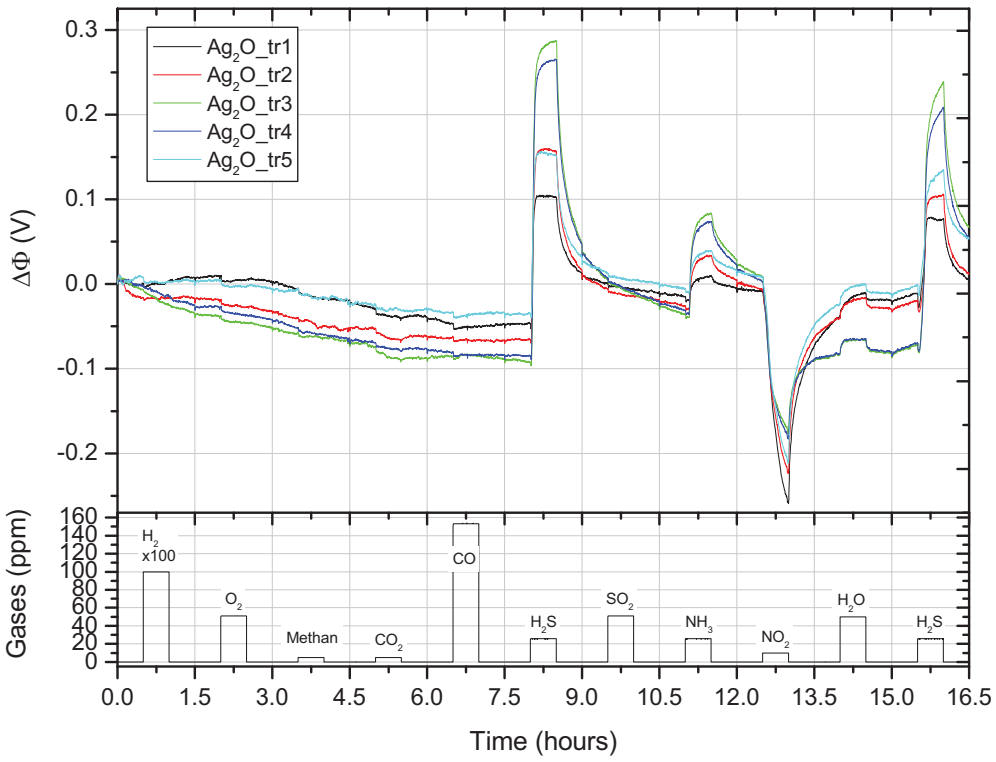

Figure 4.5. Cross sensitivity of the Ag_2O sensor at 95°C under dry conditions.

4.1.5 Long-term stability of the Ag_2O sensor

Investigation of the gas sensor with metal oxide as sensitive film has given little consideration to the problem of long-term stability. Therefore, long-term stability investigations are necessary and will be an important criterion that determines the ability of the sensors.

Long-term stability experiments were carried out one month after first conditioning. For the experiments, the Ag_2O sensor is characterized in a constant flow of dry synthetic air (100 ml/min) with interrupted 5 ppm H_2S concentrations at 95°C under dry condition. First, the sensor is exposed in a constant flow of dry synthetic air (100 ml/min) for 30 min in order to obtain stable sensor signal. Then, it is exposed to 5 ppm H_2S for 30 min. After that, H_2S is turned off for 30 min to investigate reversibility of the sensor. Finally, this cycle is repeated for a total of 6.5 hours to study reproducibility of the sensor.

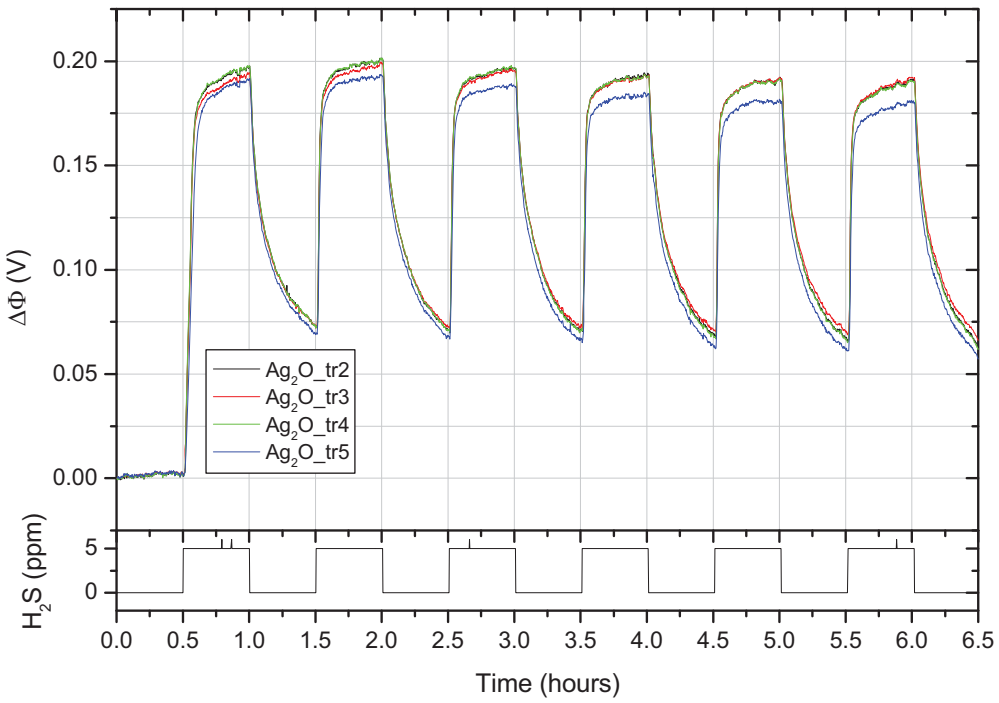

Figure 4.6. Long-term stability of the Ag_2O sensor after one month without testing at 95°C under dry conditions.

The results are shown in Fig. 4.6. The signal patterns of the sensor remain stable. Three transducers number 2, 3 and 4 have identical signal height whereas the signal of transducer number 5 changes after the third cycle of gas H_2S exposing. The base line after the third cycle is lower than the base line of previous cycles due to fast desorption process. However, reproducible signals can be observed in this condition. It means also that poisoning is not occurring at the film surface due to H_2S interaction.

4.2 Zinc oxide (ZnO) for nitrogen dioxide (NO_2) detection

Zinc oxides, particularly the ZnO phase, are thoroughly studied post-transition-metal oxides, which are popular materials for gas-sensing application next to the tin oxides [51]. ZnO has been known as a sensing material to detect reducing and oxidizing gases such as O_2 [52], CO [53], NO_2, H2, and CH4 [51]. Unfortunately, this material has poor stability in humid condition, long-term instability and poor selectivity.

The surface of ZnO semiconductor based gas sensor plays an important role for sensing properties. NO_2 adsorption on the surface generates an acceptor like surface state because NO_2 captures electrons from the bulk conduction band. This causes a broadening of the depletion layer near the surface and thus the work function changes [21, 25, 54].

Accordingly, ZnO film coated gates were mounted on the FG-FET chips in order to measure the work function change of the film due to NO_2 interaction. Sensing properties of the ZnO sensor with respect to various NO_2 concentrations were measured as a function of temperature and humidity. Moreover, selectivity and stability as well as reproducibility of the sensor were investigated at the optimal operating temperature.

4.2.1 Temperature effect on the ZnO sensor

Operating temperature of the sensor is one of the most important parameters because adsorption and desorption are temperature activated processes [25]. Increasing the temperature improves the sensor's sensitivity to test gases. On the other hand, the temperature has an effect on the physical properties of the film. Therefore, the investigation of temperature influence was carried out to obtain optimum operating temperature of the sensor.

The thermal behavior of the ZnO sensor in the temperature range between room temperature and 165°C under dry condition is depicted in Fig. 4.7. The sensor response depends strongly on temperature and concentration. The signals decrease with the increasing temperature and concentration. Optimal operation temperature of the sensor is achieved at 165°C, a temperature at which negligible base line changes and a fast response time t_{50}~10 s as well as reversible signals to NO_2 gas exposure are observed. Whereas, at operating temperature lower than 95°C, the sensor signals need more than 15 min to return to base line because desorption process related with the surface residence time of molecules NO_2 depends on the temperature. The surface residence time decreases exponentially with the increased temperature.

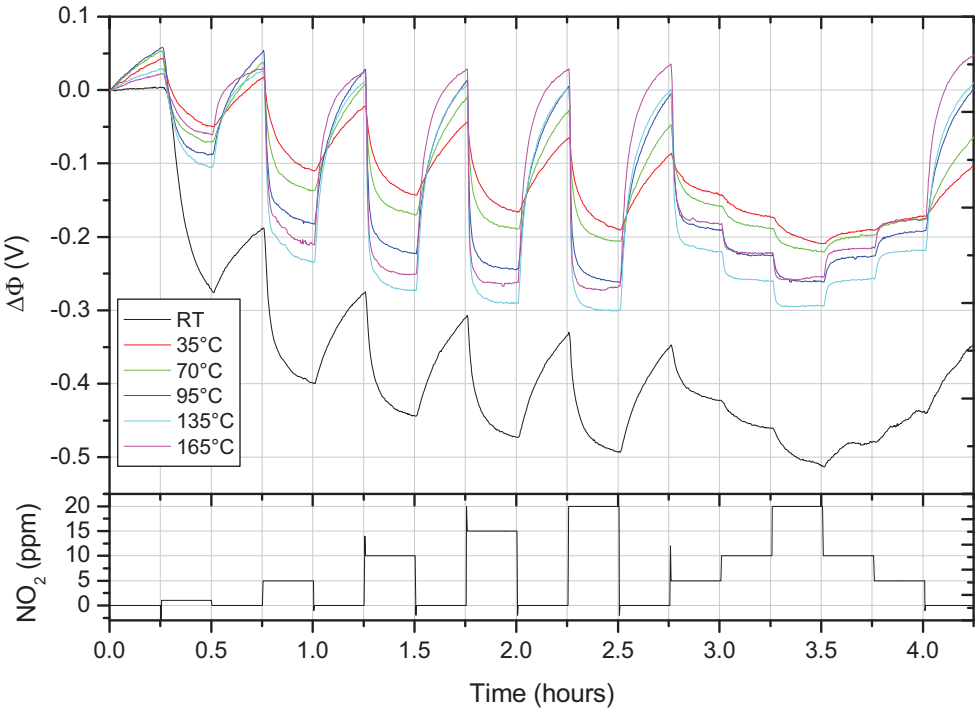

Figure 4.7. Temperature effect on the ZnO sensor during measurements of various NO_2 concentrations under dry conditions.

4.2.2 NO_2 concentration dependence of the ZnO sensor

NO_2 concentration dependence of the ZnO sensor was measured by exposing the sensor in a constant flow of dry synthetic air (100 ml/min) with interrupted 1-20 ppm NO_2. The measurements were carried out at optimum operating temperature of 165°C under dry condition. Procedure of the measurement is described as follow: first, the sensor is exposed in a constant flow of dry synthetic air (100 ml/min) for 15 min to get a stable sensor signal. Then, it is exposed to NO_2 for 15 min to observe its sensitivity. Afterwards, reversibility of the sensor signal is tested by turned off exposing NO_2 for 15 min. Finally, this cycle is repeated for several times with increased NO_2 concentrations.

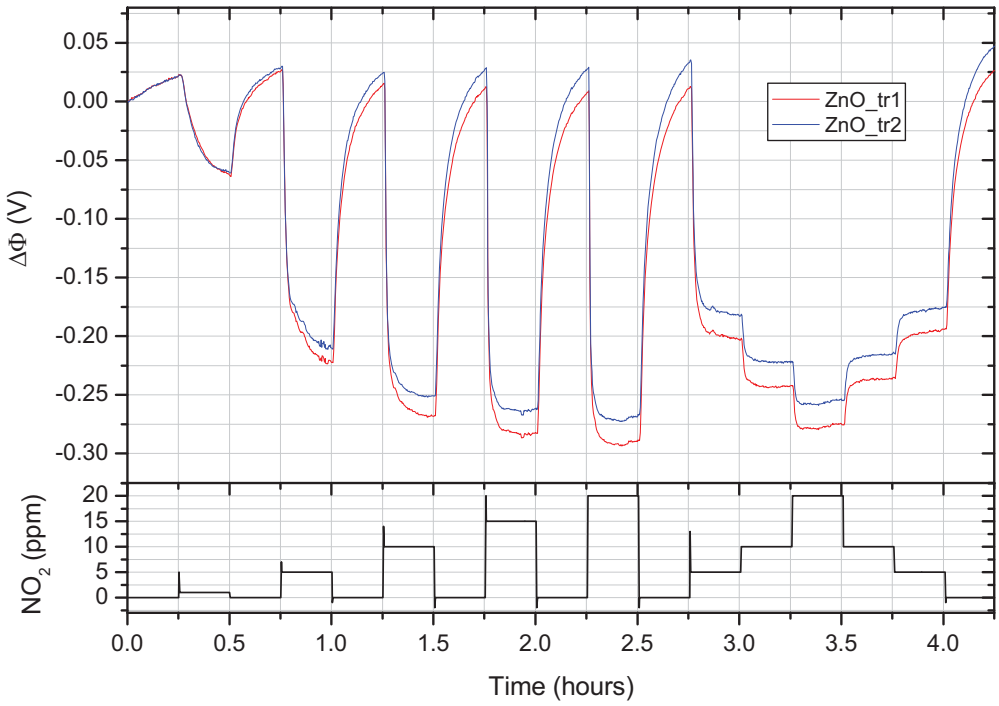

Figure 4.8. Response time of the ZnO sensor to various NO_2 concentrations at 165°C under dry conditions.

The response time of the sensor to NO_2 in a concentration range of 1-20 ppm at 165°C under dry condition is presented in Fig. 4.8. It increases and the signal height decreases with increasing concentration. The stable base line can be observed at this condition. The signal height (-250 mV) and response time (t_{50}~10 s) can be observed at 5 ppm NO_2 (maximum allowed concentration). The signals increase rapidly during measurement of 1 to 5 ppm NO_2 and are almost in saturation for concentration above 15 ppm.

Fig. 4.9 shows the NO_2 measurements in the concentration range between 200 and 2000 ppb at the operating temperature of 190°C. The increasing operating temperature is aimed to improve the sensor sensitivity. Unfortunately, the sensitivity remains low to NO_2 exposure. This is proved with response time of the sensor t_{50} is longer than 5 min at 800 ppb NO_2. With this result one can conclude that the sensor is not suitable for NO_2 detection at low concentrations. Therefore a new material as gas sensitive films for NO_2 detection at low concentration is needed.

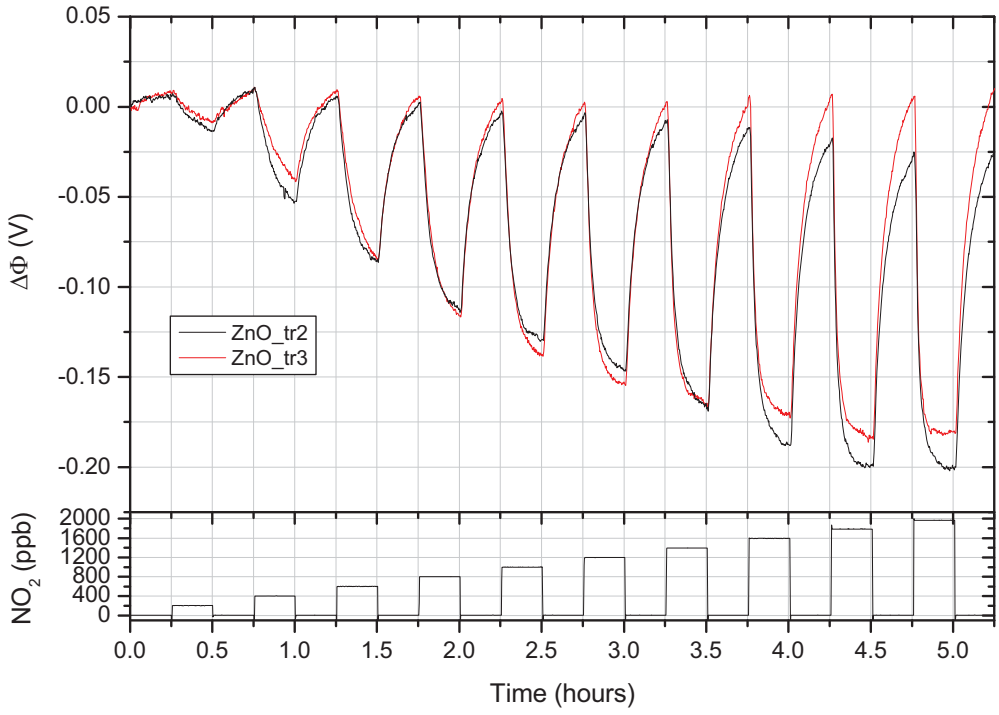

Figure 4.9. Response time of the ZnO sensor to low NO_2 concentrations at 190°C under dry conditions.

4.2.3 Humidity Effect on the ZnO sensor

The relative humidity is a serious problem for the sensor based on FG-FET device because surface current disturbs the potential measurement. The humidity influence can be reduced with the surface passivation on the FG-FET chips as presented in chapter 3. However, despite of this passivation the humidity still influences the chemical sensitive layer. From Fig. 4.10 it can be seen that sensitivity of the sensor decreases with increasing relative humidity.

Interaction between ZnO and water vapor at 165°C generates chemisorption of OH-groups on the surface. Because the binding energy of the chemisorption process is quite strong, high temperature is required to remove OH-groups [55]. The signals remain stable under humid condition during NO_2 gas exposure. The following reactions were postulated for an interaction of H_2O vapor with the ZnO surface.

$$ZnO + H_2O \rightarrow ZnOH + OH \qquad (4.4)$$

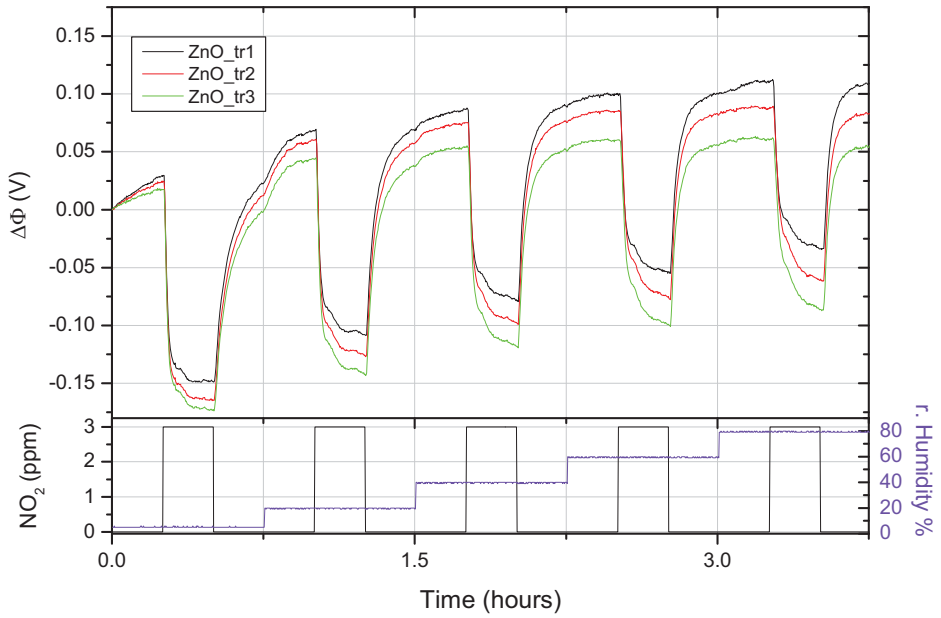

Figure 4.10. Response of the sensor to 3 ppm NO_2 exposure at 165°C under various relative humidities.

4.2.4 Cross sensitivity of the ZnO sensor

Cross sensitivity of the ZnO sensor was characterized by exposing it to H_2, CO_2, CO, O_2, H_2S, SO_2, NH_3 and H_2O vapor at 165°C under dry condition. The experiment procedure shall be as follows: first, the sensor is rinsed with synthetic air (100 ml/min) for 15 min to obtain a stable signal. Then, it is exposed towards first test gas for 15 min. Afterwards it is rinsed again with the synthetic air for 30 min in order to reduce influence of the previous exposed test gas. Finally, this circle is repeated for several times with different test gases.

Fig. 4.11 represents cross sensitivity of the sensor. It can be seen that the sensor responds to H_2, H_2S, SO_2 and NH_3. Two signals of the sensor show identical behavior to the test gases. No significant negative and positive signals are generated when the sensor is exposed to H_2, H_2S, SO_2 and NH_3 gases. A significant negative signal change (~ -220 mV) can be observed when the sensor is exposed to 2000 ppb NO_2. These results prove that the ZnO film is a promising new material with high selectivity for NO_2 detection.

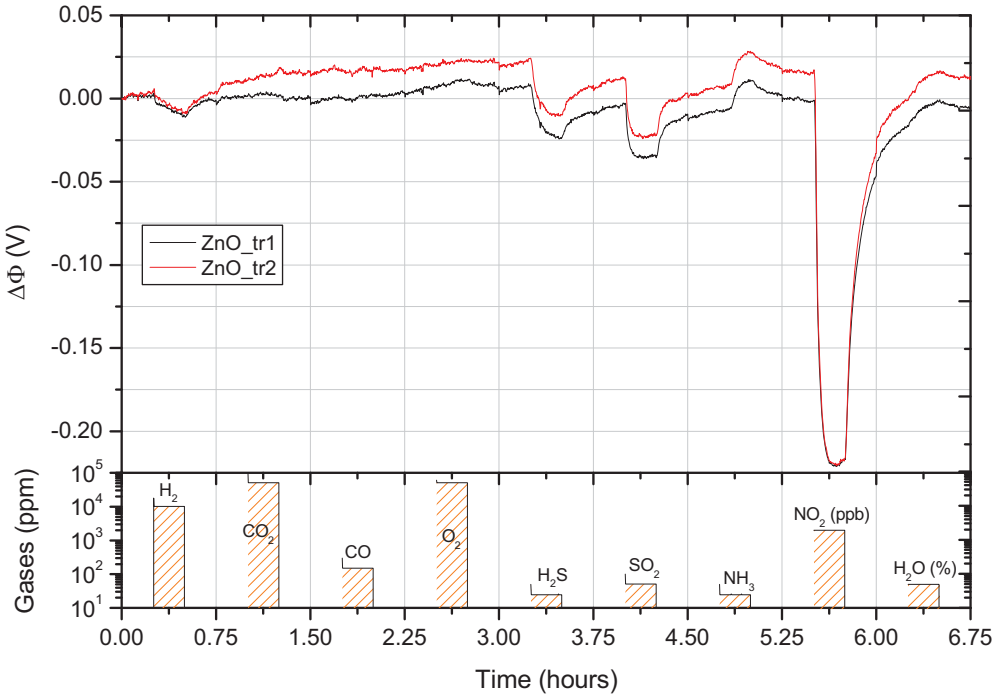

Figure 4.11. Cross sensitivity of the ZnO sensor at temperature of 165°C under dry conditions.

4.2.5 Long-term stability of the ZnO sensor

A long-term stability experiment was carried out 1.5 months after first conditioning at 165°C under dry conditions. The experiment procedure is as follows: first, the sensor is exposed in a constant flow of dry synthetic air (100 ml/min) for 30 min in order to obtain a stable sensor signal. Then, it is exposed to 5 ppm NO_2 for 30 min to observe its sensitivity. Afterwards, exposing NO_2 is turned off for 30 min to investigate reversibility of the sensor signal. Finally, this cycle is repeated for total time of 11.5 hours to study reproducibility of the sensor signal.

The results are depicted in Fig. 4.12. The signal height remains stable about 180 mV for 5 ppm NO_2. Nearly no base line drifts are observed in this condition. This proves that the sensor has well stability and reproducibility to NO_2 exposing.

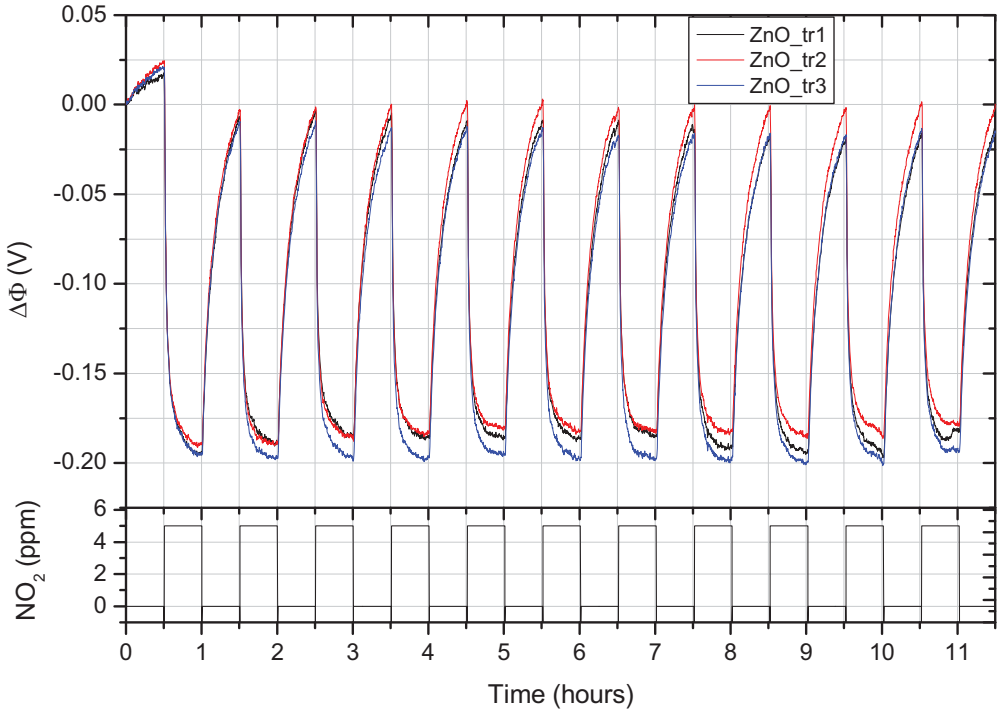

Figure 4.12. Long-term stability and reproducibility of the ZnO sensor after 1.5 months at 165°C under dry conditions.

4.3 Tin oxide/Copper (SnO_2/Cu) for nitrogen dioxide (NO_2) detection

NO_2 is still very interesting to be investigated in the concentration range of ppb because this gas is one of main pollutant. In the section 4.2 has been presented that ZnO sensor is sensitive to NO_2 in the concentration range between 1 and 20 ppm. Unfortunately, the sensor needs high temperature about 190°C to detect NO_2 at concentration below 2 ppm. In this condition, its response time is also slow.

This section is aimed to investigate sensing properties of porous SnO_2 modified with Cu clusters. Addition of Cu clusters at the SnO_2 surface is proposed to dissociate NO_2 molecules to be N and O atoms.

4.3.1 Sensing properties of the SnO_2/Cu films

Sensing properties of the films to NO_2 exposure were measured by using the FG-FET principle. In order to investigate effect of Cu clusters on NO_2 gas sensing properties, three different sensors with Cu, SnO_2 and SnO_2/Cu films as gas sensitive films were made. Fig. 4.13 shows electrical

response of the Cu, SnO_2 and SnO_2/Cu sensors to 2000 ppb NO_2 at 95°C under dry condition. It is observed that the SnO_2 film modified with Cu clusters exhibit the highest sensitivity to NO_2. Accordingly, the Cu clusters play an important role and affect on NO_2 sensitivity of the sensor because the clusters capture and dissociate NO_2 molecules, so the surface become an acceptor surface state. Due to small size of the clusters surface, interaction between the clusters with NO_2 takes short time.

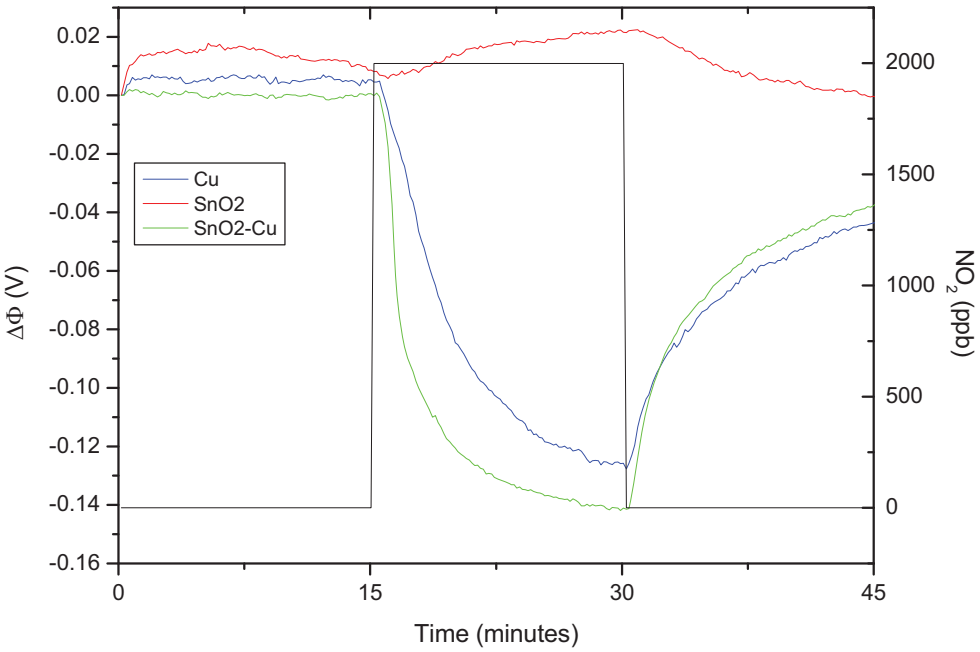

Figure 4.13. Response of Cu, SnO_2 and SnO_2/Cu sensors to 2000 ppb NO_2 at 95°C under dry conditions.

4.3.2 Temperature effect on the SnO_2/Cu sensor

An experiment corresponding to temperature effect on the sensor towards NO_2 exposure was carried out using a single transistor. This is aimed to obtain a reasonable comparison. The temperature was varied in the range between room temperature and 165°C. Each temperature value was investigated for 4.25 hours with increased NO_2 concentration exposure. Fig. 4.14 shows the response of the sensor towards NO_2 at different temperature under dry condition.

Operation at 165°C confirms that the sensor offers negligible base line change and fast response time t_{50}~10 s as well as reversible signal to low

NO_2 concentration exposure whereas operating at low temperature shows the sensor response to NO_2 exposure is very slow. The other effect can be observed that the signal height of the sensor decrease with increased temperature. It was found that optimal operating temperature of the sensor is 165°C. However, it should be note that the SnO_2/Cu sensor can be operated in the temperature range between room temperature and 165°C.

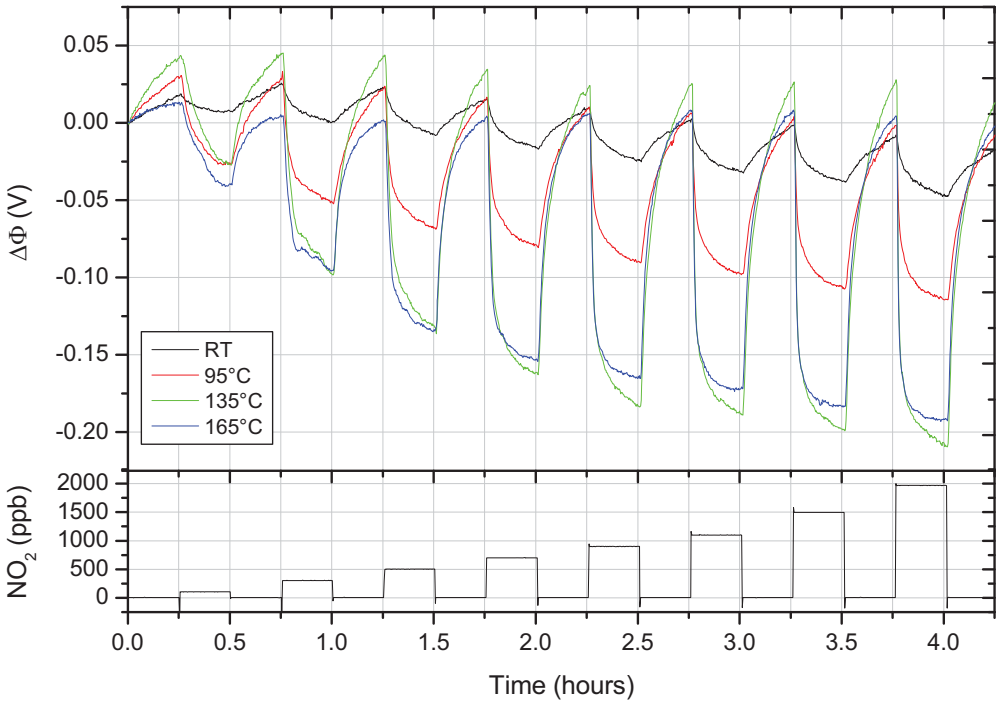

Figure 4.14. Response of the SnO_2/Cu sensor towards NO_2 in the temperature range between room temperature and 165°C under dry conditions.

4.3.3 NO_2 concentration dependence of the SnO_2/Cu sensor

Concentration is one important gas parameter. The ability of the sensors can be seen from the gas concentration value, which can be detected. Usually, the concentration dimension is in part per million (ppm) or part per billion (ppb). Investigation related to the NO_2 concentration dependence of the sensor was carried out at operating temperature of 165°C under dry condition. For measurement at humid condition the test gases are humidified by flowing dry synthetic air through a water bubbler at room temperature. Equilibrium on the film surface can be achieved with exposing the sensor in a constant flow of dry synthetic air (100 ml/min) for 15 min. To

investigate the concentration dependence of the sensor, it was exposed to several NO_2 concentrations in ppb range for 15 min. This cycle was repeated for several times.

Fig. 4.15 shows the resulting signals. The sensor depends strongly on the gas concentration. Five signals of the sensor have identical behavior to NO_2 concentration exposure. The signals decrease with increased concentrations of NO_2. Increasing concentration affect also on response time of the sensor. The response time increase with increasing concentration.

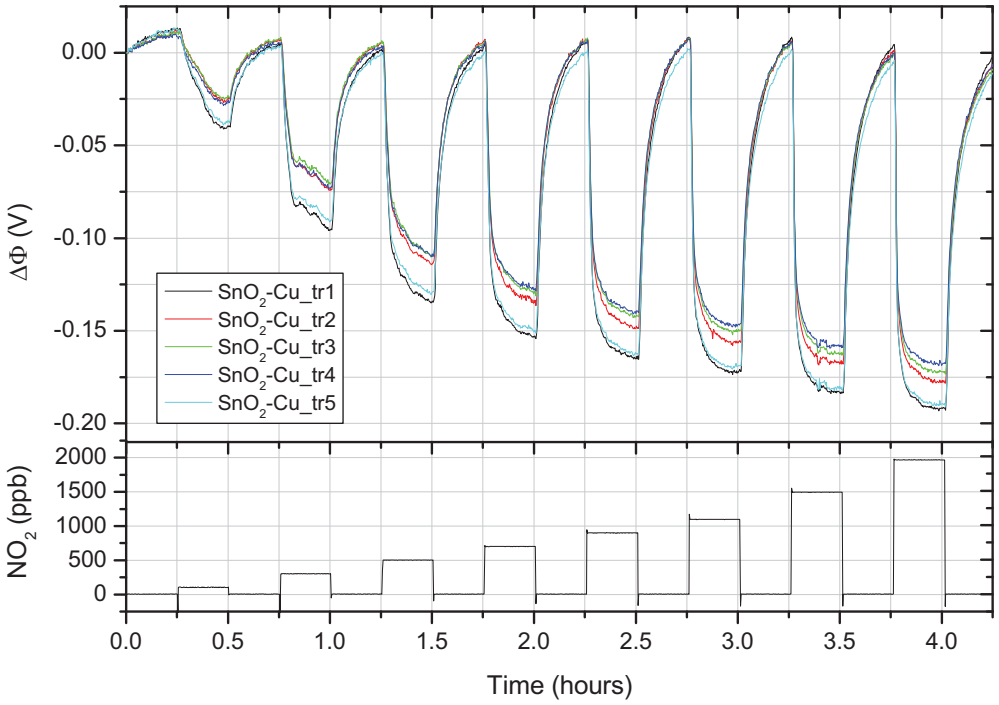

Figure 4.15. Measurement of increased NO_2 concentrations with the SnO_2/Cu sensor at 165°C under dry conditions.

4.3.4 Cross sensitivity of the SnO_2/Cu sensor

Cross sensitivity of the sensor was characterized by exposing it to H_2, CO_2, CO, O_2, H_2S, SO_2, NH_3, and H_2O vapor at 165°C under dry condition. The gases were exposed serially with interrupted the synthetic air for 30 min. Fig. 4.16 represents that cross sensitivity of the sensor is low. It responds strongly only to NO_2 with negative reversible signals and weakly to SO_2 with negative irreversible signals. It also responds very weakly to H_2S. This

indicates that porous SnO_2 film modified with Cu clusters is a promising new sensitive material for NO_2 detection at low concentrations.

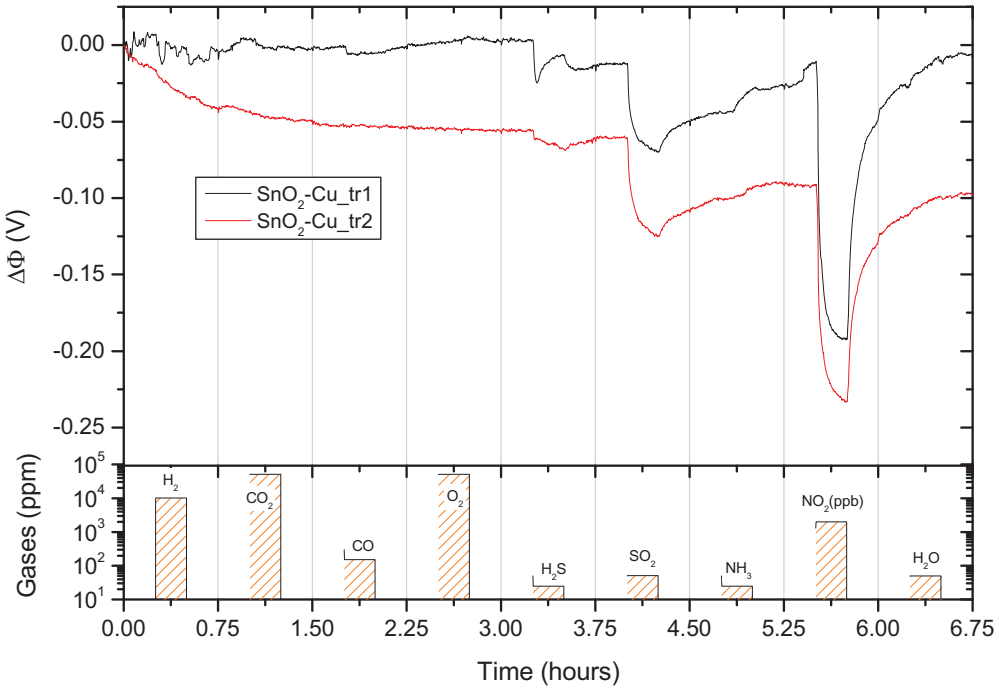

Figure 4.16. Cross sensitivity of the SnO_2/Cu sensor at 165°C under dry conditions.

Chapter 5

Modification of Pt sensor

In this chapter the modified platinum as hydrogen sensitive film in FG-FET sensor system was investigated. SEM, EDX and XPS were employed to characterize the surface of the film. Work function changes with respect to various hydrogen concentrations were measured as a function of temperature and humidity. Additionally an annealing effect on the sensing properties of the film to H_2 exposure was investigated.

5.1 Platinum (Pt)

Platinum is known as a chemical sensitive layer for hydrogen detection by the work function principle [56]. Unfortunately, the sensors have poor selectivity at room temperature. It means that the sensors react to almost all test gases as represented in Fig. 5.1. The active carbon filters have been used to reduce cross sensitivity of the Pt sensor [43]. Moreover the signals are not stable with increasing operating temperature above 95°C as depicted in Fig. 5.2.

An experiment related to investigation of unstable signal due to increasing operating temperature on the sensor was carried out. For this experiment, the sensor is exposed to H_2 in the concentration range between 1000 and 20000 ppm at a temperature of 95°C under dry conditions. At this

condition, the signals decrease rapidly to H_2 exposure at concentrations of 5000 and 7000 ppm as shown in Fig 5.2. Afterwards the signals are stable again to next H_2 exposure.

A possible explanation is as follows: the interaction between H_2 and Pt surface strongly depends on temperature [41]. The oxygen chemisorption at the Pt surface changes with temperature [57, 58]. In the temperature range between 100 and 500°C, O_2^- converts into O^- specie at the surface by taking one electron from the bulk conduction electron (ionosorption) [59]. As a consequence, OH-groups are formed at the surface when it is exposed to H_2. This is proved by the rapid decreasing signals during H_2 exposure because free electrons, which are generated in the forming OH-groups, transfer from the surface to the bulk conduction electron and induces an accumulation layer near the surface. Afterwards, H atoms interact with Pt-OH at the surface. The following reaction is related to interaction OH-groups and hydrogen on the Pt surface [60]

$$OH_{ads} + H_{gas} \rightarrow H_2O_{ads} \tag{5.1}$$

$$H_2O_{ads} + O_{gas} \rightarrow 2\,OH_{ads} \tag{5.2}$$

The ‘gas’ and ‘ads’ indicate the gaseous as well as at the Pt absorbed condition of the respective molecules and atoms. Both of the reactions are a valid mechanism to form synthetic water with Pt as catalyst. The reversible signals of the sensor show that the mechanism is also reversible. The signals are stable from room temperature to 165°C. Unfortunately the sensor has still a problem with its long-term stability due to decomposition of OH-groups.

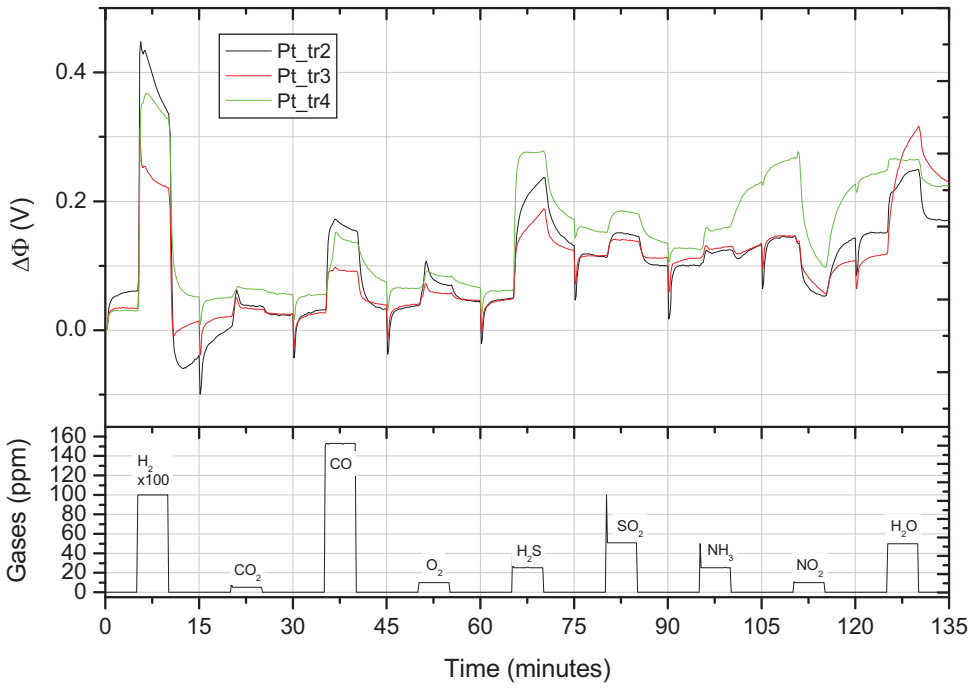

Figure 5.1. Cross sensitivity of the Pt sensor at room temperature under dry conditions.

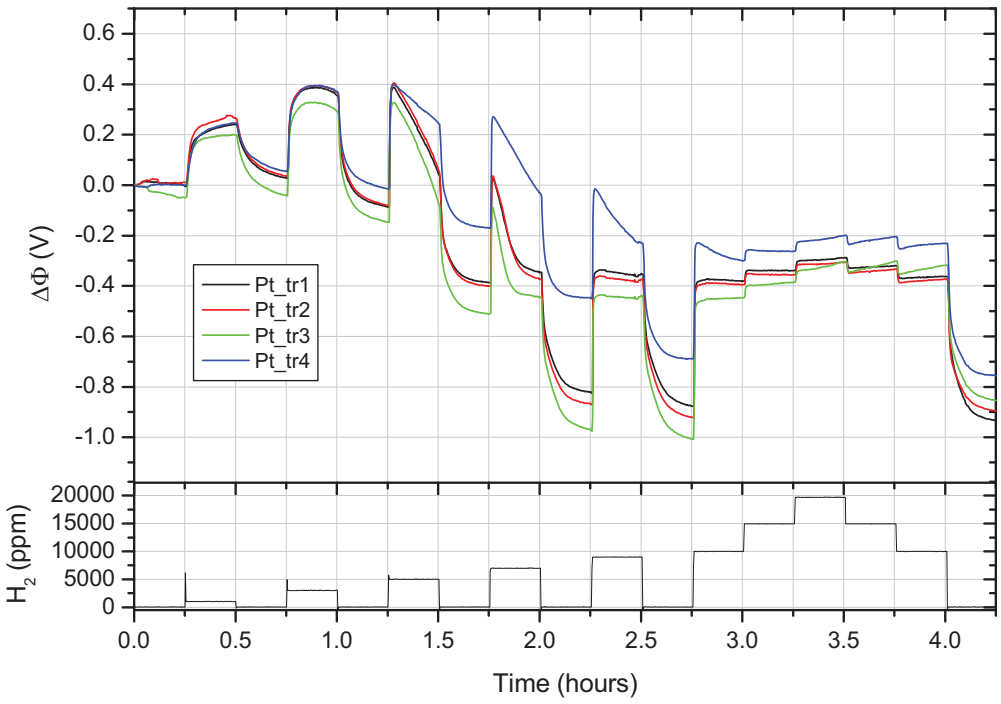

Figure 5.2. Characteristic of the Pt sensors to H_2 concentration at 95°C under dry conditions.

5.2 Modified platinum with tin oxide (Pt/SnO_2)

The first SnO_2 based gas sensors were developed by Taguchi in the 60s [61-63] and sensors of this company are still among the leading SnO_2 gas sensors. SnO_2 is a wide band gap n-type semiconductor, which crystallizes in the rutile structure (tetragonal structure, space group D_{4h}^{14} or – in another notation – $P4_2/mnm$) like for example TiO_2, CeO_2 or GeO_2 [64, 65]. With an optical band gap of 3.6 eV, this material has a low conductivity at room temperature, but its conductivity can be increased by introducing dopants that also are importance to tailor SnO_2 based gas-sensors to higher sensitivity and selectivity towards gases of interest. The used dopants are for example Pd [34], Pt [46, 66], Sb [67] or V [68].

The sensing mechanism is based on the fact that the adsorption of oxygen on the semiconductor surface can cause a significant change in the electrical resistance of the material. The formation of adsorbed oxygen results an electron-depletion surface layer due to electron transfer from the oxide surface to oxygen [69].

5.2.1 Preparation of the SnO_2 films

Pure tin (Sn) was thermally evaporated on the gates. In order to achieve an oxidation reaction between Sn and O_2, a micro leak was used to adjust an oxygen pressure of $2x10^{-2}$ mbar in the vacuum chamber. The evaporation rate was kept between 0.05-0.1 nm/s for a total film thickness of 50 nm. Thickness of the film was measured by using a quartz micro balance frequency of 6 MHz.

5.2.1.1 Surface characterization

Chemical compositions of the films were analyzed by using XPS. The analysis result can be seen in Fig. 5.3. The binding energy spectrum is dominated by core level peaks of tin and oxygen with concentrations of 50% and 37%, respectively. This result shows that the obtained films are non-stoichiometric SnO_2.

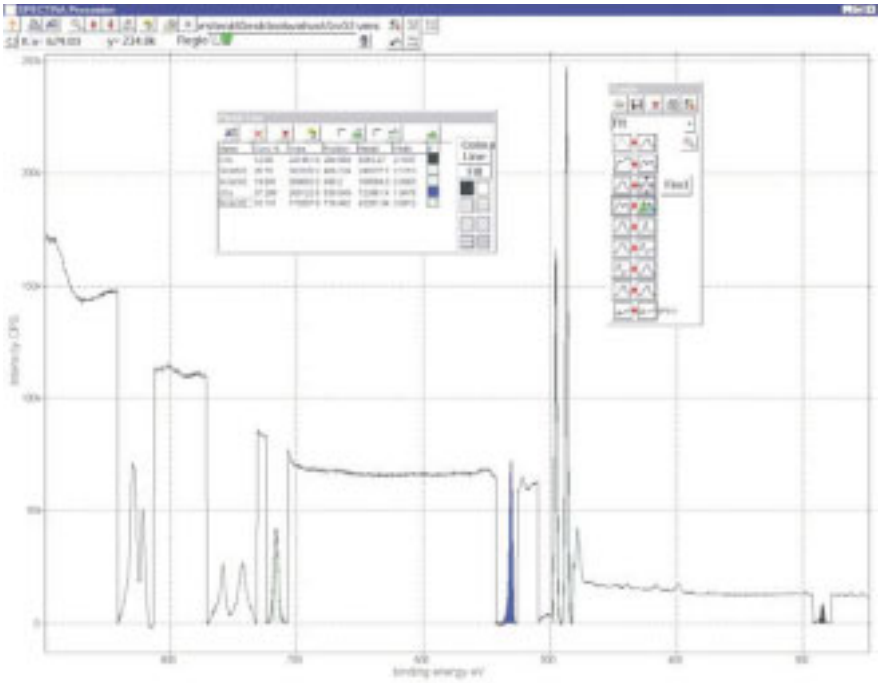

Figure 5.3. Typical XPS survey spectrum of the used Pt/SnO_2 surface.

Surface morphology of the film was characterized by using SEM. The obtained porous SnO_2 films of 50 nm are always transparent. The characterization result can be seen in Fig. 5.4. Many cracks and porous can be observed on the surface with a width less than 25 nm.

The film was also characterized by using EDX to determine the qualitative composition of the surface. The characterization was done at 5 keV primary electron energy, 6 nA beam current and (4 μm x 3 μm) area. These parameters have been used to make sure that the characterization is only near to the surface. At these parameters, electron beam strikes the surface of a conducting sample up to a depth of 50 nm. It can be seen that an EDX signal from Pt was measured also. This is a proof for the porosity of the film. N-peak appears at the surface because oxygen, which is used in oxidizing process, consists of 2 ppm nitrogen.

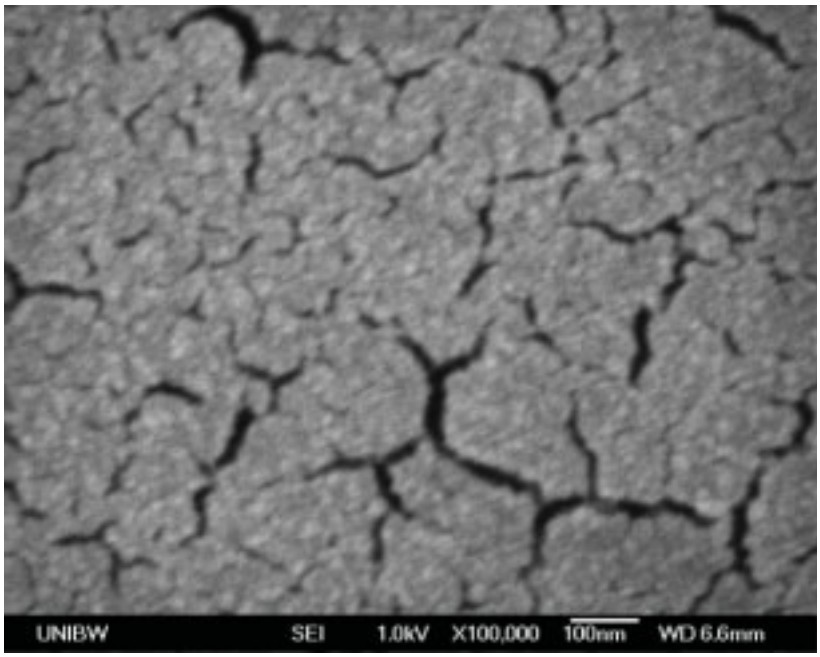

Figure 5.4. SEM image of the Pt/SnO_2 surface.

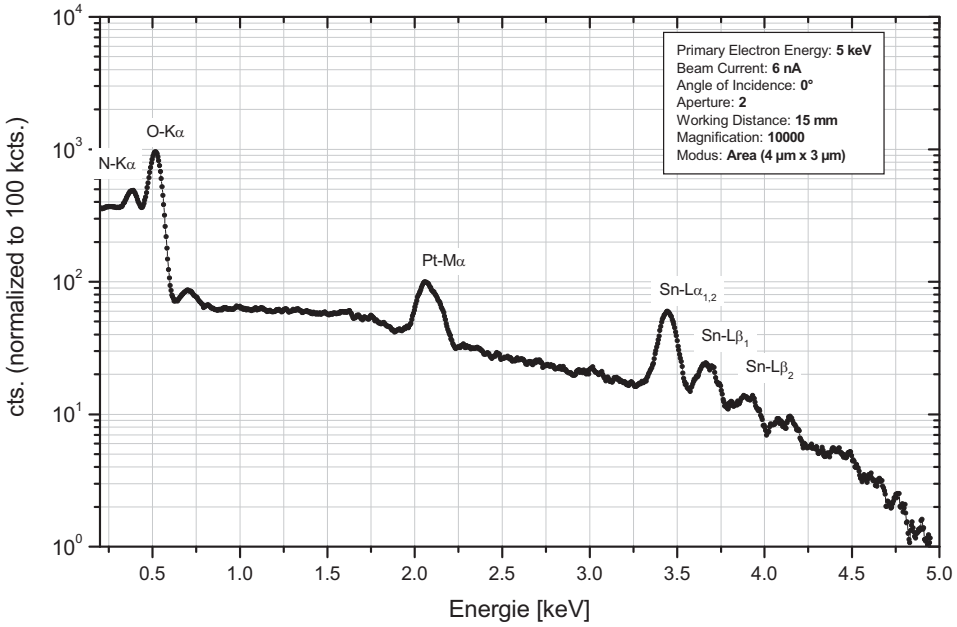

Figure 5.5. EDX measurement of the Pt/SnO_2 surface.

5.2.1.2 Effect of porous SnO_2 on the Pt surface

Effect of porous SnO_2 on the Pt surface related to H_2 detection was investigated by Dr. G. Lillienkamp and B. Borkenhagen at TU-Clausthal. For this investigation samples of Pt and Pt/SnO_2 films were made at UniBw Munich. Both of the samples were attacked with electron beam (1 μA, 0.6 eV,

10 s) in a Low Energy Electron Microscope (LEEM). Fig. 5.6 and 5.7 show condition of the Pt and Pt/SnO_2 surfaces before and after electron bombardment, respectively.

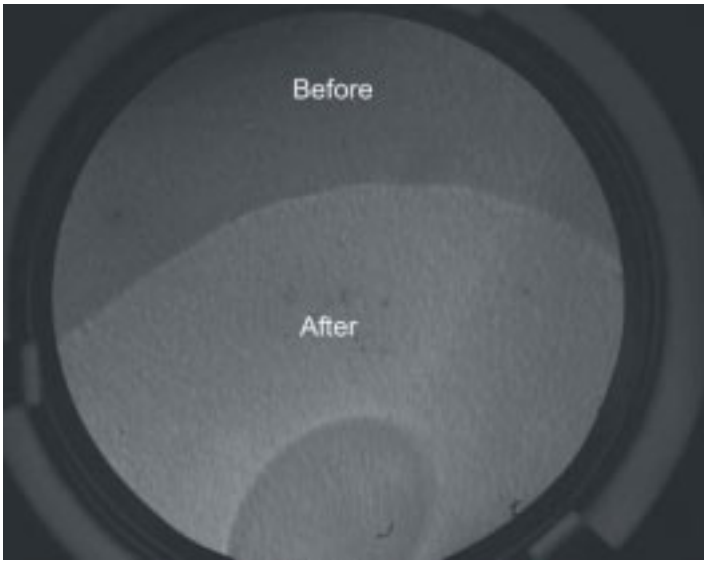

Figure 5.6. LEEM image of the Pt surface before and after electron beam bombardment.

Figure 5.7. LEEM image of the Pt/SnO_2 surface before and after electron beam bombardment.

The electron beam changes the surface in a similar way as H_2. After the bombardment the contrast is enhanced at the Pt surface. A possible reason is that reduction reaction of Pt-O is occurring due to electron bombardment. Because pure Pt surfaces show more contrast. On the other

hand, the SnO_2 surface change is not observed due to electron beam bombardment.

Work function changes of the Pt/SnO_2 film due to H_2 and O_2 interactions were measured by using LEEM at room temperature. Fig. 5.8 shows that $\Delta\Phi$ is negative (-0.32 V) when the surface is exposed to $1x10^{-5}$ mbar of H_2 and positive (0.42 V) when the surface is exposed to $1x10^{-5}$ mbar of O_2. During the vacuum process the work function remains. The work function change still occurs although the Pt surface is coated with porous SnO_2. Accordingly we conclude that the interaction between adsorbed O_2 and H_2 occurs not at the SnO_2 surface but at interface between Pt and SnO_2.

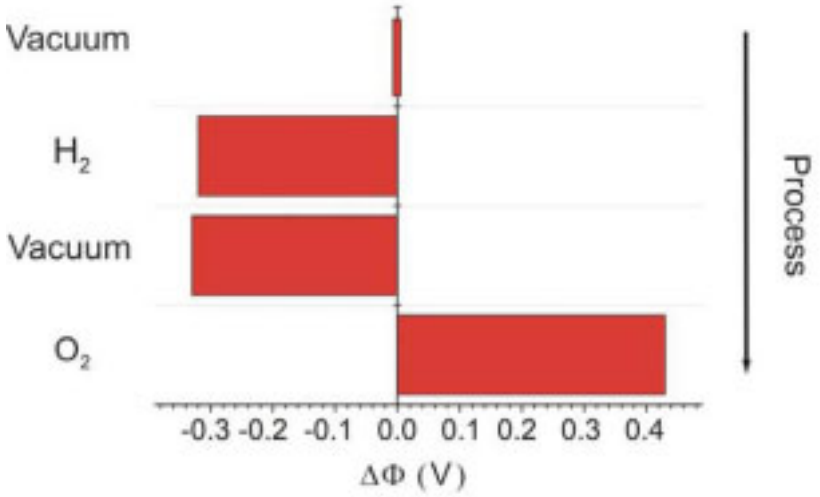

Figure 5.8. Work function change measurement by using the LEEM.

5.2.1.3 Interaction between SnO_2 and H_2

An experiment corresponding to interaction between H_2 molecule and SnO_2 was also carried out. For this experiment, titanium (Ti) was deposited on the gate by using DC sputtering. Then SnO_2 was thermally evaporated on it. Titanium has been used because it does not react with H_2 molecules. Sensing property of the Ti/SnO_2 sensor was investigated with exposing it to 10000 ppm H_2 in synthetic air at a temperature of 95°C under dry conditions.

Fig. 5.9 shows that the sensor does not respond to H_2 exposure. A work function change is not observed due to H_2 interaction. This proves that no interaction between adsorbed H_2 and O_2 molecules at SnO_2 is occurring without Pt as catalyst.

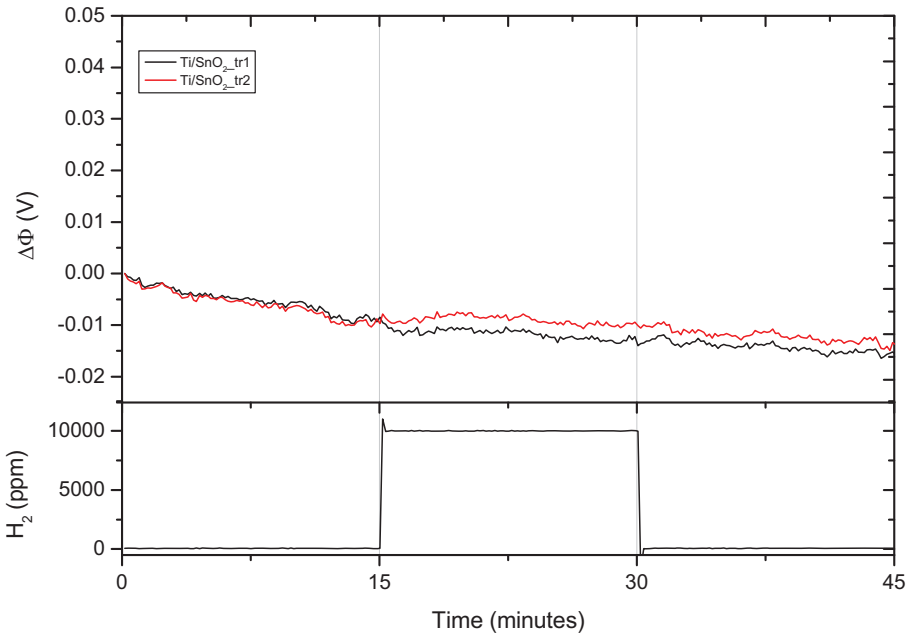

Figure 5.9. Response of the Ti/SnO_2 sensor to H_2 at temperature of 95°C under dry conditions. No interaction between H_2 molecules and SnO_2.

5.2.2 Gas sensing mechanism

It has been known that non-stoichiometry of SnO_2 is an n-type semiconductor [64, 65]. Therefore the species, which tend to trap electron from the semiconductor are easily adsorbed. Under usual operating conditions with synthetic air (20% O_2 in 80% N_2) the SnO_2 is mainly covered by oxygen species [70].

Reactions of adsorbed oxygen at Pt/SnO_2 with H_2 are based on the Schottky barrier, as schematically shown in Fig. 5.10. The Schottky barrier is formed at the interface between Pt and SnO_2 by the electron transfer from SnO_2 to Pt because the value of the Pt work function (5.65 eV) is higher than the electron affinity of SnO_2 (4.49 eV) [71].

At room temperature the equilibrium of the O_2^- coverage with gaseous O_2 is approached slowly. With increasing temperature O_2^- and O^- convert to $2\,O^-$ and O^{-2} with taking one electron from the bulk conduction electron, respectively. This causes an increasing density of surface charge related to decreasing conductivity and increasing work function of SnO_2 (see Fig. 5.10, a). The reactivity of O^-, which is dominant species, is high, whereas O^{-2}

species are unstable and do not play important role in determining the sensitivity [59, 69]. Therefore, the oxygen adsorption can be written as

$$O_2 + 2e^- \leftrightarrow 2\,O^- \tag{5.3}$$

If the sensor is exposed to mixture gas from H_2 and synthetic air, H_2 diffuses through the SnO_2 film to the interface between Pt and SnO_2. Thus, the Pt surface (catalyst) dissociates H_2 into H atoms. Subsequently the hydrogen atoms migrate to adsorption or reaction sites on the SnO_2 surface (spill over effect). Adsorbed hydrogen atoms act as donors, which provide additional free electrons into the bulk conduction electron and induce an accumulation layer [69]. As a result the conductivity increases and the work function decreases (see Fig. 5.10, b). In any case, a dissociation of the hydrogen molecule is required because adsorbed H_2 molecules do not change the work function. The reaction between adsorbed hydrogen and oxygen atoms at the interface is as following

$$H + O^- \rightarrow OH + e^- \tag{5.4}$$

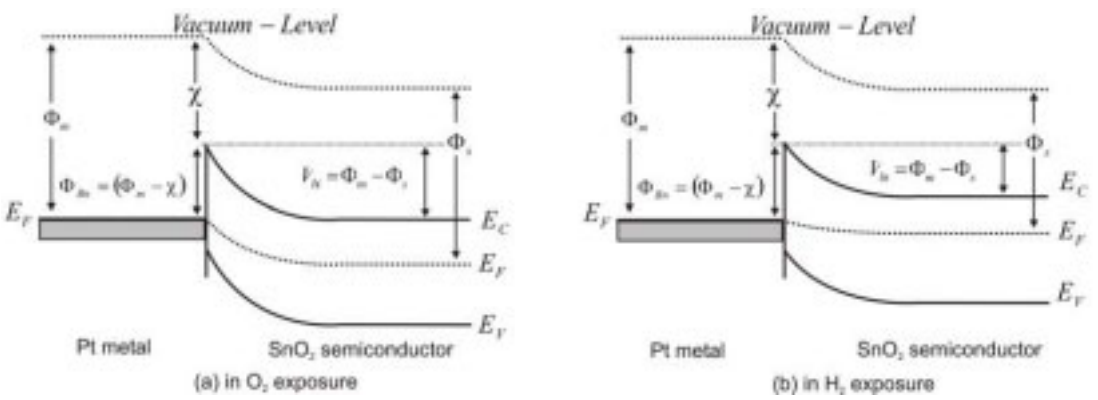

Figure 5.10. H_2 sensing mechanism based on the Schottky barrier at the interface between Pt and SnO_2.

5.2.3 Sensing properties of Pt/SnO_2 film

Sensing properties of Pt and Pt/SnO_2 films to various H_2 in concentration range between 1000 and 9000 ppm were investigated in FG-FET sensor system at temperature of 95°C under dry conditions. The sensor is exposed to each H_2 concentration for 30 min. Afterward the sensor is rinsed with synthetic dry air for 30 min in order to observe their reversibility.

It can be seen from Fig. 5.11 that signals of the Pt sensor (black lines) drift at 9000 ppm H_2 exposure and the unstable base line is observed. On the other hand, signals of the Pt/SnO_2 sensor (red lines) can well detect various H_2 concentrations. The unstable signals are not observed anymore. Furthermore the base line remains stable. In this case, non-stoichiometry of SnO_2 provides reactive oxygen atoms species O^- when the sensor is exposed to synthetic air. Due to the species at SnO_2 relative mobile with temperature [72], they react with dissociated H_2 molecules. This reaction is not occurring at the Pt surface but at SnO_2 surface near the interface due to the spill-over effect when the sensor is exposed to H_2.

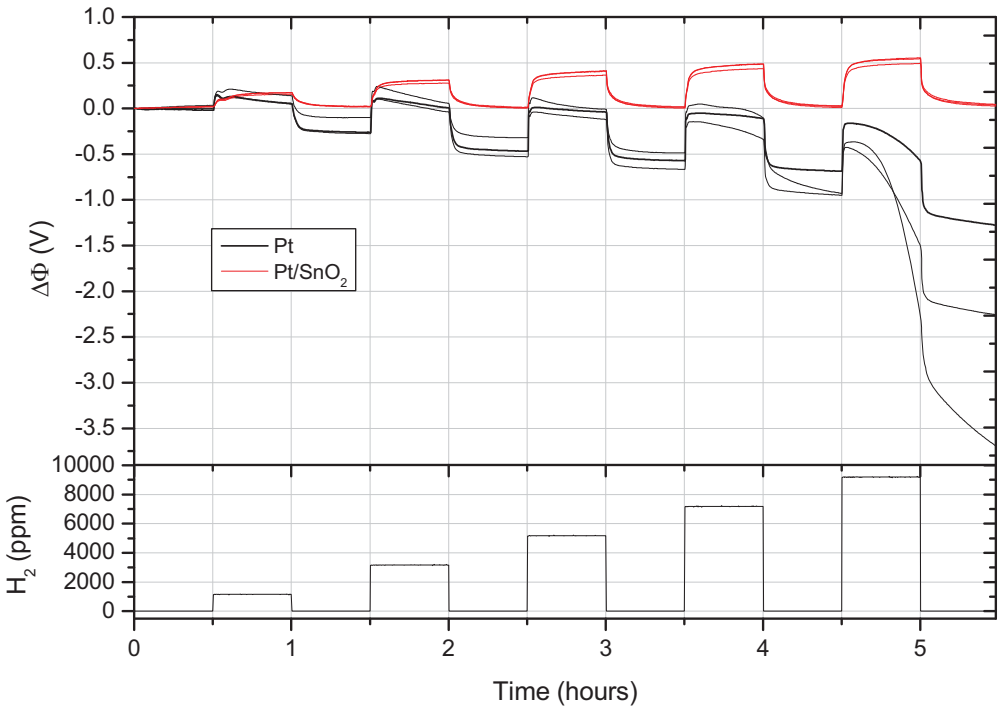

Figure 5.11. Comparison of sensing characteristic between the Pt and Pt/SnO_2 sensors at 95°C under dry conditions.

5.2.3.1 Temperature effect on the Pt/SnO_2 sensor

Temperature is an important parameter of the sensor because diffusion on and in the SnO_2 surface depends on temperature. In order to investigate temperature influence the sensor is exposed to various H_2 concentrations between room temperature and 165°C. The temperature is achieved by using an integrated poly-heater.

Fig. 5.12 represents the temperature influence on the sensor. It can be seen that the sensor depends strongly on temperature. Response of the sensor to H_2 exposure increases with increasing temperature. At room temperature the sensor responds slowly to H_2 exposure. The signal needs more than 15 min to return to the base line. Above 135°C a signal drift is observed. Possibility of reason is that reaction between hydrogen and oxygen atoms is occurring at the Pt surface. The best sensor response is exhibited at an operating temperature of 95°C.

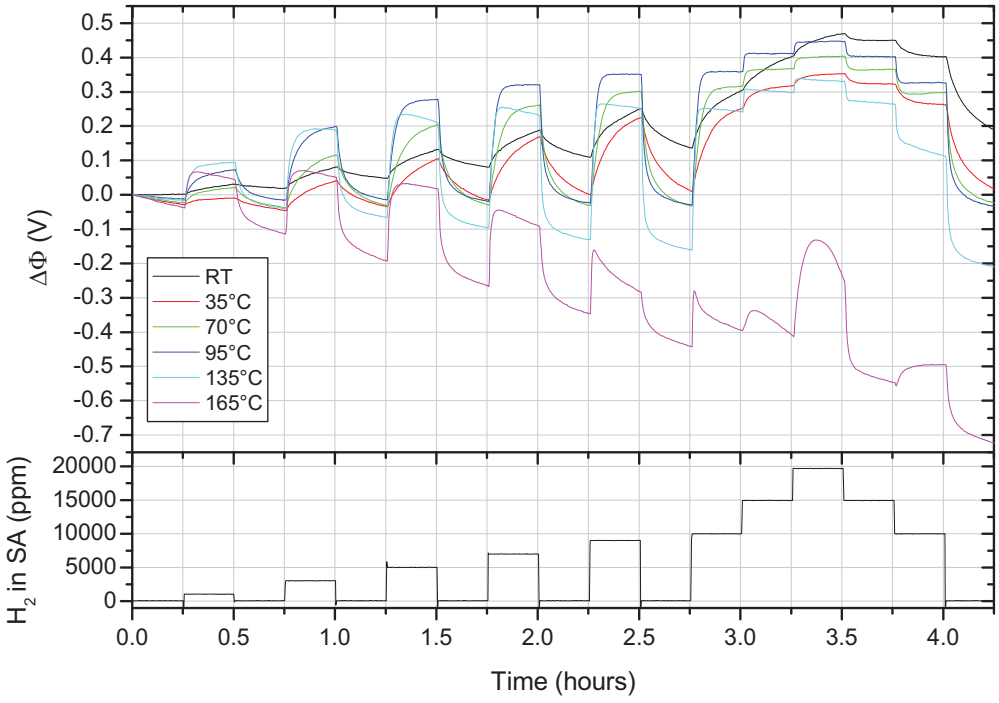

Figure 5.12. Temperature effect on the Pt/SnO_2 sensor under dry conditions.

5.2.3.2 H_2 concentration dependence of the Pt/SnO_2 sensor

The response of the Pt/SnO_2 sensor with respect to various H_2 concentrations was firstly investigated at the operating temperature of 95°C under dry conditions. Equilibrium on the surface can be achieved with exposing the sensor in a constant flow of dry synthetic air (100 ml/min) for 15 min. In order to examine sensitivity and reversibility of the sensor, it is exposed to various H_2 concentrations for 15 min. Then it is rinsed with synthetic dry air for 15 min. This cycle is repeated several times.

Fig. 5.13 shows the sensor response towards various H_2 concentrations at 95°C under dry conditions. Two signals of the sensor show same type of response to H_2 exposure. The signals increase with increasing H_2 concentration. At a concentration above 7000 ppm, the signals reach the steady state very quickly with response time t_{50}~10 s.

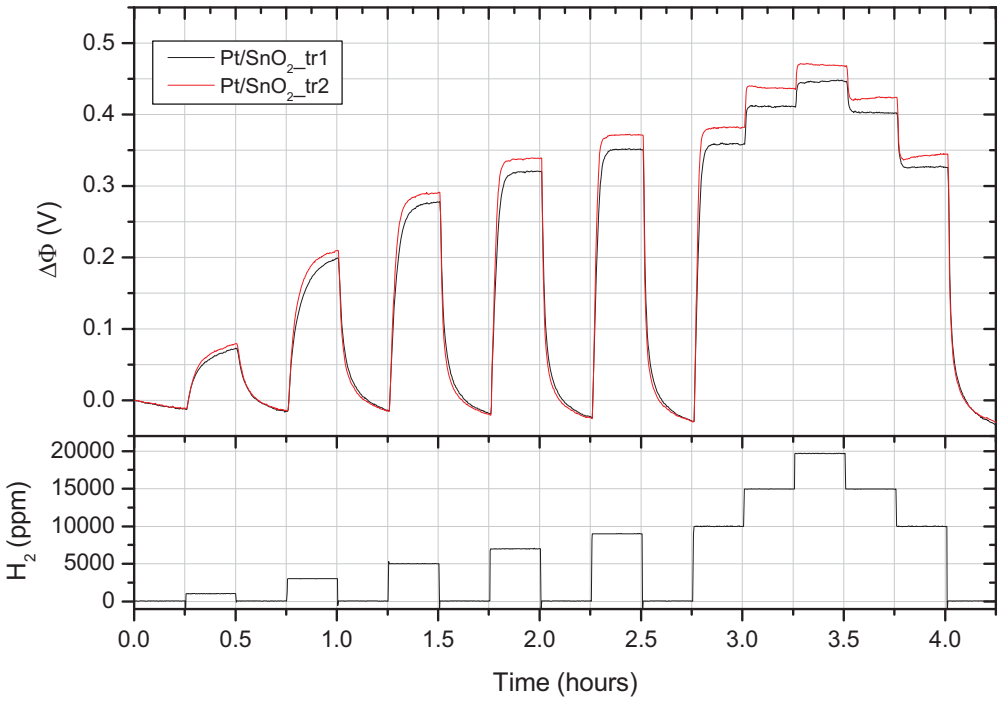

Figure 5.13. Response of the Pt/SnO_2 sensor to various H_2 concentrations at operating temperature of 95°C under dry conditions.

The logarithmic dependence of response on the H_2 concentration is shown in Fig. 5.14. The signal increases linearly with increasing logarithmic H_2 concentration. The logarithmic dependence of the response on the concentration permits the use of the FG-FETs over a wide concentration range. The obtained linier fit is as follows:

$$\Delta\Phi = 0.3\frac{\mathrm{V}}{\mathrm{ppm}} \cdot \mathrm{c}(\mathrm{H}_2) - 0.9\mathrm{V} \qquad (5.5)$$

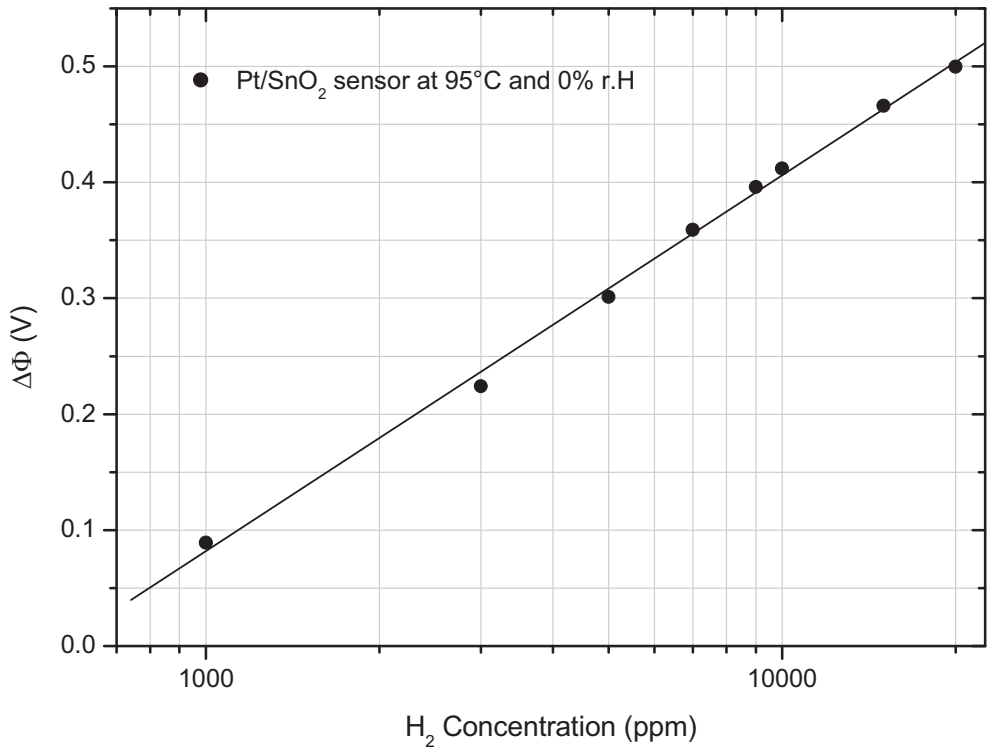

Figure 5.14. Calibration curve of the signal at 95°C under dry conditions.

5.2.3.3 Humidity effect on the Pt/SnO_2 sensor

To analyze mixed gas behavior especially reduction in sensitivity of the sensor to H_2 gas exposure with increasing the humidity, measurements of various H_2 concentrations were carried out under dry and humid condition at 95°C. The concentration was humidified by flowing dry synthetic air through a water bubbler at room temperature.

Fig. 5.15 represents humidity effect on the sensor. The signal corresponding to work function change $\Delta\Phi$ decreases with increasing relative humidity at each H_2 concentration. In humid condition H_2O molecules diffusion through the cracks affect and play important role in decreasing sensitivity of the sensor. At low temperature desorption can be attributed to adsorbed H_2O molecules [59].

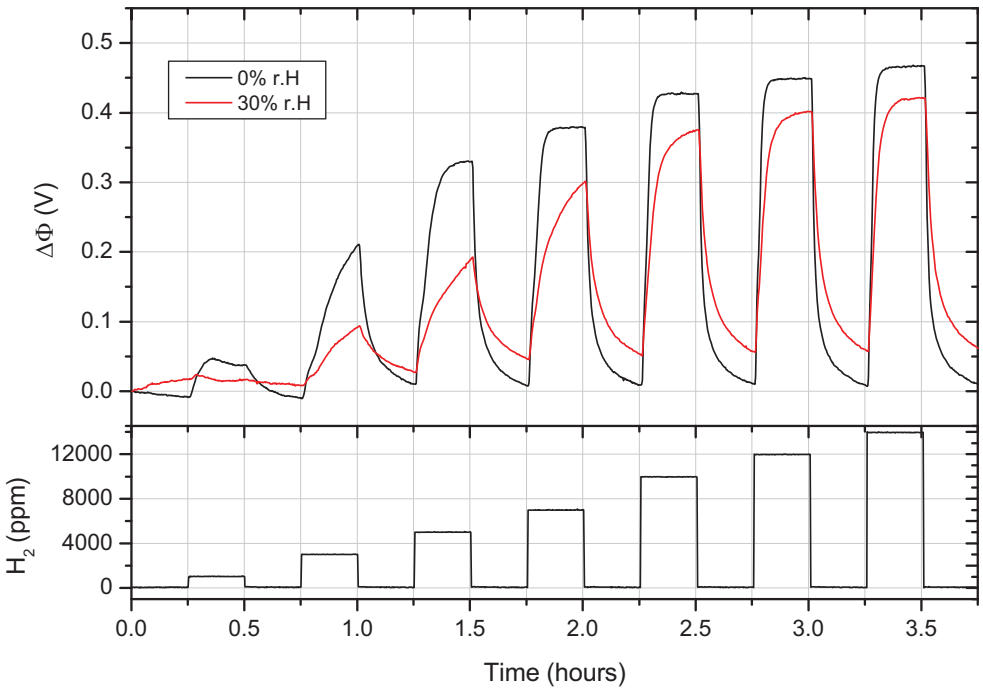

Figure 5.15. Response of the Pt/SnO2 sensor to various H_2 concentrations at operating temperature of 95°C under dry and humid (30% r.h) conditions.

With raising the temperature up to 135°C, the sensitivity in humid atmosphere significantly increases as showed in Fig. 5.16. At this condition H_2O molecules are adsorbed at the SnO_2 surface and dissociated into formation of OH-groups. These processes generate an electron and an oxygen vacancy as postulated in eq. (5.6) and (5.7). The electron and the oxygen vacancy on the right-hand side of the eq. have to move towards the bulk and become effective as a donor. This can improve the sensitivity of the sensor when it is exposed to H_2 because the bulk conduction electron accepts electrons not only from resulting reduction reaction between H_2 and adsorbed O^- species but also from the dissociating H_2O. The following reactions were postulated for the dissociate interaction of water with SnO_2 [69, 73].

$$H_2O + Sn_{lat} + O_{lat} \rightarrow (HO - Sn_{lat}) + (O_{lat}H)^+ + e^- \quad (5.6)$$

or

$$H_2O + Sn_{lat} + O_{lat} \rightarrow 2(HO - Sn_{lat}) + V_O \quad (5.7)$$

with V_O: Oxygen vacancy

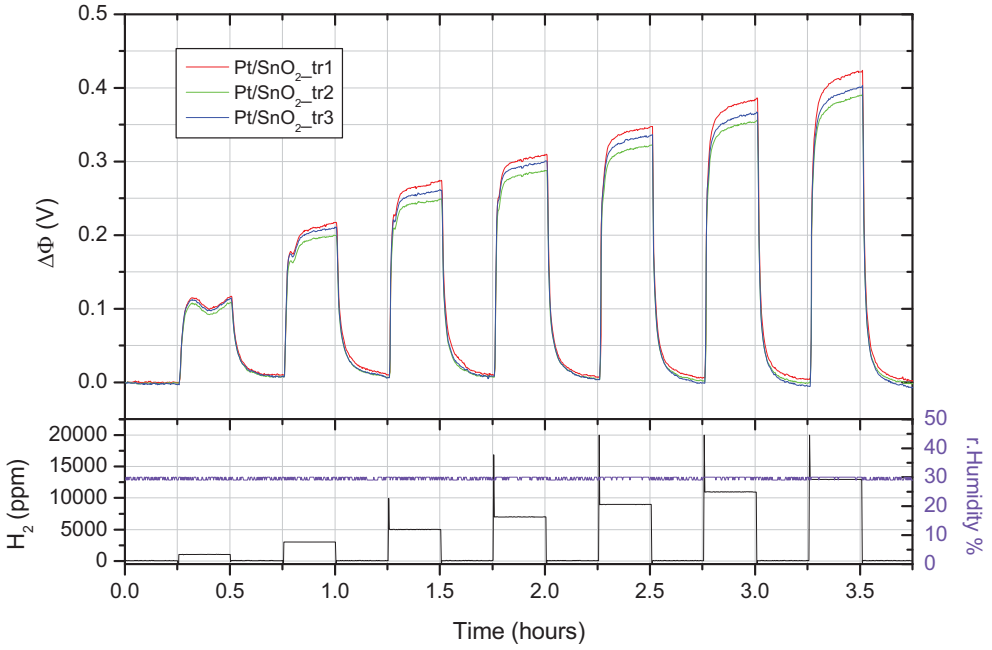

Figure 5.16. Response of the Pt/SnO2 sensor to various H_2 concentrations at operating temperature of 135°C and 30% relative humidity.

5.2.3.4 Cross sensitivity of the Pt/SnO_2 sensor

The cross sensitivity of the sensor was characterized by exposing it to H_2, CO_2, CO, O_2, H_2S, SO_2, NH_3 and H_2O vapor at 95°C under dry conditions. Each test gas is exposed for 30 min. Afterwards the sensor is rinsed for one hour to avoid the previous test gases effect.

Fig. 5.17 shows the cross sensitivity of the sensor. The sensor has well selectivity at 95°C under dry condition. The cross sensitivity is reduced compared to pure Pt. Three signals of the sensor have identical behavior to test gases. No significant signal changes are generated if the sensor is exposed to the test gases. CO sensitivity of the Pt/SnO_2 film is not observed as has been reported by J. Y. Yun [74]. NH_3 being the only exception.

A possible reaction between Pt and ammonia has been predicted by I. Lundström [75]. The signal height depends on temperature. Adsorption of ammoniac at the Pt surface decreases with increasing temperature, because the desorption process increases with increasing temperature. Therefore at temperature of 95°C only few molecules can be adsorbed at the surface.

From Fig. 5.17 it can be seen that the increasing signal due to NH_3 interaction is about 300 mV. The response time is slow and the signal needs more than 30 min to return to base line when the NH_3 is turned off. The chemical reaction of ammonia at the Pt surface in qualitative is explained as following [76]

$$NH_{3\,gas} \leftrightarrow NH_{3\,ads} \tag{5.8}$$

$$NH_{3\,ads} + O_{ads} \rightarrow NH_{ads} + H_2O \tag{5.9}$$

$$2NH_{ads} + O_{ads} + O_2 \rightarrow 2NO + H_2O \tag{5.10}$$

The forming H_2O at the surface plays important role in ammonia detection. Reaction of Pt sensor to ammonia in synthetic air at temperature of 75°C has been investigated by Dr. M. Leu [77].

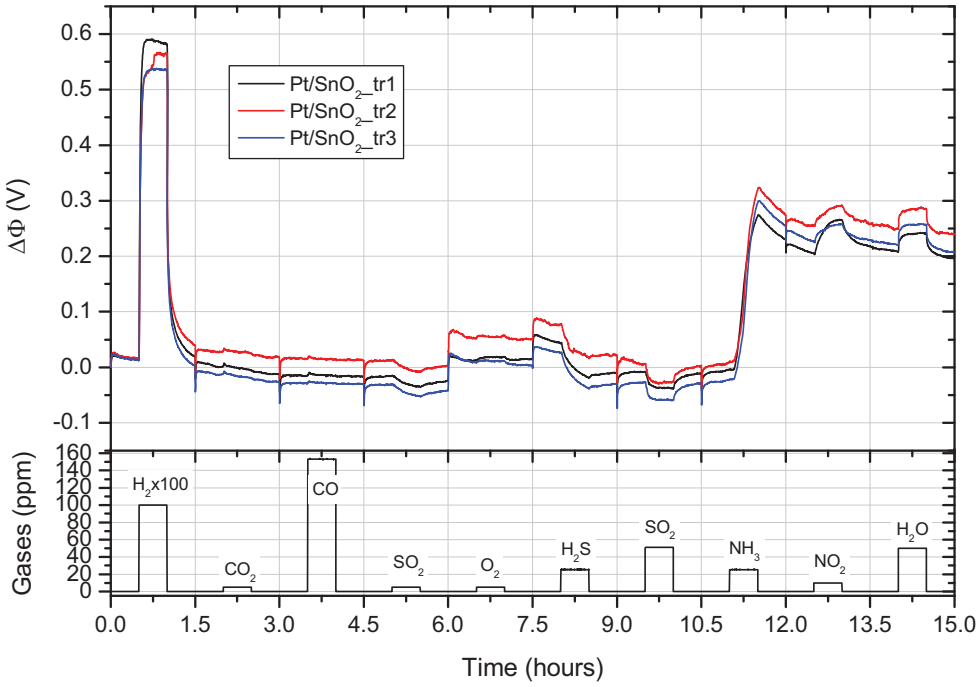

Figure 5.17. Cross sensitivity of the Pt/SnO_2 sensor at 95°C under dry conditions.

5.2.3.5 Long-term stability of the Pt/SnO_2 sensor

The stability is one important criterion that determines the ability of the sensors. An experiment on long-term stability (see Fig. 5.18) represents that the sensor signals remain stable to 10000 ppm H_2 gas exposure at 95°C

under dry condition after 2 months. The signal height of ~400 mV is observed at this concentration. The reproducibility of the output signals is very well. It is observed in eleven cycles of H_2 exposure. The stable and reproducible signals prove that the porous non-stoichiometric SnO_2 film is suited to significantly stabilize the hydrogen response of the Pt surfaces in FG-FETs. However the Pt/SnO_2 sensor is not yet satisfying because its response to H_2 is slow compared to the Pt sensor.

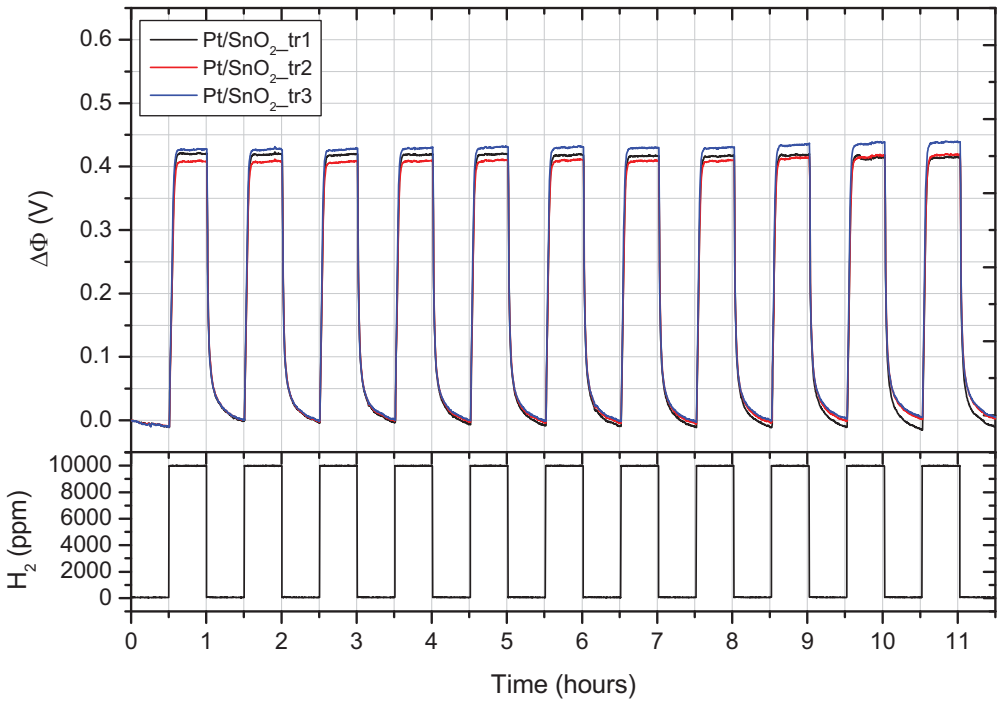

Figure 5.18. Long-term stability of the Pt/SnO_2 sensor to 10000 ppm H_2 at 95°C under dry conditions after 2 months.

5.2.4 Enhanced stability of the Pt/SnO_2 sensor at high temperatures

Stability of the sensor at high temperatures and H_2 concentrations is one of the problems which are considered. It was presented previously that the signals of sensor are not stable above 135°C, although the porous SnO_2 films have been coated on the Pt surfaces. Therefore, in order to enhance the sensor's stability at high temperatures, a pre-treatment at the surface is needed. Procedure of the pre-treatment is as follow: before the sensor is used, it is exposed in a constant flow of dry synthetic air (100 ml/min) for 15 min. Then it is exposed to 1000 and 7000 ppm H_2 in synthetic air with the

interrupted synthetic dry air. The pre-treatment is carried out at 165°C under dry conditions to create OH-groups at the SnO_2 surface. The forming OH-groups can be observed with decreasing signals of the sensor. From Fig. 5.19 can be seen that the forming OH-groups occurs at first and second cycles. Afterwards, the signals are stable again.

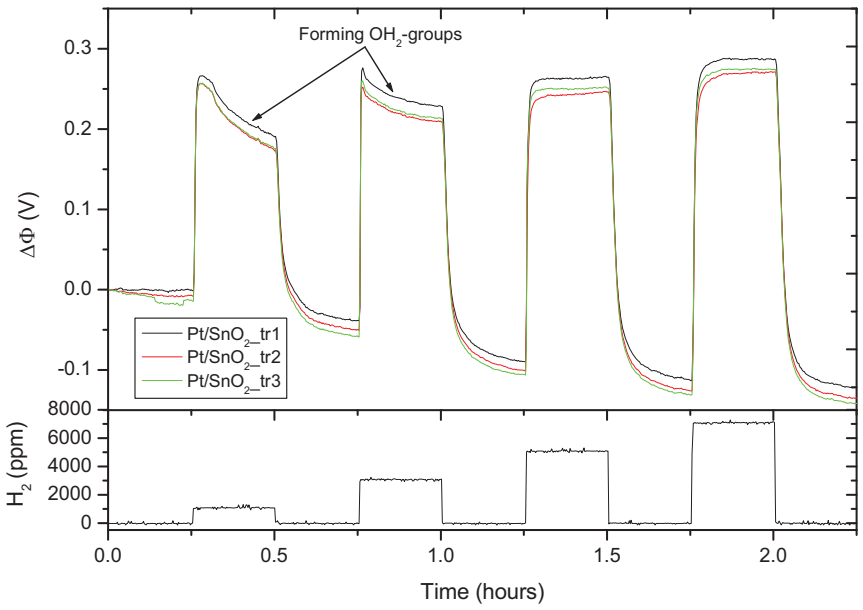

Figure 5.19. Pre-treatment on the Pt/SnO_2 (50 nm) sensor at temperature of 165°C under dry conditions.

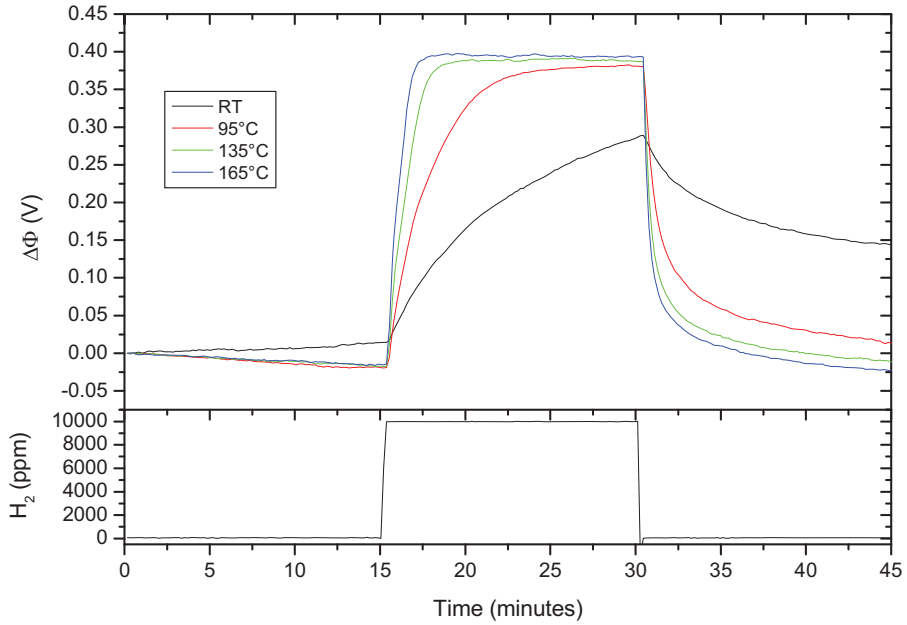

Figure 5.20. Temperature effect on the Pt/SnO_2 (50 nm) sensor to H_2 under dry conditions after the pre-treatment.

Response of the sensor after the pre-treatment was examined to 10000 ppm H_2 exposure in a temperature range between room temperature and 165°C. Fig. 5.20 shows that the signal drift is not observed again at operating temperature above 135°C. The signal is stable and reversible at high temperatures but it has still a problem with its long-term stability.

5.2.5 Improving sensitivity of the Pt/SnO_2 sensor at room temperature

As we have known that the sensor still has disadvantage in H_2 detection at room temperature as shown in Fig. 5.20. H_2 sensitivity of the sensor at room temperature decreases rapidly because of SnO_2 film. In case of the gas sensing mechanism, the reaction between H_2 molecules and adsorbed O atoms species at the SnO_2 surface occurs after H_2 molecules were dissociated by Pt at interface of Pt/SnO_2. This means that H_2 molecules have to diffuse through the SnO_2 film. As a consequence, the molecules need more energy or high temperature to diffuse the film because the process of diffusing particle depends strongly on temperature.

In order to cut short the distance for a diffusing particle, the reduction of the SnO_2 film thickness was achieved. The thickness reduction should be done carefully in order to obtain selectivity of the sensor. Several SnO_2 thicknesses have been tried to achieve optimal results. The SnO_2 thickness of 35 nm exhibits the best result to detect H_2 at room temperature as well as keep the selectivity of the sensor.

The SnO_2 films were deposited by thermally evaporation on the gates. The same parameters of the evaporation have been used. The obtained films with thickness of 35 nm were characterized by using SEM. Fig. 5.21 shows SEM image of the resulting films. The films remain porous and look similarly with the previous obtained films.

The response of the Pt/SnO_2 (35 nm) sensor to H_2 after the pre-treatment with dry synthetic air was examined to 10000 ppm H_2 exposure for 15 min at various temperatures under dry conditions. Fig. 5.22 shows that the sensor can well detect 10000 ppm H_2 exposure in a temperature range between room temperature and 165°C. The signals reach quickly steady state with response time of t_{90} is around 10 s at all temperatures. The signal height

decreases with elevated temperatures up to 135°C. This causes the surface residence time τ of H_2 is too short due to elevated temperature. As a result only few hydrogen atoms react with adsorbed oxygen.

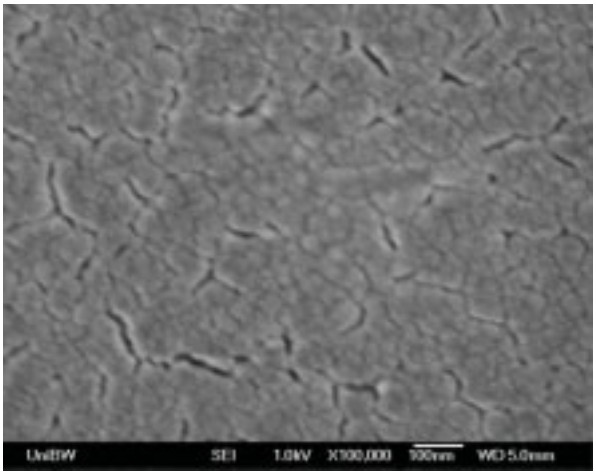

Figure 5.21. SEM image of the SnO_2 surface with thickness of 35 nm.

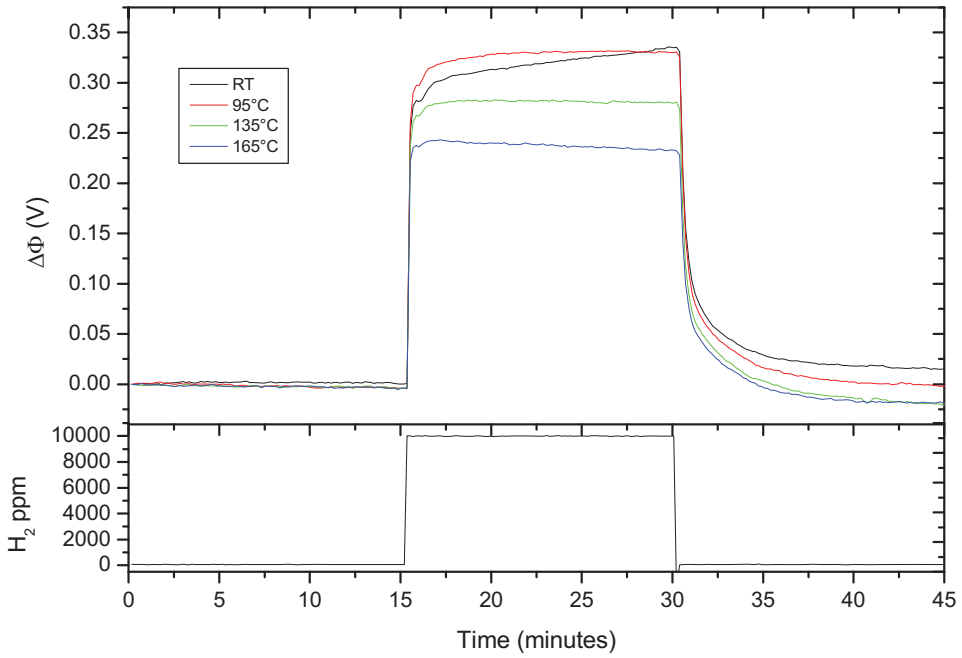

Figure 5.22. Temperature effect on the Pt/SnO_2 (35 nm) sensor to 10000 ppm H_2 under dry conditions after the pre-treatment.

Fig. 5.23 shows the response of the Pt/SnO_2 (35nm) sensor to various H_2 concentrations at room temperature under dry conditions. It can be seen that the sensor can well detect H_2 exposure in a concentration range between 1000 and 20000 ppm. Three signals of the sensor exhibit identical behavior to H_2 exposure. The signals can quickly reach steady state at almost all H_2 test

concentrations with the response time t_{90} is about 10 s. At 20000 ppm H_2 the signals can not reach steady state. This phenomenon may not occur if the sensor is previously rinsed with the synthetic dry air (regeneration of the sensor) after 15000 ppm H_2 exposure. It is found that the sensor needs a time for recovery O^- at the SnO_2 surface. However, the stable base line is observed during H_2 concentration measurements.

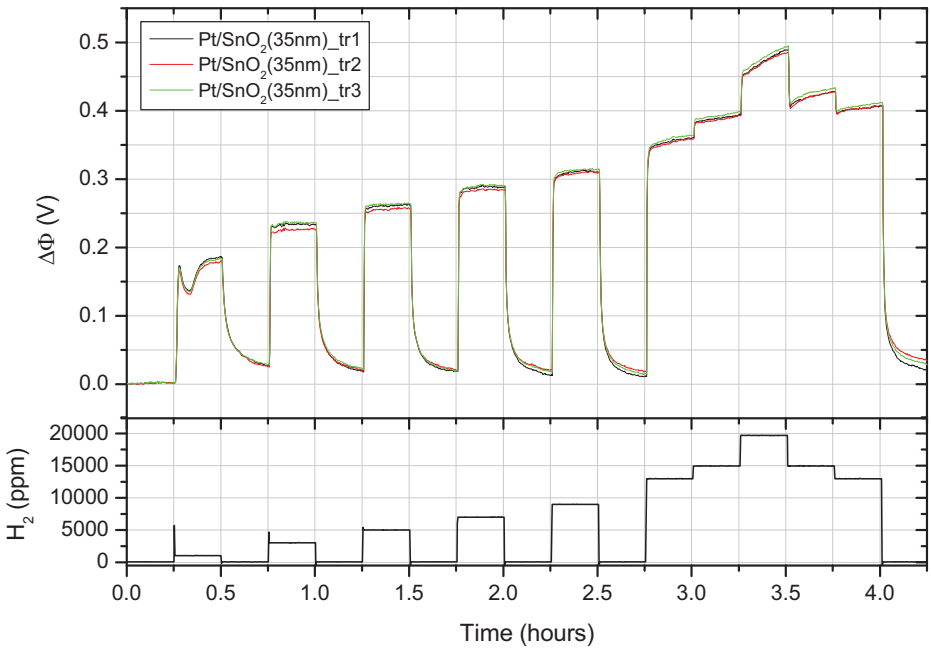

Figure 5.23. Response of the Pt/SnO_2 (35 nm) sensor to various H_2 concentrations at room temperature under dry conditions.

To analyze the H_2 concentration dependence of the sensor, it was exposed in the synthetic dry air flow with interrupted 1000-20000 ppm H_2. Each value of $\Delta\Phi$ due to H_2 interaction was taken at the beginning and ending of H_2 exposure. Then their difference was plotted to H_2 concentration. Fig. 5.24 describes the H_2 dependence of the sensor. The obtained characteristic of the Pt/SnO_2 (35 nm) sensor associated to H_2 concentration dependence is different from the obtained characteristic of the Pt/SnO_2 (50 nm) sensor. Signal of the Pt/SnO_2 (35 nm) sensor increases linearly with increasing H_2 concentration. The obtained linier fit is as follows:

$$\Delta\Phi = 1.5 \cdot 10^{-5} \frac{V}{ppm} \cdot c(H_2) + 0.2V \qquad (5.11)$$

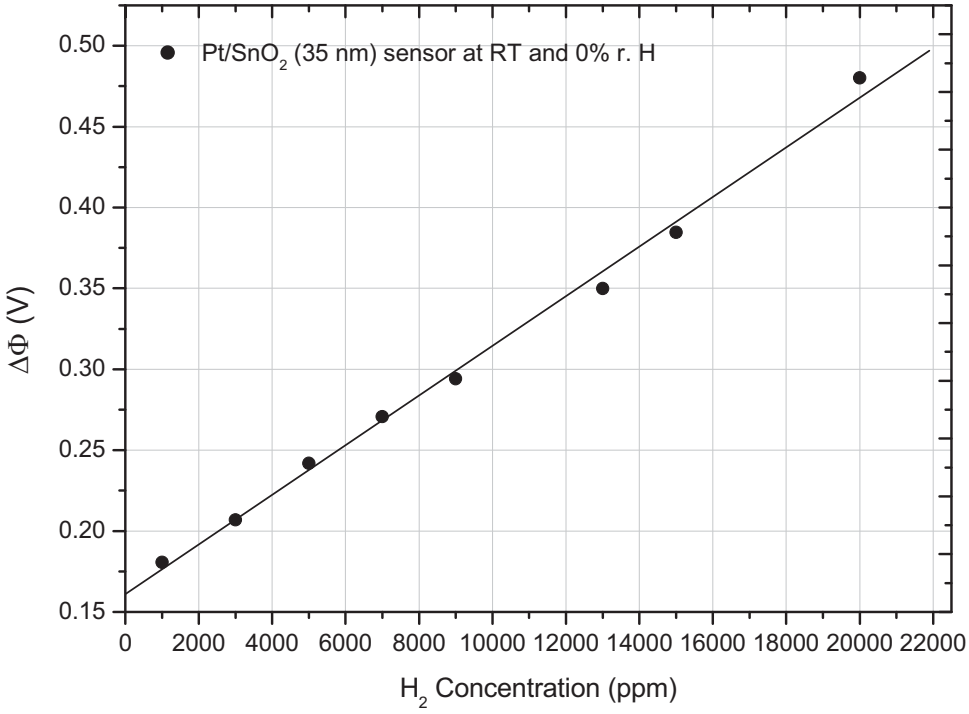

Figure 5.24. H_2 concentration dependence of the Pt/SnO_2 (35 nm) sensor at room temperature under dry conditions.

H_2 measurement at humid conditions was carried out with interrupted H_2 concentration from 1000 to 13000 ppm at room temperature under 30% relative humidities. The H_2 concentration was humidified by flowing dry synthetic air through a water bubbler at room temperature.

Fig 5.25 represents that the Pt/SnO_2 (35 nm) sensor can be still used to detect H_2 at low concentrations although the sensor signals can not achieve saturation condition at each H_2 concentration measurement for 15 min. However, reducing sensitivity of the sensor due to mixed H_2 with H_2O vapor is not significantly occurring because reducing thickness of SnO_2 films also reduces adsorption of H_2O vapor.

The cross sensitivity of the sensor was investigated by exposing it to H_2, CO_2, CO, O_2, H_2S, SO_2, NH_3 and H_2O vapor at room temperature under dry conditions. The result (see Fig. 5.26) proves that the sensor's selectivity can be improved particularly its sensitivity to NH_3. Signal drift due to NH_3 interaction is only 100 mV.

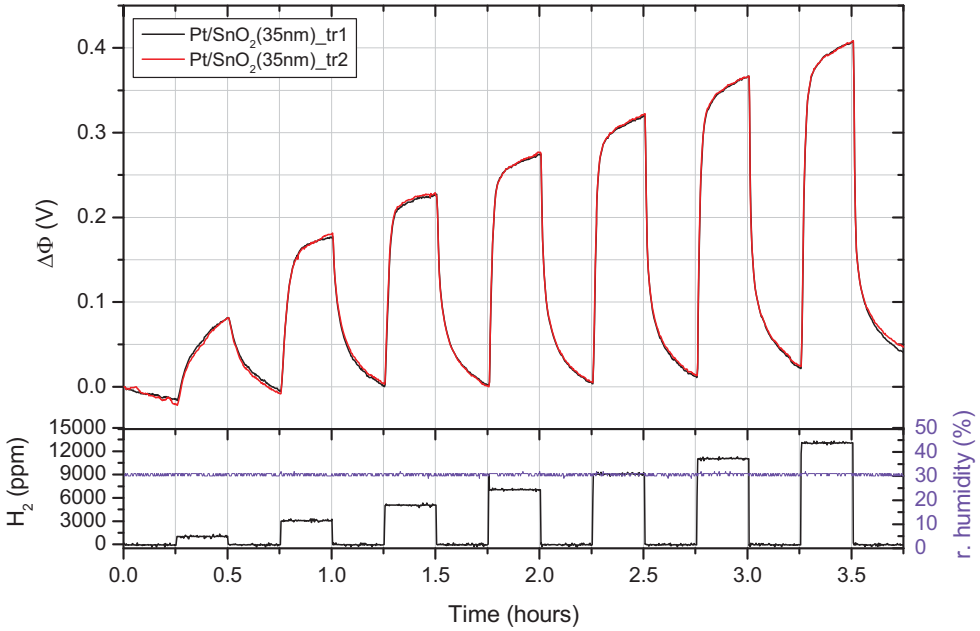

Figure 5.25. H_2 measurement with Pt/SnO_2 (35 nm) sensor at room temperature under 30% relative humidity.

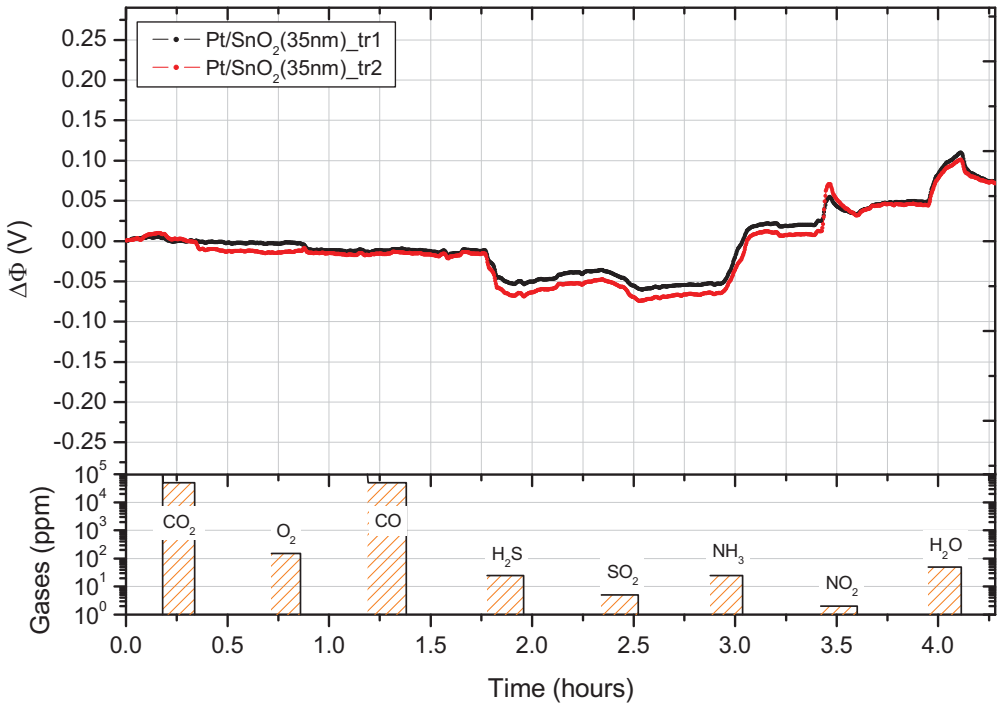

Figure 5.26. Cross sensitivity of the Pt/SnO_2 (35 nm) sensor at room temperature under dry conditions.

5.2.6 Annealing effect

To enlarge cracks or porousity at the SnO_2 surface, the layers have been annealed. With expectation, H_2 molecules can easy diffuse through the surface. In this model, cracks at the surface act as pathways for H_2 diffusion. The advance investigation about cracks on the surface has been carried out by Z. Tang [78]. Investigation of cracks on the metal oxides has been also reported previously [79, 80].

The Pt/SnO_2 films coated gates were annealed by using horizontal furnace (Carbolite) in oxygen flow of 600 cm^3/min. The temperature was ramped up to 600°C at rate of 5°C/min. Then the temperature was dwelled for 30 min. Afterwards the temperature was naturally ramped down to room temperature. The cooling process generates cracks on the surface [78].

Fig. 5.27 shows the film before and after the surface was annealed. It can be seen that significant change at the surface occurs after the annealing. At the annealed surface appear more cracks than at the un-annealed surface. On the other hand, the EDX characterization (see Fig. 5.28) shows that the qualitative composition of the surface is almost unchanged. Si being the only exception.

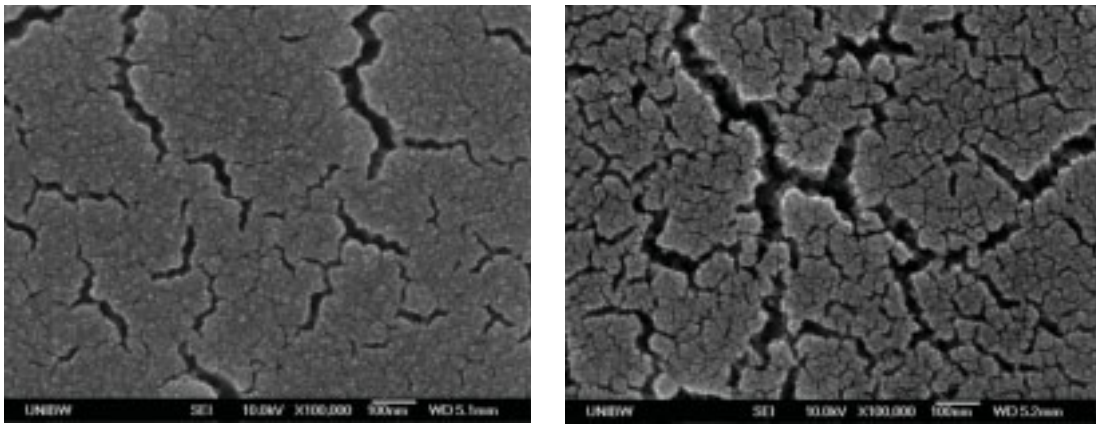

(a) before annealing (b) after annealing

Figure 5.27. SEM images of the Pt/SnO_2 surface after and before annealing in oxygen at 600°C.

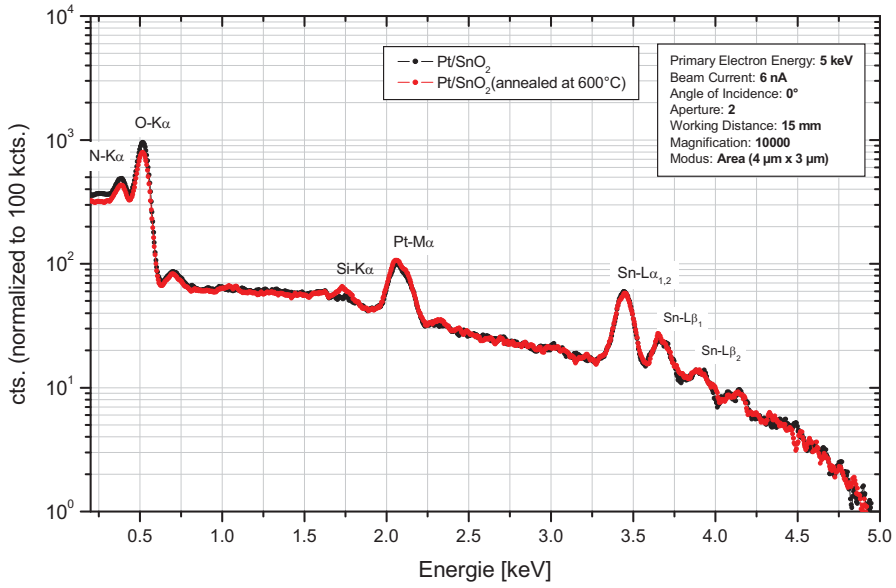

Figure 5.28. EDX characterization of the Pt/SnO_2 surface before and after annealing in oxygen at 600°C.

The sensor's sensitivity to H_2 exposure was examined at 95°C under dry conditions. It is exposed in a constant flow of synthetic dry air (100 ml/min) with interrupted 1000-20000 ppm H_2. Unfortunately, the Pt/SnO_2600 sensor is also not sensitive to H_2 exposure. Three signals of the sensor show identical behavior to H_2 exposure as represented in Fig. 5.29.

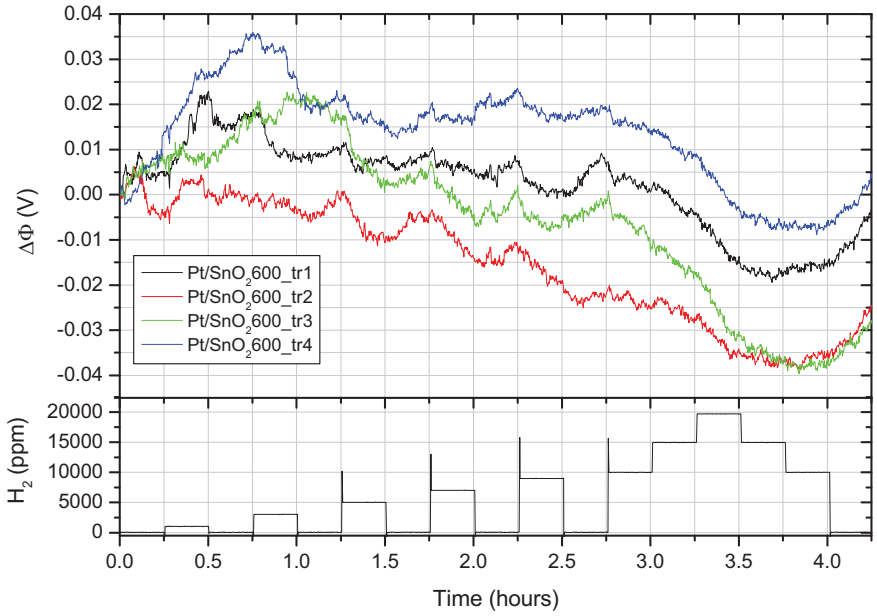

Figure 5.29. Response of the Pt/SnO_2600 sensor to elevated H_2 concentrations at various temperatures under dry conditions.

In order to explain this result, the Ti/Pt film was annealed at 600°C in oxygen flow of 600 cm^3/min for 30 min. The annealed surface was studied by using SEM and EDX.

Fig. 5.30 shows the surface morphology of the Ti/Pt film and the same film after annealing at 600°C. Before annealing the Ti/Pt film is dense. After annealing material clusters appear at the surface with cluster size of about 0.1 μm. Fig. 5.31 shows cross sections of the film after and before annealing. Before the annealing the thickness of each film can be visibly observed. After the annealing the borders between Ti and Pt films disappear. Total thickness of the film increases up to 875.6 nm. A possible explanation is the growth of micro-grains of $TiSi_2$ inside the film. This causes clusters at the surface and increases total thickness of the film.

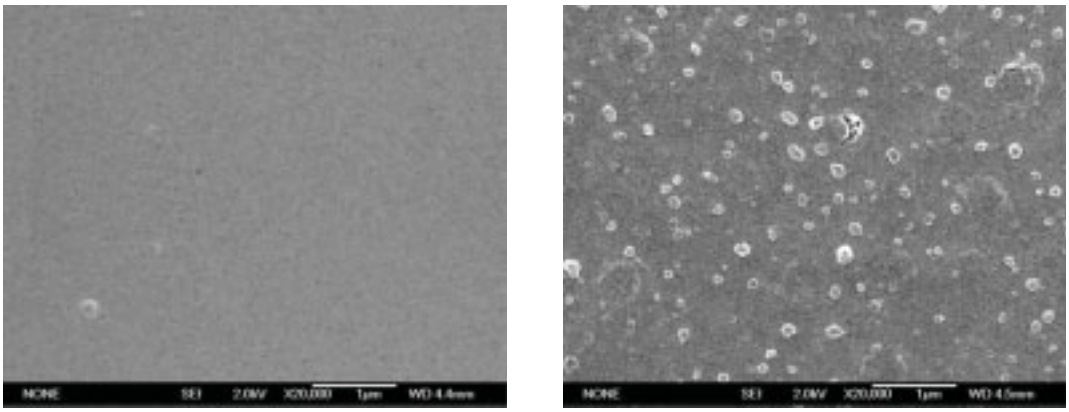

(a) before annealing (b) after annealing

Figure 5.30. SEM images of the Ti/Pt surface after and before annealing in oxygen at 600°C.

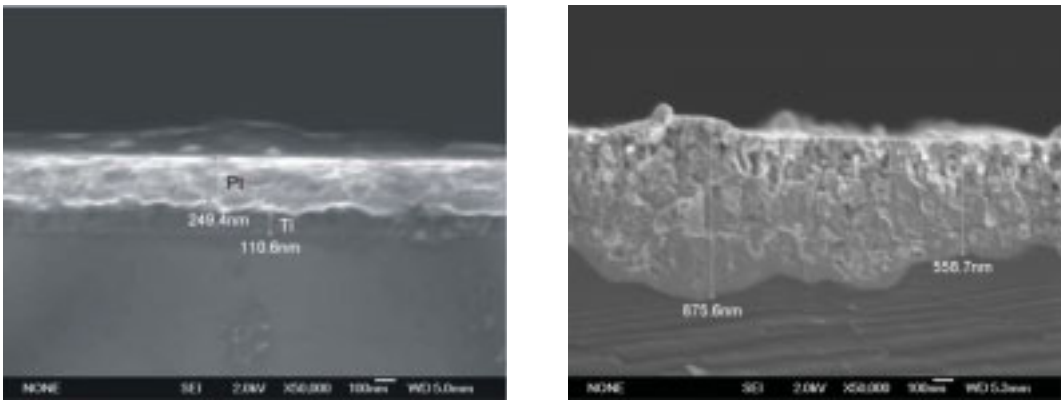

(a) before annealing (b) after annealing

Figure 5.31. The cross sections of the Ti/Pt film thickness after and before annealing in oxygen at 600°C.

The qualitative compositions of the films were characterized by using EDX at primary electron energy of 15 keV. The characterization (see Fig.5.32) shows that before the annealing the spectrum is dominated by Pt peak. After the annealing Ti, Si and O-peaks are observed beside the Pt-peak. With this result it can be found that obviously Ti reacts with Si to form $TiSi_2$.

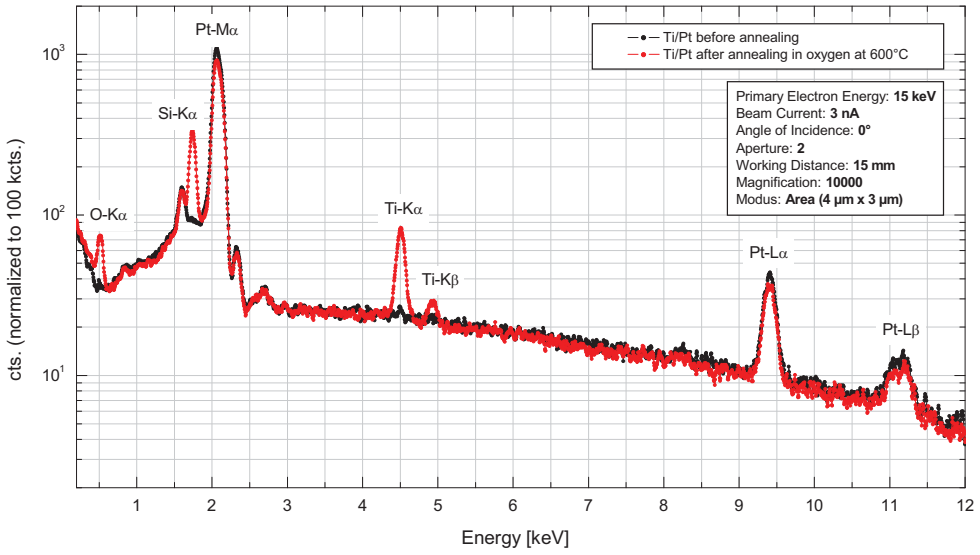

Figure 5.32. The EDX spectrum of the Ti/Pt surface after and before annealing in oxygen at 600°C.

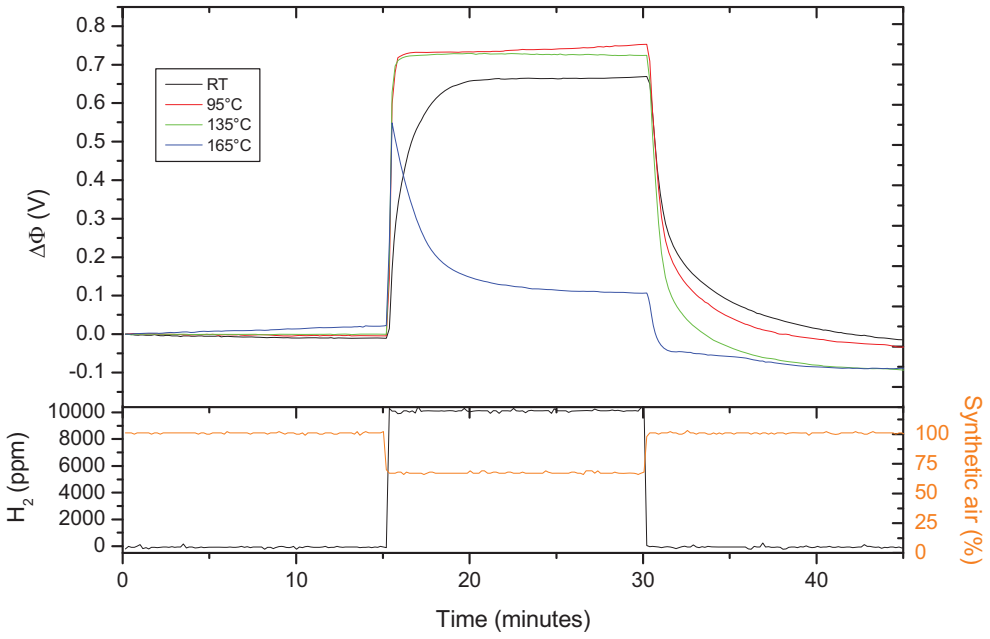

Figure 5.33. Response of the Ti/Pt600 sensor to 10000 ppm H_2 at various temperatures under dry conditions.

Properties of the Ti/Pt600 sensor were studied by exposing it to 10000 ppm H_2 at different temperature under dry conditions. Fig. 5.33 shows that the sensor can be used very well to detect 10000 ppm H_2 exposure. The operating temperature range, sensitivity and response time of the sensor can be improved. The sensor signal is stable up to operating temperatures of 135°C with response time t_{90} about 10 s. At operating temperature of 165°C the sensor signal drifts rapidly due to oxygen chemisorption and formation of OH-groups at the Pt surface. An experiment corresponding to long-term stability of the sensor confirms that the base line of the sensor decreases significantly in the beginning of H_2 measurement. However, the annealing process degrades the Pt/SnO_2 sensor significantly. The possible reason is the replacement of Pt by micro-grains of $TiSi_2$ and PtSi at the surface.

To confirm the role of gas sensing mechanism, additional experiments have been conducted by depositing 10 nm Pt on the SnO_2 surface. The SnO_2 films were prepared on the Si/Ti gates under the same conditions as described in section 5.2.1. Afterwards Pt was deposited by DC sputtering. Finally, the gates were annealed in oxygen at 600°C for 30 min.

Fig. 5.34 shows surface morphology of the Pt/SnO_2 and SnO_2/Pt/Cu surfaces after annealing in oxygen at 600°C. Many cracks at both of the surface are observed with width of ~50 nm, whereas surface color of the SnO_2/Pt/Cu is brighter than surface color of Pt/SnO_2. It is clear that the bright color is caused by Pt thin film.

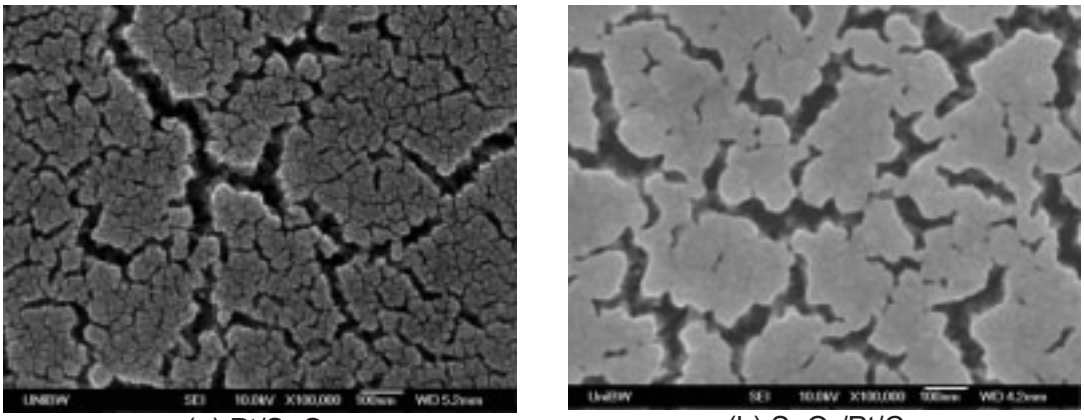

(a) Pt/SnO_2 (b) SnO_2/Pt/Cu

Figure 5.34. SEM image of Pt/SnO_2 and SnO_2/Pt/Cu surface after annealing in oxygen at 600°C.

The resulting EDX measurement at primary electron energy of 5 keV is represented in Fig. 5.35. It can be seen that the EDX spectrum is dominated by Pt, Sn and Cu peaks. The quantitative composition of Pt is much bigger than the others, because Pt thin film is at upper layer. Cu peak appears due to insufficient Pt source at the DC sputtering, so that material of Pt carrier, which is made from Cu, is also deposited on the surface. Oxygen peaks are not observed at the moment because the EXD does not work properly at binding energy below 750 eV.

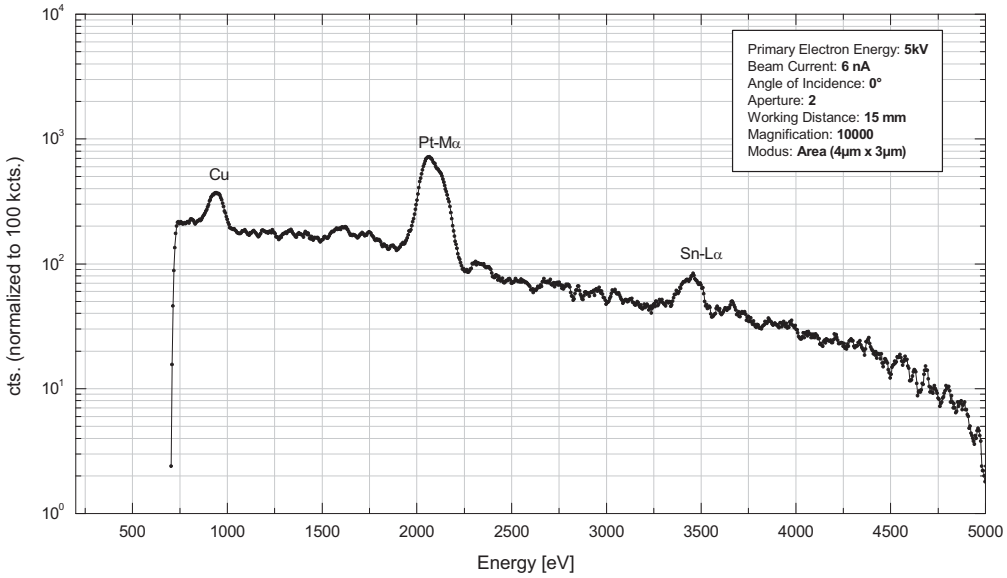

Figure 5.35. The EDX spectrum of the SnO_2/Pt/Cu surface after the annealing in oxygen at 600°C.

Properties of the SnO_2/Pt/Cu600 sensor were investigated by exposing it to elevated H_2 concentrations at various temperatures under dry conditions. Fig. 5.36 shows that the sensor can be used to detect H_2 concentrations up to 20000 ppm at all temperatures with slow response time. The decreasing signal height of the sensor compared to the SnO_2/Pt sensor is observed. Maximum signal height of the sensor is observed at about 171 mV for 20000 ppm H_2 exposure at room temperature under dry conditions. As is known from literature in section 1.2.4 the spill-over effect will optimally occur if the catalyst particles are located at the surface of bigger metal oxide grains and are homogenously distributed on the surface. In the present case the Pt catalyst particles are not big enough, so spill-over effect on the Pt catalyst is not

optimally occurring. However, these results prove that the H_2 sensing mechanism of Pt/SnO_2 sensor occur at the interface between Pt and SnO_2 films due to the Schottky barrier and the spill-over effect.

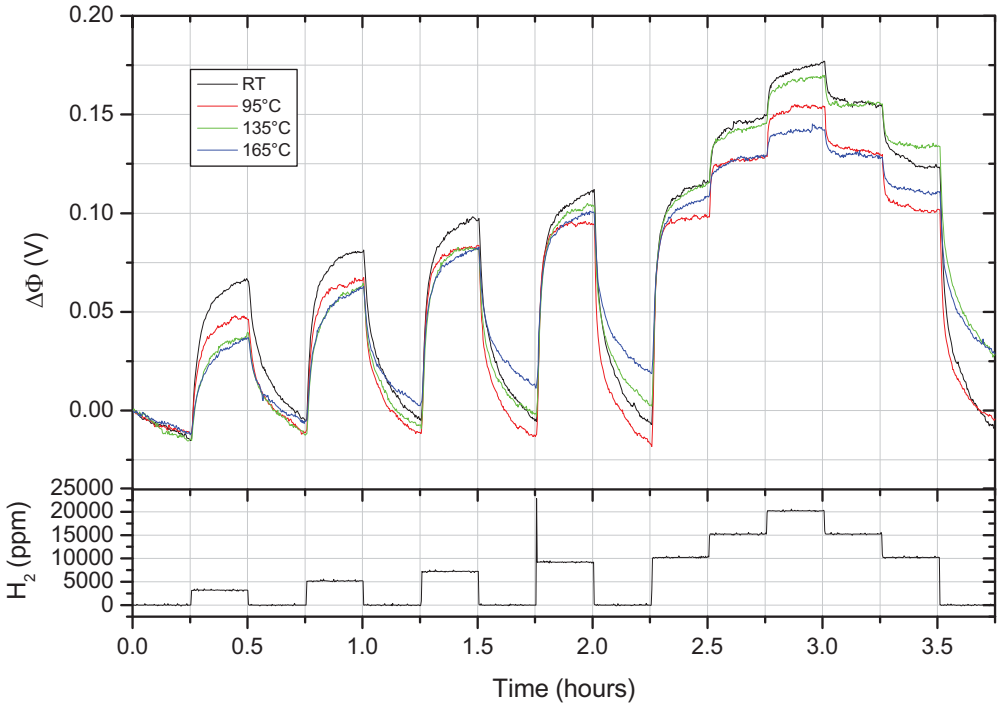

Figure 5.36. Response of the SnO_2/Pt/Cu600 sensor to elevated H_2 concentrations at various temperatures under dry conditions.

5.3 Application of Pt and Pt/SnO_2 films in other sensor configurations

In order to investigate the ability of Pt and Pt/SnO_2 films for hydrogen detection, the films were used in different sensor systems. Hydrogen sensors based on Lundstrom-FET/Suspended Gate FET (SGFET) were prepared by Micronas GmbH in Freiburg. A schematic of the sensor can be seen in Fig. 5. 37 [81]. Pt85 sensor uses Pt + 35 nm SnO_2 and Pt92 sensor uses Pt + 50 nm SnO_2, whereas Pt102 sensor uses Pt on Ti as gas sensitive films. Stability of the sensors to various hydrogen concentrations were tested for different temperatures and humidities. For this experiment, the sensors were put in a climatic chamber.

The resulting experiment is shown in Fig. 5.38. The Pt85 and Pt92 sensors exhibit identical behavior to H_2 exposure. The sensors can work well at elevated temperature. Afterwards, the sensors can not detect H_2 when

temperature is decreased down to room temperature. Signals of the sensors decrease rapidly. Obviously the chemical composition changes at the SnO_2 films due to H_2 interaction at high temperature. On the other hand, the Pt102 sensor is well suited to detect H_2 at low temperatures but signal of the sensor decreases rapidly at high temperature. Furthermore, base line of the sensor decreases significantly in the beginning of H_2 measurement because the Pt surface adsorbs oxygen atoms in order to achieve an equilibrium condition for a reaction between H_2 and O_2.

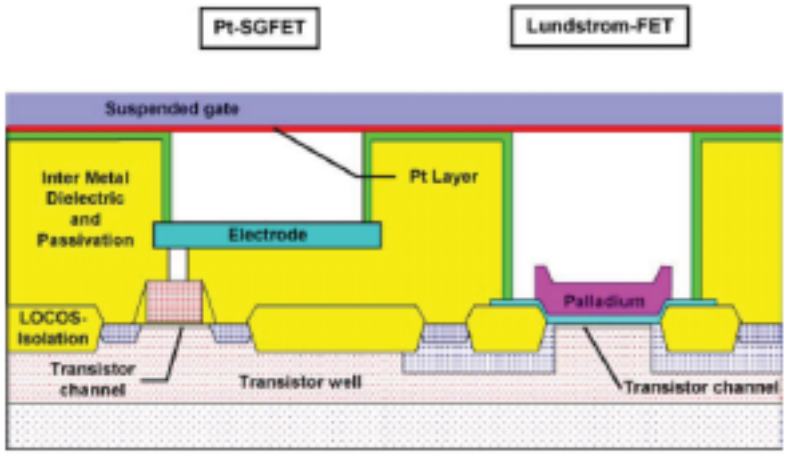

Figure 5.37. Schematic of the Lundstrom-FET/SGFET double sensor in CMOS technology.

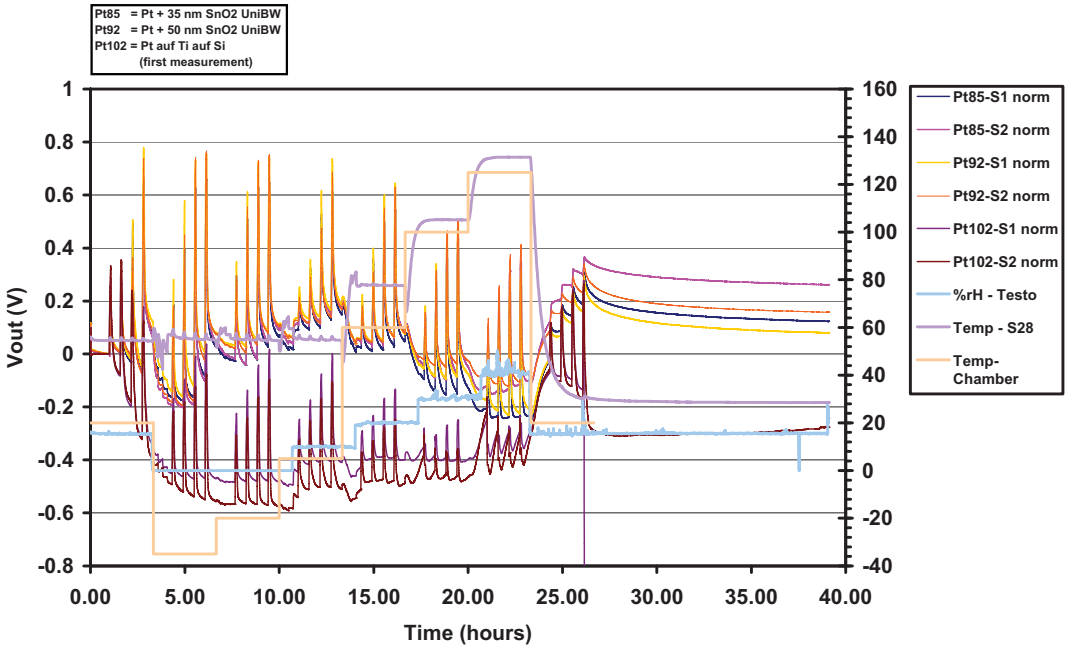

Figure 5.38. Stability of the Pt85, Pt92 and Pt102 sensors to H_2 exposures at different temperatures and humidities. The experiment was carried out at Micronas GmbH in Freiburg.

5.4 Titanium silicide / platinum ($TiSi_2$/Pt)

We have demonstrated performance of the Pt and Pt/SnO_2 films based on the FG-FET sensor system for H_2 detection. The results show that there are still problem, particularly with humidity and temperature. Several strategies have been explored to fabricate a sensor with high sensitivity, selectivity and stability at low operating temperatures. Unfortunately, the results are still not satisfying.

In this section we concern nano-grains of titanium silicide ($TiSi_2$) with Pt catalyst as a new gas sensitive film in FG-FET sensor systems for H_2 detection. The advantages of the $TiSi_2$/Pt sensor are

1. A high sensitivity and selectivity to high H_2 concentrations at low temperature.
2. A stable base line and fast response time t_{90} ~10 s.
3. No significant humidity effect up to 70% relative humidity
4. High long-term stability.
5. Simple preparation of nano-grains of $TiSi_2$/Pt.

More than half of the elements in the periodic table react with silicon to form silicides. The most interesting silicides are derived from the metals of the groups IVB, VB, VIB and VIIIB of the periodic table of elements (see Appendix A). The first three groups are called the refractory metal silicides and the fourth group is called the near noble silicides. The Ti-Si system belongs to group IVB [82, 83].

At present the widely accepted sequence for reaction of a Ti film on a Si substrate is the following as described in Fig. 5.39

1. Around 200 °C intermixing of the two materials occurs (diffusion of silicon into the titanium) [84, 85].
2. Up to temperatures of 500 °C further intermixing of Ti and Si occurs (some TiO and Si islands appear) [86].
3. At 450-500 °C the C49 $TiSi_2$ metastable phase nucleates.
4. The stable C54 phase appears at temperatures ranging from 600-850°C (depending on the layer thickness) [87].

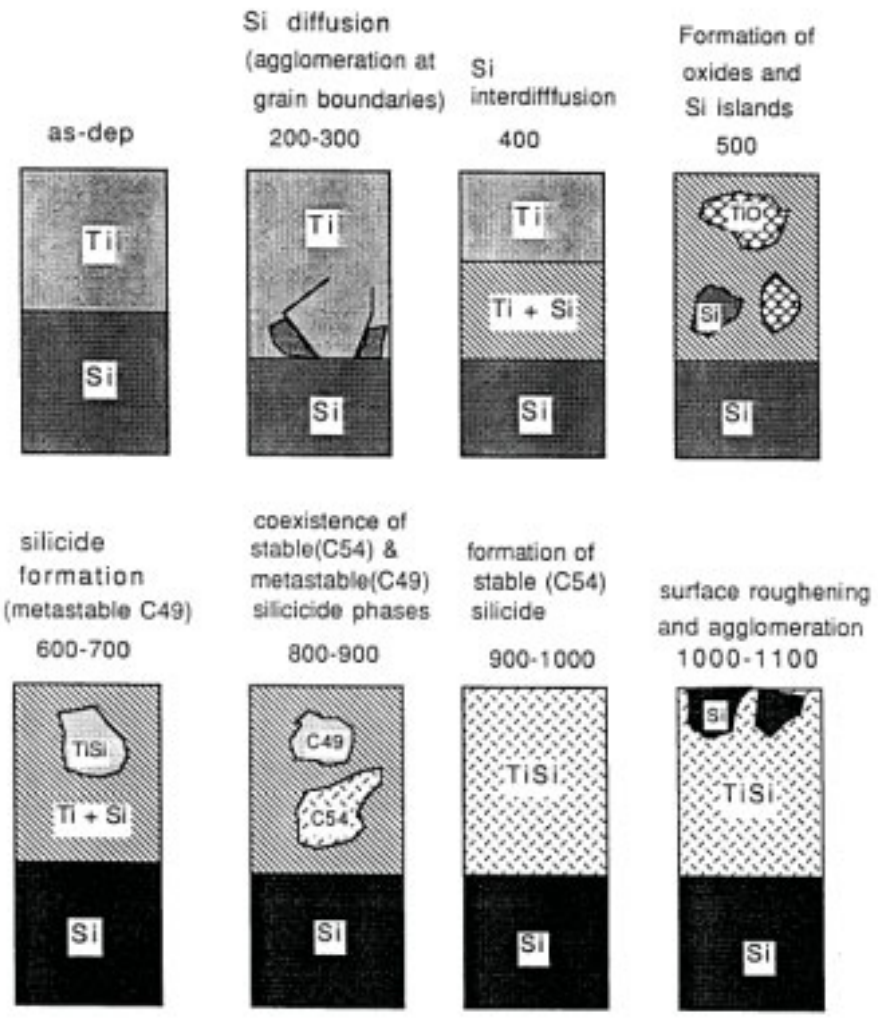

Figure 5.39. The $TiSi_2$ formation sequences [86].

5.4.1 Preparation and characterization of $TiSi_2$/Pt film

For film preparation, 110.6 nm of Ti and 249.4 nm of Pt films were deposited by using DC sputtering on p-doped Si gates. Afterwards, the gates were annealed by using horizontal furnace (Carbolite) in oxygen flow of 600 cm^3/min. The temperature was ramped up to 800°C at rate of 20°C/min. Then, the temperature was dwelled for 30 min. Finally, the temperature was naturally ramped down to ambient temperature.

The surface morphology of the resulting films is shown in Fig. 5.40. It is found that in this condition, nano-grains of $TiSi_2$ grow inside the films whereas Pt film opens and forms dense islands of Pt on the grains.

Fig. 5.41 shows the EDX spectrums of the film composition before and after the annealing in oxygen at 600°C and 800°C. Ti, O and Si-peaks appear

besides Pt-peaks after annealing in oxygen at 600°C and 800°C. The EDX spectrum of the annealed film shows similar behavior.

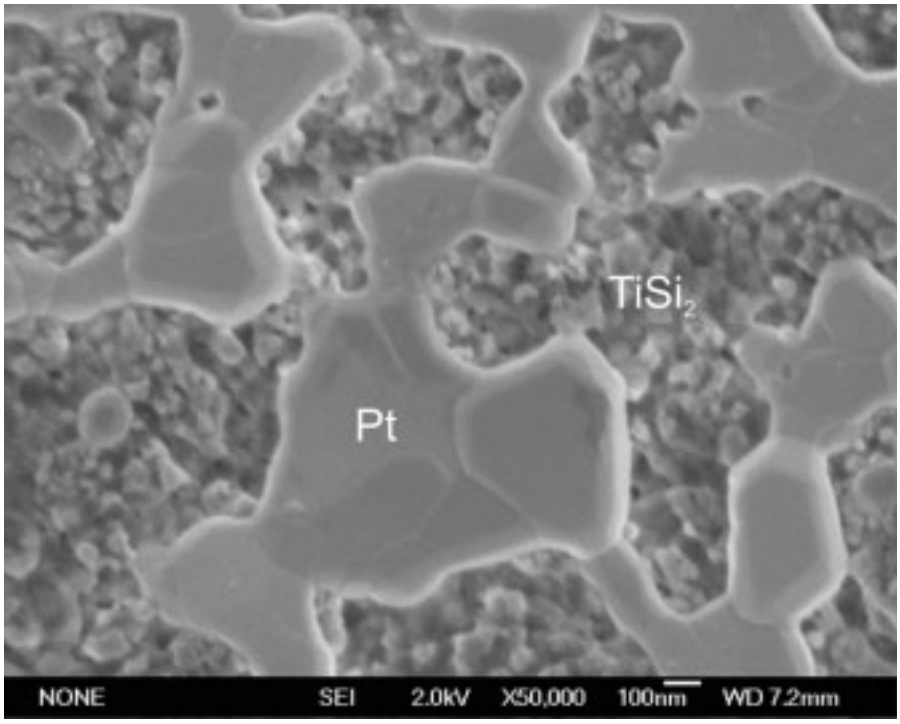

Figure 5.40. SEM images of the Ti/Pt surface after annealing in oxygen at 800°C.

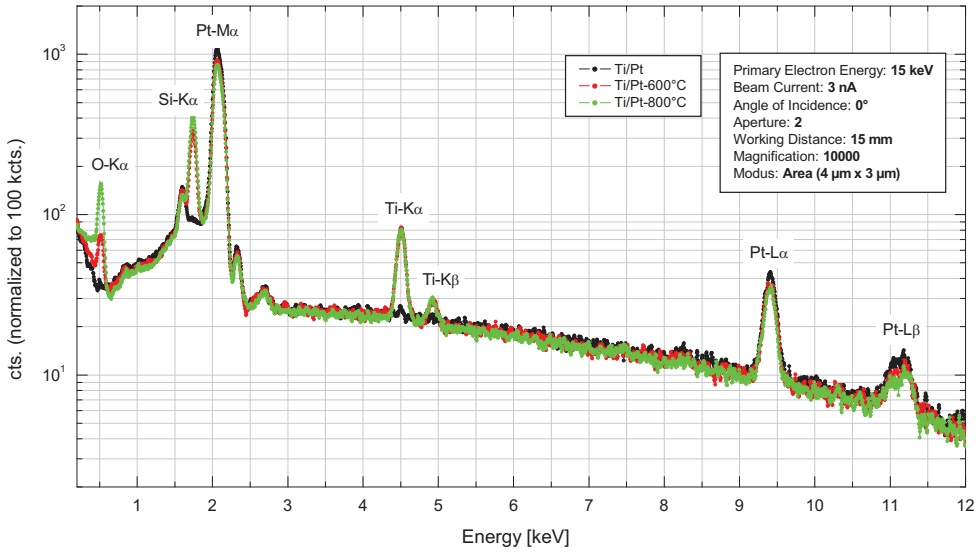

Figure 5.41. EDX spectrum comparison of the Ti/Pt film before and after annealing in oxygen at 600°C and 800°C.

5.4.2 Gas sensing mechanism

The gas sensing mechanism still is based on the Schottky barrier and the spill-over effect due to the presence of dispersed metallic catalyst. The Schottky barrier is formed at the interface between $TiSi_2$ and Si [88].

When the sensor is exposed to synthetic air (20% O_2 and 80% N_2), the Pt catalyst dissociates directly O_2 molecule into O^- atom species. These species spill over onto $TiSi_2$. This causes an increasing height of the Schottky barrier and broadening of depletion layer at the conduction band near the surface of $TiSi_2$. As a result, the conductivity decreases and the work function of $TiSi_2$ increases.

Pt catalyst also dissociates directly H_2 molecule into H atoms, when the sensor is exposed to a mixture from H_2 and synthetic air. These atoms spill over onto $TiSi_2$ and react there with the O^- atom species. Adsorbed hydrogen atoms act as donors, which provide additional free electrons and induce an electron accumulation layer. As a result the conductivity increases and the work function of $TiSi_2$ decreases leading to an increasing sensor signal.

5.4.3 Sensing properties of $TiSi_2$/Pt film

Sensing properties of a $TiSi_2$/Pt film to H_2 exposure was characterized by using FG-FET sensors. Work function changes with respect to various hydrogen concentrations have been measured as a function of temperature and humidity. Cross sensitivity and long-term stability of $TiSi_2$/Pt800 sensor were also investigated.

Temperature effect on the sensor was observed in the temperature range between room temperature and 165°C under dry conditions. H_2 sensitivity of the sensor was examined by exposing it to H_2 in the concentration range between 3000 ppm and 20000 ppm at each test temperature.

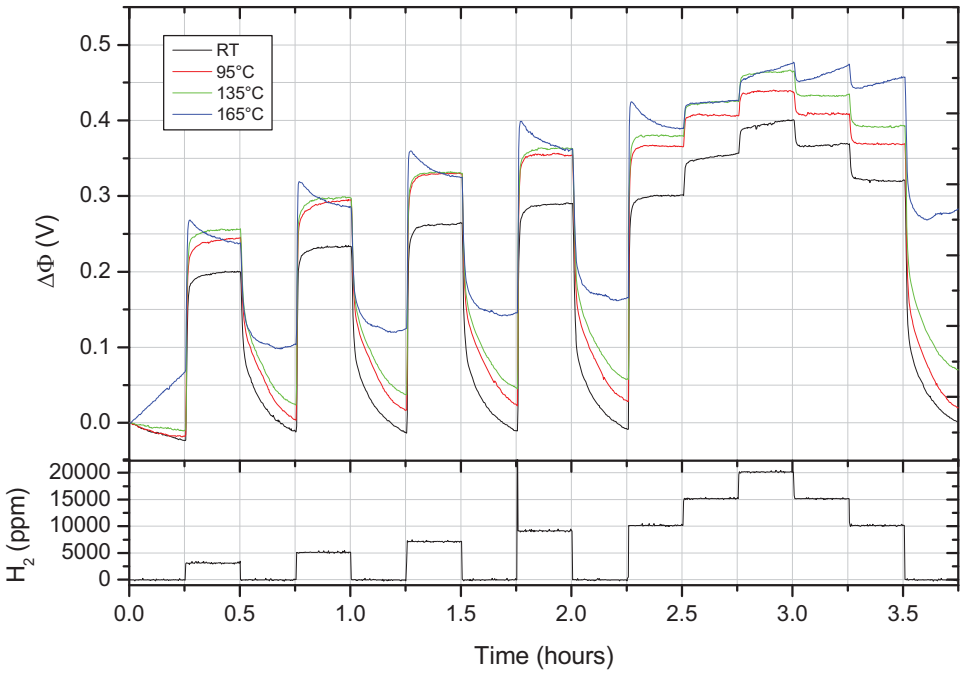

Figure 5.42. Temperature effect on the $TiSi_2$/Pt800 sensor under dry conditions.

Fig. 5.42 represents the thermal behavior of the sensor. The film, which is used in this sensor, shows nearly no temperature dependence up to 135°C. From room temperature up to 135°C, there are nearly no change of the signal height of the sensor at each measurement at the same H_2 concentration. No significant change of the response time (t_{90}~10 s) can be observed due to elevated concentration and temperature. At operating temperature of 165°C significant base line change of the sensor is observed due to chemisorption of oxygen at the film.

The response of the sensor with respect to various H_2 concentrations was investigated at room temperature under dry conditions. Equilibrium on the surface can be achieved with exposing the sensor in a constant flow of dry synthetic air (100 ml/min) for 15 min. In order to examine sensitivity and reversibility of the sensor, it is exposed to various H_2 concentrations for 15 min. Then it is rinsed with synthetic dry air for 15 min. This cycle is repeated several times.

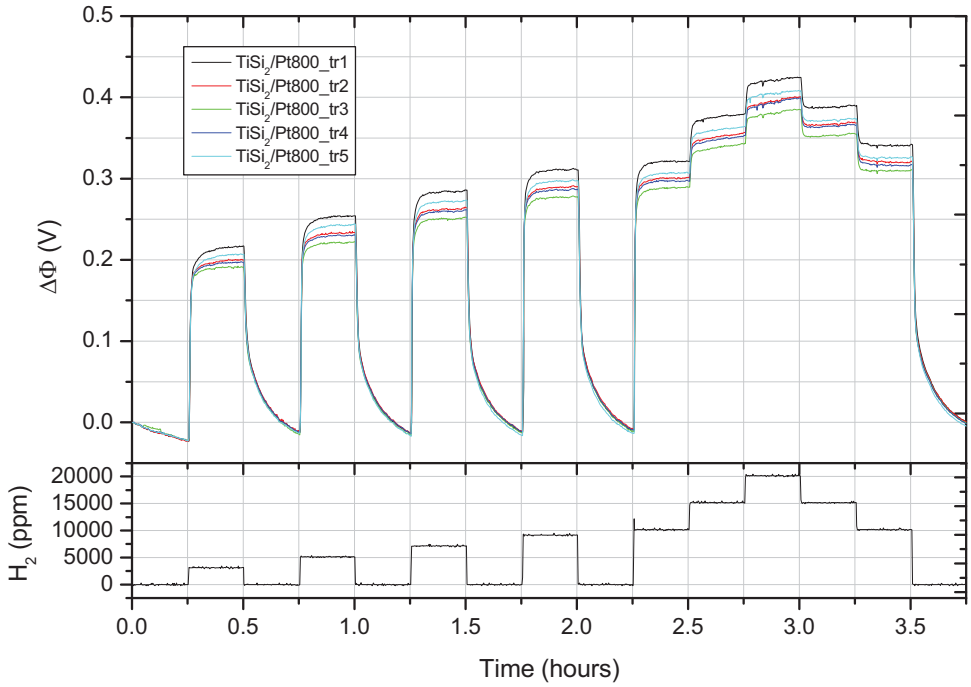

Figure 5.43. Dynamic response of the $TiSi_2$/Pt800 sensor to various H_2 concentrations at room temperature under dry conditions.

Fig. 5.43 shows the dynamic response of the sensor to various H_2 concentrations at room temperature under dry conditions. The sensor can well distinguish H_2 concentrations. No significant change of the response time (t_{90}~10 s) and the base line can be observed due to increased H_2 concentrations. The dependence of response on the H_2 concentration is shown in Fig. 5.44. The signal of the sensor increases linearly with increasing H_2 concentrations. The resulting fit linier is as follow

$$\Delta\Phi = 1.1 \cdot 10^{-5} \frac{V}{ppm} \cdot c(H_2) + 0.2V \qquad (5.12)$$

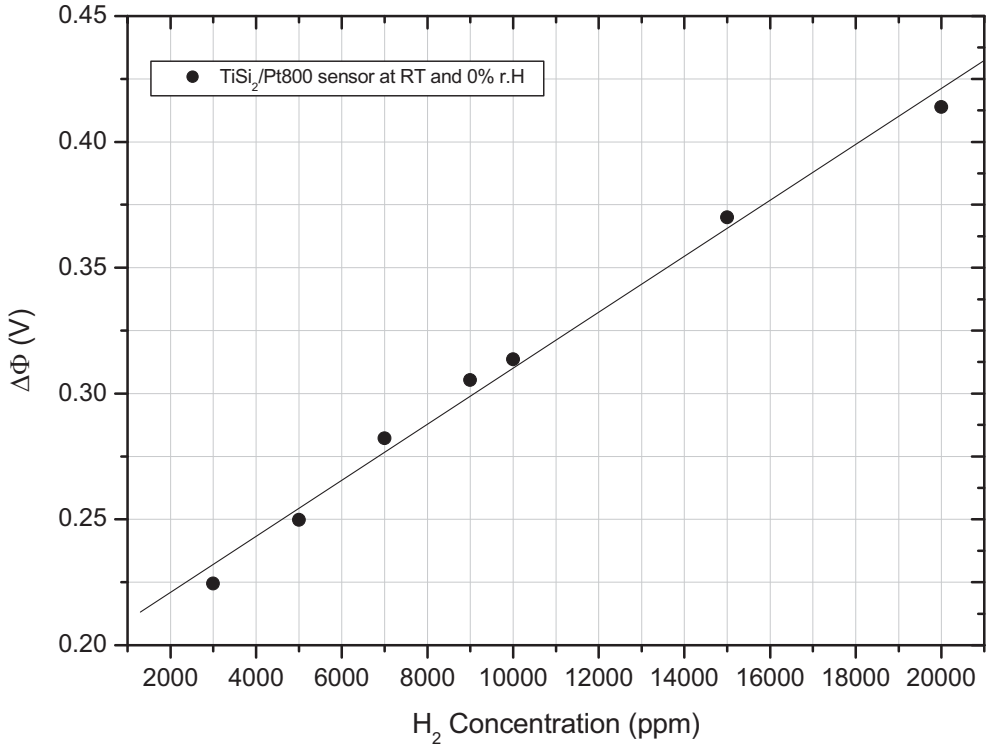

Figure 5.44. H_2 concentration dependence of the $TiSi_2$/Pt800 sensor at room temperature under dry conditions.

Sensing properties of the films were also tested by exposing the sensor to high H_2 concentrations in argon (Ar). Dynamic response of the sensor to high H_2 concentrations at room temperature under dry conditions is represented in Fig. 5.45. The signals increase with increasing H_2 concentrations up to 50000 ppm. The response time t_{90} is about 10 s at all test concentrations. The base line remains stable at this condition. It can be observed that the signals at 10000 ppm H_2 in argon (Ar) are 100 mV above the value for H_2 in synthetic air and return faster to the base line because Ar reduces oxide at the surface like H_2. The reproducibility of the signals is very well. This has been proved by measuring H_2 concentrations from 50000 ppm to 10000 ppm. Height of the signals remains stable about 400 mV for 10000 ppm H_2.

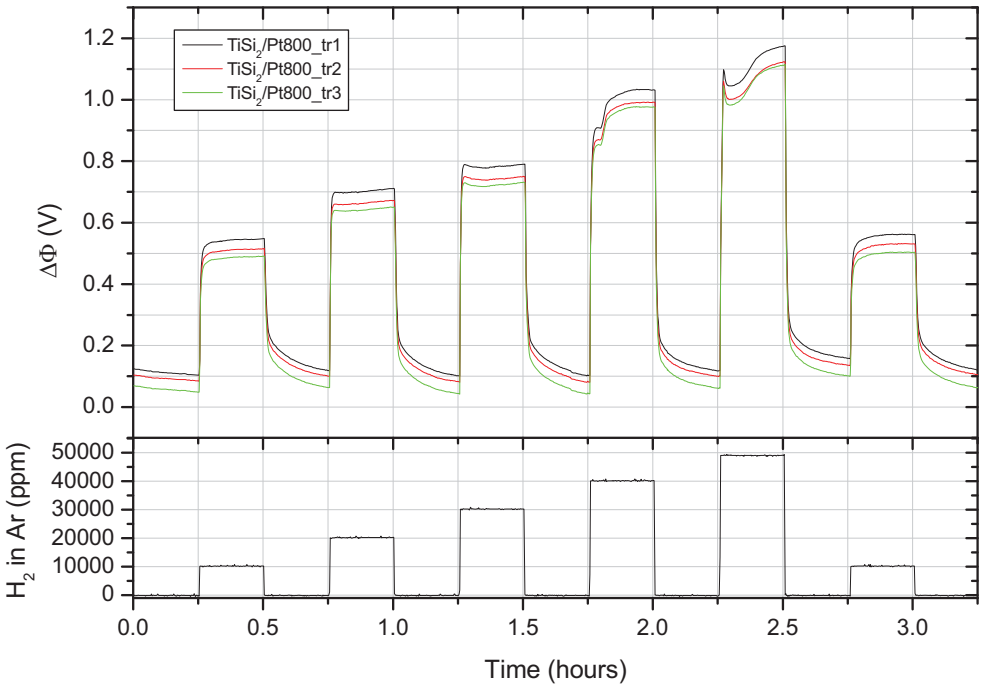

Figure 5.45. Dynamic response of the $TiSi_2$/Pt800 sensor to high H_2 concentrations in argon at room temperature under dry conditions.

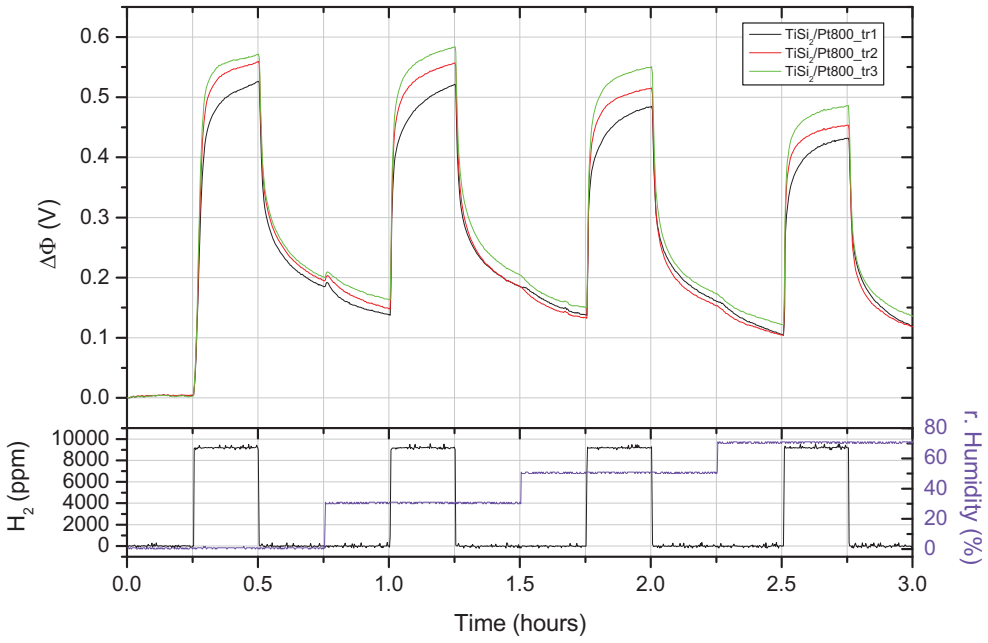

Figure 5.46. Humidity effect on the $TiSi_2$/Pt800 sensor at room temperature.

The humidity effect was investigated by exposing the sensor to relative humidities up to 70% at room temperature. Fig. 5.46 describes humidity effect of the sensor. No significant change of the signals can be observed due to raised relative humidity. The signals remain stable when the humidity is elevated.

An experiment related with reproducibility of the sensor was carried out at room temperature under dry conditions. The sensor is exposed to 10000 ppm H_2 for 30 min, and then it is rinsed with synthetic air for 30 min. This cycle is repeated for eight times.

Fig. 5.47 represents the reproducibility of the sensor signals to 10000 ppm H_2 measurements. Reproducible signals of the sensor can be well observed in this experiment. The height of the signals remains stable at ~ 300 mV with response time t_{90}~10 s during the measurement. Furthermore, no significant base line change of the sensor can be observed.

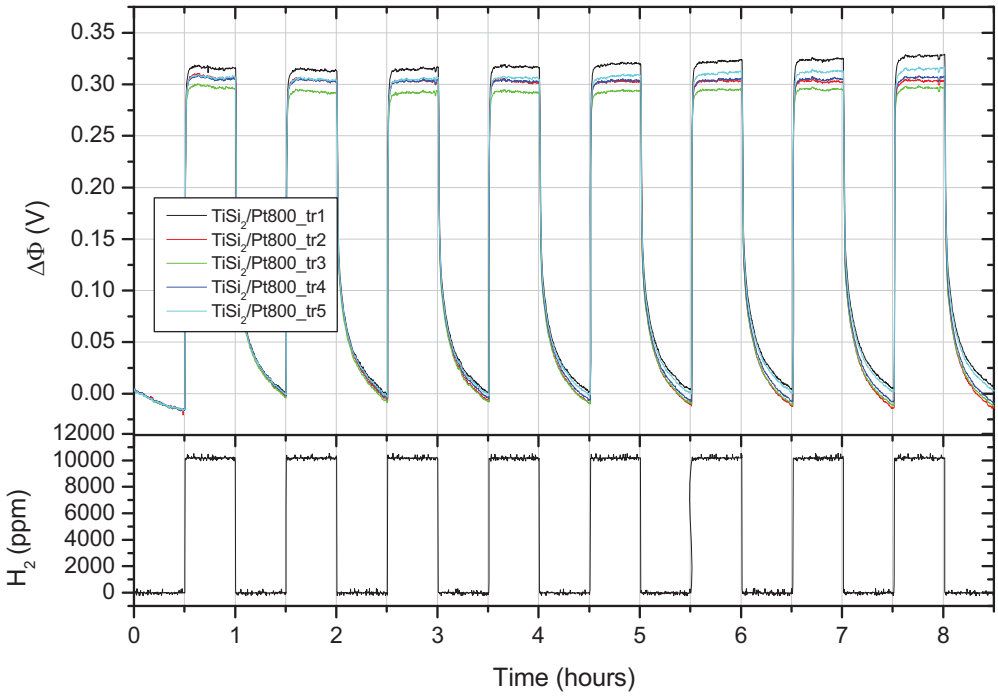

Figure 5.47. Reproducibility of the $TiSi_2$/Pt sensor signals to 10000 ppm H_2 in synthetic air at room temperature under dry conditions.

Long-term stability of the sensor was investigated at 60°C under 30% relative humidity after six days without testing. The sensor is exposed to constant flow of dry synthetic air for 15 min with interrupted 5000, 10000 and

20000 ppm H_2 for 15 min. Afterwards it is rinsed with synthetic air for 24 hours. This cycle is repeated.

Fig. 5.48 represents the long-term stability of the sensor. The signal pattern and the base line of the sensor still remain stable in the beginning of the measurement after six days without testing. The signals need more than 15 min to achieve real base line of the sensor. No significant humidity effect can be observed when the sensor is exposed to H_2 in humid conditions.

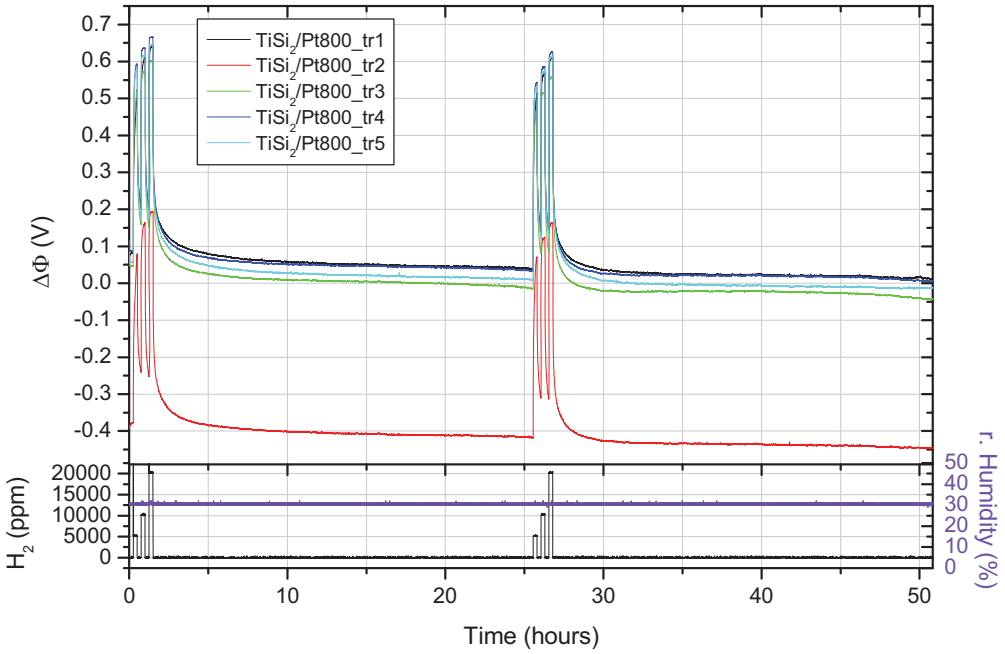

Figure 5.48. Long-term stability of the $TiSi_2$/Pt800 sensor to H_2 at 60°C under 30% relative humidity after six days without testing.

Fig. 5.49 shows the cross sensitivity of the sensor at 60°C under 30% relative humidity. It can be observed that the cross sensitivity is very low. Five different sensors exhibit the same behavior to the test gases. The sensors respond to H_2, CO_2 and H_2S exposure. Advance experiment confirms that CO_2 sensitivity of the sensors is caused by memory effect. However, it should be noted that the sensors respond strongly only to H_2. These results prove that the $TiSi_2$/Pt films are a new and very promising candidate as gas sensitive films for H_2 detection at high concentrations in FG-FETs.

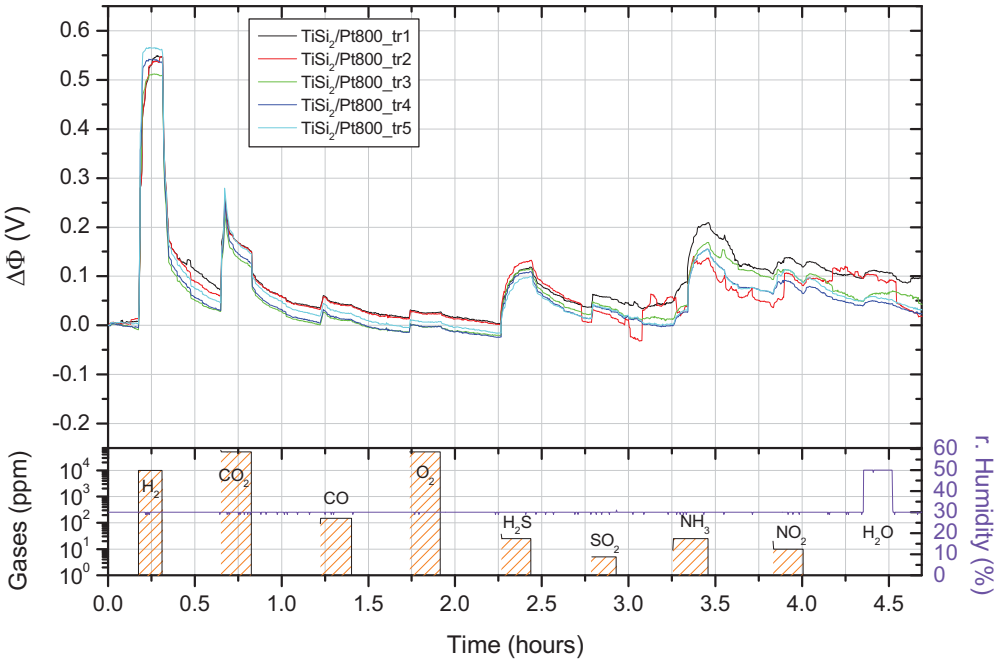

Figure 5.49. Cross sensitivity of the $TiSi_2$/Pt800 sensor at 60°C under 30% relative humidity.

Chapter 6

Conclusions

In a final evaluation, it was concluded that

1. Ag_2O films, which are used in FG-FETs, are suitable for H_2S detection in the concentration range between 2 and 50 ppm at 95°C under dry conditions.
2. ZnO films are a promising new material as gas sensitive film for 2-20 ppm NO_2 detection at T< 200°C in FG-FETs.
3. SnO_2/Cu films are suitable for NO_2 detection at low concentrations below 2 ppm and low temperatures in FG-FETs.
4. Non-stoichiometric porous SnO_2 is suitable to significantly stabilize the hydrogen response of Pt surfaces in FG-FETs but a serious problem with the humidity influence remains.
5. $TiSi_2$/Pt800 films are a promising new system for H_2 detection in the concentration range between 3000 and 20000 ppm in FG-FETs. The sensor offers **high sensitivity**, **selectivity**, **reproducibility**, **long-term stability** and **negligible base line change** at a temperature range from room temperature to 135°C under dry and humid conditions with **response time (t_{90}~10 s)**.
6. Combination between catalyst and material support is very interesting to be investigated. FG-FET sensors can be optimized and it is still possible to obtain a variety of combinations, which can be used as sensitive films for other gases.

Appendix A

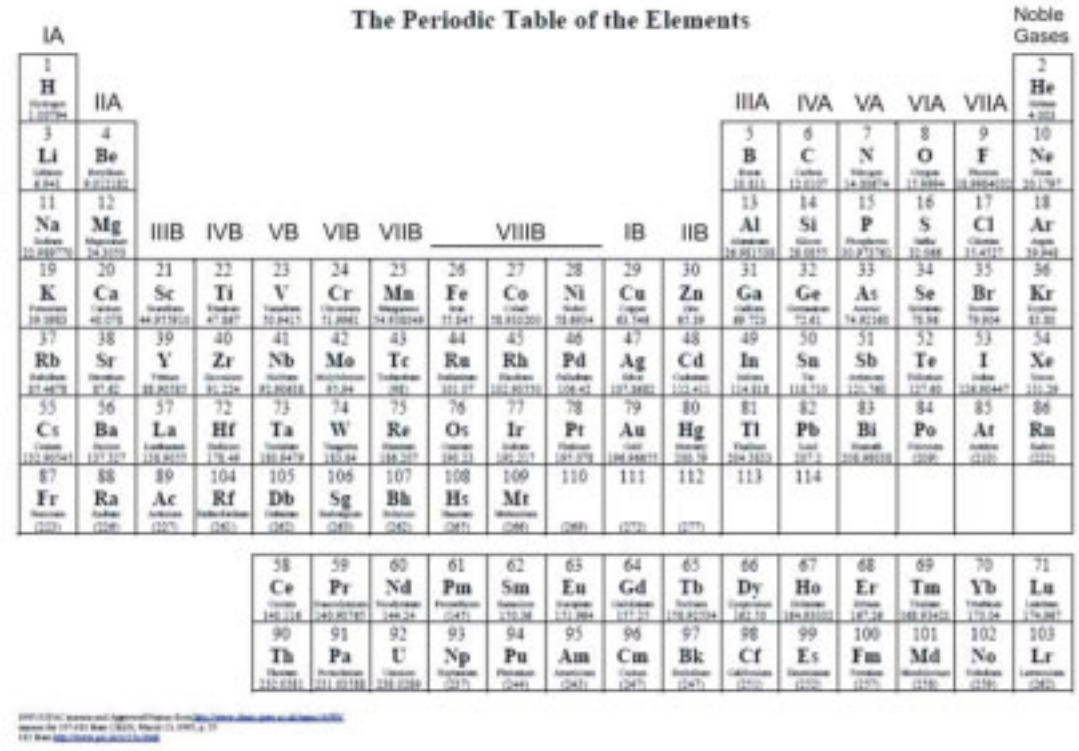
The Periodic Table of the Elements
IA
IIA
IIIB
IVB
VB
VIB
VIIB
VIIIB
IB
IIB
IIIA
IVA
VA
VIA
VIIA
Noble Gases
H
He
Li
Be
B
C
N
O
F
Ne
Na
Mg
Al
Si
P
S
Cl
Ar
K
Ca
Sc
Ti
V
Cr
Mn
Fe
Co
Ni
Cu
Zn
Ga
Ge
As
Se
Br
Kr
Rb
Sr
Y
Zr
Nb
Mo
Tc
Ru
Rh
Pd
Ag
Cd
In
Sn
Sb
Te
I
Xe
Cs
Ba
La
Hf
Ta
W
Re
Os
Ir
Pt
Au
Hg
Tl
Pb
Bi
Po
At
Rn
Fr
Ra
Ac
Rf
Db
Sg
Bh
Hs
Mt
110
111
112
113
114
Ce
Pr
Nd
Pm
Sm
Eu
Gd
Tb
Dy
Ho
Er
Tm
Yb
Lu
Th
Pa
U
Np
Pu
Am
Cm
Bk
Cf
Es
Fm
Md
No
Lr

List of figures

References

[1] T. Amamoto, Sensors and Actuators B1 (1990) 226.
[2] Y.-K. Jun, Sensors and Actuators B 107 (2005) 264.
[3] W.-T. Moon, Sensors and Actuators B 115 (2006) 123.
[4] K. D. Schierbaum, Sensors and Actuators B 4 (1991) 87.
[5] Y. Xu, Sensors and Actuators B 14 (1993) 492.
[6] L. Zheng, Sensors and Actuators B 66 (2000) 28.
[7] C. Baratto, Sensors and actuators B 109 (2005) 2.
[8] T. Iwanaga, Sensors and Actuators B 93 (2003) 519.
[9] Y. Shimizu, Sensors and Actuators B 83 (2002) 195.
[10] O. K. Varghese, Sensors and Actuators B 93 (2003) 338.
[11] I. Lundström, J. Appl. Phys. 46 (1975) 3876.
[12] J. S. Chung, in IMCS, Gaiterburg, 1996.
[13] Z. Gergintschew, Sensors and Actuators B 35-36 (1996) 285.
[14] G. Freitag, in Eurosensors XVIII, Roma, 2004, p. 648.
[15] T. Knittel, in IEEE Sensors, 2003, p. 191.
[16] T. Sulima, in IEEE, Irving, USA, 2005.
[17] W. Widanarto, in 11th IMCS, Brescia, Italia, 2006, p. 162.
[18] W. Widanarto, in XX EUROSENSORS, Vol. 1, Göteborg, Sweden, 2006, p. 306.
[19] I. Eisele, Sensors and Actuators B 78 (2001) 19.
[20] S. M. Sze, Semiconductor devices physics and technology, John Wiley and Sons, New York, 1985.
[21] K. Hauffe, Adsorption, Walter de Gruyter, Berlin, 1974.
[22] M. J. Madou, Chemical sensing with solid state device, Academic Press Inc., New York, 1989.
[23] V. F. Kiselev, Adsorption processes on semiconductor and dielectric surfaces, Springer-Verlag, Berlin Heidelberg, 1985.
[24] M. W. Roberts, Chemistry of the metal-gas interface, Clarendon Press, Oxford, 1978.
[25] S. R. Morrison, The chemical physics of surfaces, Plenum Press, New York, 1977.
[26] S. Harbeck, Characterisation and functionality of SnO_2 gas sensors using vibrational spectroscopy, PhD thesis Eberhard-Karls-Universität Tübingen, 2005.
[27] N. Barsan, Journal of Electronics 7 (2001) 143.
[28] W. Göpel, Sensors and Actuators B 26-27 (1995) 1.
[29] S. Hahn, SnO_2 thick film sensors ultimate limits: Performance at low O_2 and H_2O concentrations: Size reduction by CMOS technology,, PhD thesis Eberhard-Karls-Universität, Tübingen, 2002.
[30] P. B. Weisz, J. Chem. And Phys. 21 (1953) 1531.
[31] S. G. Chang, J Vac. Sci. Tech. 17 (1980) 366.
[32] J. Bock, Selektives und rekalibrierbares Sensorsystem zur Messung charakteristischer Verbindungen in Röstprozessen am Beispiel der Kaffeeröstung, PhD thesis Justus-Liebig-Universität, Gießen, 2000.

[33] K. Jun, Die Gasempfindlichkeit der gesputterten Zikoxid-dünnschichten unter dem periodischen Gaswechsel-Meßverfahren, PhD thesis TU Hamburg-Harburg, Hamburg, 1993.
[34] N. Yamazoe, Sensors and Actuators 4 (1983) 283.
[35] S. R. Morrison, Sensors and Actuators 2 (1982) 329.
[36] D. Bianchi, Journal of catalysis 38 (1975) 135.
[37] S. Bergmann, Festkörper, Walter de Gruyter, Berlin• New York, 1992.
[38] W. Thomson, in Phil. Mag Vol. 46, 1898, p. 82.
[39] M. Burgmair, Einsatz von Metalloxiden in Gas Sensor, PhD thesis UniBw, Munich, 2003.
[40] M. Burgmair, Sensors and Actuators B 95 (2003) 183.
[41] K. Scharnagl, Feldeffekttransistoren mit Luftspalt für den Nachweis von Wasserstoff, PhD thesis UniBw, Munich, 2002.
[42] J. F. Moulder, Handbook of X-rayphotoelectron spectroscopy, Perkin-Elmer Corporation, Physical Electronics Division, Minnesota, 1992.
[43] T. Knittel, Stabilisierung von Gassensoren auf FET-Basis, PhD thesis UniBw, Munich, 2005.
[44] S. T. Shishiyanu, Sensors and Actuators B 107 (2005) 379.
[45] N. P. Benner, Präparation und Optimierung von SnO_2-Schichten und deren Reaktivität, PhD thesis Justus-Liebig Universität, Giesen, 2004.
[46] B. Esfandyarpour, Sensors and Actuators B 100 (2004) 190.
[47] Z. Ling, Sensors and Actuators B 102 (2004) 102.
[48] R. S. Niranjan, IEEE (2003)
[49] N. S. Ramgir, Sensors and Actuators B 107 (2005) 708.
[50] J. Tamaki, Sensors and Actuators B 95 (2003) 111.
[51] G. Eranna, Central electronics engineering research institute Pilani, India, 2004.
[52] F. Chaabouni, Sensors and Actuators B 100 (2004) 200.
[53] H. Gong, Sensors and Actuators B 115 (2006) 247.
[54] G. Telipan, IEEE (1997)
[55] A. Karthigeyan, Sensors and Actuators B 78 (2001) 69.
[56] M. Zimmer, Mikrosensoren auf Transistor-Basis zur Wasserstoff- und Ozondetektion, PhD thesis UniBw, Munich, 2003.
[57] J. L. Gland, Surface Science 95 (1980) 587.
[58] G. Lindauer, Surface Science 126 (1983) 301.
[59] N. Yamazoe, Surface Science 86 (1979) 335.
[60] B. Kasemo, Physical review letters 44, 23 (1980) 1555.
[61] N. Tagushi, Vol. Patent 45-38200, Japan.
[62] N. Tagushi, Vol. Patent 47-38840, Japan.
[63] N. Tagushi, Vol. Patent 3 644 795, US.
[64] K. D. Schierbaum, Elektrische und spektroskopische Untersuchungen an Dünnschicht-SnO_2-Gassensoren, PhD thesis Eberhard-Karls Universität, Tübingen, 1987.
[65] M. Sinner-Hettenbach, SnO_2 (110) and Nano-SnO_2: Characterization by surface analytical techniques, PhD thesis Eberhard-Karls Universität Tübingen, 2000.
[66] D. Kohl, Sensor and Actuators B 1 (1990) 158.
[67] K. Suzuki, Sensors and Actuators B 24-25 (1995) 773.
[68] B. Hivert, Sensors and Actuators B 26-27 (1995) 242.
[69] D. Kohl, Sensors and Actuators 18 (1989) 71.

[70] M. Sriyudthsak, Sensors and Actuators B 13-14 (1993) 139.
[71] R. D. Delgado, in an electrochemical approach, Barcelona, 2002.
[72] W. Hellmich, Sensors and Actuators B 43 (1997) 132.
[73] G. Heiland, Chemical sensor technology, Kodansha, Tokyo, 1988.
[74] J. Y. Yun, CO-Gas sensing characteristics of Pt/SnO_2 thin composite film, Pusan National University, Korea, 2000.
[75] I. Lundström, Physica Scripta 18 (1978) 424.
[76] A. Spetz, Journal of Applied Physics 64 No. 3 (1988) 1274.
[77] M. Leu, Suspended gate feldeffekt-transistoren: reaktionsmechanismen für den gasnachweis und signalanalyse, PhD thesis UniBw, Munich, 1995.
[78] Z. Tang, Sensors and Actuators B 79 (2001) 39.
[79] J. Lee, Thin solid films 370 (2000) 307.
[80] E. Sonder, J. Appl. Phys. 58 (11) (1985) 420.
[81] C. Wilbertz, Sensors and Actuators A 123-124 (2005) 2.
[82] F. Jedema, Surface Morphology of Nanoscale $TiSi_2$ Epitaxial Islands on Roughened Si (100) and their Schottky Barrier Height, North Carolina State University in Raleigh, NC USA, 1996.
[83] M. Slotboom, North Carolina State University in Raleigh, NC USA, 1993.
[84] R. J. Nemanich, in Mat. Res. Soc. Symp, Vol. Proc. 94, 1987, p. 139.
[85] R. J. Nemanich, IEEE J. Quantum Electronics 25 (1989) 997.
[86] R. W. Fiordalice, North Carolina State University, 1988.
[87] K. Nomoto, J. Appl. Phys. 79 (1996)
[88] J. Oh, Electrical Characterization of $TiSi_2$ Nanoscale Islands by Scanning Probe Microscopy, PhD thesis North Carolina State University, Raleigh North Carolina, 2001.

Acknowledgments

First of all, I would like to thank *Prof. Dr. I. Eisele* for providing the great opportunity to pursue a Ph.D. at *Institut für Physik, Univesität der Bundeswehr München* and for interesting thesis topic. He provided extremely valuable suggestions and corrections. He inspired me with his enthusiasm about the achievements. I would like also to thank him for financial support.

I would like to thank *Prof. Dr. H. Baumgärtner* for *das Gutachten*. With it, I can extend my DAAD scholarship.

Thanks go to my colleagues at sensor group *Dr. Markus Burgmair, Kwanchai Anothainart, Dr. Thorsten Knittel, Thomas Galonska and Christoph Senft* for cooperation and interesting discussion about the entire sensor.

This work could not have been completed without the help and support of many people. To them I would like to express my deepest gratitude. In particular I would like to thank *Oliver Senftleben* for SEM and EDX characterizations, *Dr. Tanja Stimpel* for XPS characterization.

Many thank to *Frau Grüner* and *Dr. H. Pollack*, who have helped me to find a beautiful apartment and for all administrative processes at *Universität der Bundeswehr* and *Landratsamt Mariahilfplatz – München.*

Also, I am happy to thank all colleagues at *institut für physik*, *Dr. Torsten Sulima, Mathias Born, Thomas Zilbauer, Martin Schlosser, Andreas Aßmuth, Lothar Höllt, Markus Reinl, Markus Schindler, Ulrich Abelein, Peter Iskra, Dr. Alexandra Ludsteck, Dr. Gunter Freitag, Dr. Matthias Schmidt, Dr. Krishna K. Bhuwalka, Herr P. Ciecierski, Frau K. Bächle, Hans Messerosch, Walter Funke, Michael Meyer and Andreas Rippler* for their help and interesting scientific as well as non-scientific discussions.

Many thank to DAAD for providing a long-term scholarship program from October 2003 – Marc 2007.

Many thank to my parents, who have supported me in my academic way and also special thanks to my wife *Tutik Ningrahayu* and my daughter *Wida Ayu Larasati* for their understanding during accompany me in Germany.

R. Wahyu Widanarto